Evolution of the B cell repertoire in a spontaneous model of experimental autoimmune encephalomyelitis (EAE)

Florent Salvador

THESE

Présentée en vue de l'obtention du grade de

DOCTEUR EN SCIENCES
DE L'UNIVERSITE DE LILLE

Ecole doctorale : Biologie - Santé
Spécialité : Immunologie, Neurologie

Par
Florent Salvador

Le 02 avril 2021

Titre :

Évolution du répertoire des lymphocytes B dans un modèle spontané d'encéphalomyélite auto-immune expérimentale

Directeur de thèse : Pr Hélène Zéphir

Co-directeur de thèse : Dr Lennart Mars

Jury :

Pr Sylvain Dubucquoi	Président
Dr Nicolas Collongues	Rapporteur
Dr Cécile Delarasse	Rapporteur
Dr Anneli Peters	Examinateur

DOCTORAL THESIS

A thesis submitted in fulfilment of the requirements for the degree of :

DOCTOR OF PHYLOSOPHY
UNIVERSITY of LILLE

Doctoral school : Biologie - Santé
Speciality : Immunology, Neurology

By
Florent Salvador

2021, April 2nd

Title :

Evolution of the B cell repertoire in a spontaneous model of experimental autoimmune encephalomyelitis (EAE)

Thesis director : Pr Hélène Zéphir

Thesis co-director : Dr Lennart Mars

Jury :

Pr Sylvain Dubucquoi	President
Dr Nicolas Collongues	Rapporteur
Dr Cécile Delarasse	Rapporteur
Dr Anneli Peters	Examiner

Acknowledgements.

I would like to warmly thank all the people with who I have enjoyed working, who have helped, supervised, advised and comforted me and from whom I have learned so much:

- Many thanks to Dr. Nathalie Journiac, in particular for her expertise and her invaluable help in the daily conduct of animal experiments.

- Thanks to my colleagues from the NEMESIS (Neuro-inflammation and Multiple Sclerosis) team and more broadly from the LIRIC (Lille Inflammation Research International Center) and the LilNCog (Lille Neuroscience and Cognition). I would like to thank in particular Dr. Laure Deramoudt and Dr. Shin-Yi Yu.

I would like to thank my friends for the good times spent together in the difficult times.

I would also thank my family and especially my parents for their kind support.

Finally, I would like to particularly thank my partner Julia for her very special daily support as well as her encouragement.

Acknowledgements.

I would like to thank my thesis supervisor, Pr. Hélène Zéphir, and my thesis co-supervisor, Dr. Lennart Mars. Thank you for having accompanied me, given me their trust and transmitted their complementary knowledge. I am honored to have contributed to this beautiful and ambitious project.

I would like to thank Pr. Sylvain Dubucquoi, Dr. Cécile Delarasse, Dr. Nicolas Collongues, and Dr. Anneli Peters who have honored me with the privilege of sitting on this jury and evaluating my thesis work. Special thanks to Dr. Anneli Peters, for her great contribution to the elaboration of this ambitious project and Dr Bertrand Meressse for his advises during the monitoring PhD committee.

I would also like to thank:

- The cytometry and cell sorting platform of the Bio Imaging Center of the University of Lille, especially Nathalie Jouy and Emilie Floquet.

- The Genomic platform of Lille, especially Dr.Frédéric Leprêtre and Dr.Martin Figeac.

- Dr Thomas Guerrier and Julie Boucher.

Acknowledgements.

We thank:

- Dr. Dieter Jenne from the Ludwig-Maximilians-University of Munich for sharing reagents and protocols for MOG protein production in HEK-Ebna cells.

- Dr. Gurumoorthy Krishnamoorthy and Pr Hartmut Wekerle from the Ludwig-Maximilians-University of Munich for generously sharing protocols, scientific advice and the TCR^{1640} and IgH^{MOG} mouse models.

- Pr. Masayuki Kuraoka from the Research Institute for Biomedical Sciences of Tokyo University of Science for sharing protocols and 40LB feeder cells used for single cell culture of B cells.

Acknowledgements.

We thank for funding:

- ARSEP (fondation pour l'aide à la recherche sur la sclérose en plaques): call for Proposal 2016.

- Roche Foundation, Dr. Camille Brochier and Dr. Franck Delevacq.

Address:16, boulevard Carnot,
59800 Lille, France
Phone: 06 72 15 82 51
Email: florent.salvador@inserm.fr

Florent SALVADOR

FORMATION

- **2017-2021 : PhD program, Doctoral school Biology Health of Lille, France**
  Thesis director: Dr Hélène Zéphir (Contact: helene.zephir@chru-lille.fr)
  Laboratory: Neuro-inflammation and Multiple Sclerosis, UMRS Inserm 1172.
  Subject: Evolution of the B cell repertoire in a spontaneous model of experimental autoimmune encephalomyelitis (EAE). Article submitted in Frontiers in Neurosciences journal.

- **2014-2016 : Master, Biology Health Ecology, Signaling and Integrated Systems in Biology**
  EPHE (École Pratique des Hautes Etudes) 75014 Paris / **Sorbonne University** 75005 Paris.

- **2014 : Bachelor of Science, Sciences of Biotechnology**
  Pierre et Marie Curie University 75252 Paris.

- **2013 : Intensive general program for top-ranking higher education establisments, Biomedical Research**
  ESTBA (École Supérieure des Techniques de Biologie Appliquée) 75020 Paris.

- **2010-2012 : Two-year technical degree in Biology, Bioanalysis and Controls**
  ESTBA (École Supérieure des Techniques de Biologie Appliquée) 75020 Paris

- **2010 : High-school degree, STL, Speciality: Biology and Biological engineering**
  Notre-Dame les oiseaux 78480 Verneuil.

PROFESSIONAL EXPERIENCE

- **2017-2021 (4 years) : PhD program, Doctoral school Biology Health of Lille, France**
  PhD student [Transcriptomic analysis of B cell repertoire in a a spontaneous model of experimental autoimmune encephalomyelitis (EAE): Recombinant protein production and purification, construction of protein complexes, Westernbloting, cell culture, cell differentiation, cell sorting, ELISA, RNA purification, PCR, animal experimentation].

- **2015-2016 (2 years) : Cochin Institut, INSERM, Paris**
  Team «Biologie des phagocytes» (Contact: florence.niedergang@inserm.fr)
  [Study of the infection mechanisms involved in infection with an emerging strain of non-typhoid hyperinvasive *Salmonella* typhimurium (SiNT) on human macrophages derived from blood monocytes: Infection kinetic, cell culture, cell differentiation, cell sorting, Cytokine detection, recombinant protein production and purification, Westernblot.

- **2014 (CDD 1 year) : Cochin Institut, GENOM'IC Plateform, CNRS, Paris**
  GENOM'IC plateform (Contact: franck.letourneur@inserm.fr)
  [High-throughput sequencing on Ion Proton sequencer (Life Technology): Preparation of Ampli-seq Exome, Target-seq and RNA-seq samples; Ion PI chip loading, primary analyzes of sequencing data and estimation of data quality].

- **2013 (8 months) : Cochin Institut , INSERM, Paris**
  Equipe «Biologie des phagocytes» (Contact: florence.niedergang@inserm.fr)
  [Role of dendritic cells to transfer antigen to B cells: regulatory mechanisms and effect on humoral responses by immunostaining, recycling kinetics, bi-photon microscopy, cell culture].

Contents.

List of Abbreviations.

40LB	40L BAFF feeder cells
AID	activation Induced Cytosine Deaminase
ALN	axillary lymph nodes
APC	allophycocyanine
ARSEP	fondation pour l'aide à la recherche sur la sclérose en plaques
AU	arbitrary unit
BAFF	B-cell activating factor
BBB	blood brain barrier
BCR	B cell receptor
BV	brilliant violet
cDNA	complementary deoxyribonucleic acid
CFA	complete Freund adjuvant
CLNs	cervical lymph nodes
CNS	central nervous system
CSF	cerebrospinal fluid
CSR	class Switch Recombination
CXCL	circulating chemiokine ligand
EAE	experimental autoimmune encephalomyelitis
ECL	electrochemiluminescence
ELISA	enzyme-linked immunosorbent assay
FACS	flow cytometry analysis
FITC	fluorescein isothiocyanate
GC	germinal center
GFP	green fluorescent protein
GM-CSF	granulocyte macrophage colony-stimulating factor
GWAS	genome-Wide Association Studies data
HEK	human embryonic kidney
HLA	human Leukocyte Antigen
HRP	horseradish peroxidase
Ig	immunoglobulin
iGB	induced germinal center B cells
IgH	heavy chain of immunoglobulin
IgL	light chain of immunoglobulin
IL	interleukin
ILN	inguinal lymph node
PBS	phosphate-buffered saline
PE	phycoerythrin
PerCP	peridinin-chlorophyll-protein complex
PNA	peanut agglutinin
MBP	myelin basic protein
MHC	major Histocompatibility Complex
MLN	mesenteric lymph node
MOG	myelin oligodendrocyte glycoprotein
MOGAD	myelin oligodendrocyte glycoprotein autoimmune disease
MOG_{biot}	recombinant murin myelin oligodendrocyte glycoprotein biotinylated
MOG_{m}	recombinant myelin oligodendrocyte glycoprotein monomer

MOG_{tet}	recombinant murin myelin oligodendrocyte glycoprotein tetramerized
MRI	magnetic resonance imaging
MS	multiple sclerosis
NMO	neuromyelitis optical
NTL	non transgenic littermate
NRF2	NF-E2-related factor 2
PLP	proteolipoprotein
PP	Payer patches
PPMS	primary progressive multiple sclerosis
RNA	ribonucleic acid
RRMS	relapsing-remitting multiple sclerosis
SD	standard deviation
SEM	standard error of the mean
SHM	somatic hypermutation
SNP	single Nucleotide Polymorphisms
SPMS	Secondary progressive multiple sclerosis
TCR	T-cell receptor
TMB	tetramethylbenzidine
WT	wild type

Abstract.

The project aims clarifying the involvement of B cells in the initiation and progression of multiple sclerosis (MS) using a transcriptomic analysis of B cells in cervical lymph nodes (CLNs) and brain of a transgenic mouse model of spontaneous experimental autoimmune encephalomyelitis (EAE). In this model called TCR^{1640}, transgenic TCR (T cell receptor) for $MOG_{92\text{-}106}$ are supposed to recruit MOG-specific B cells from the endogenous repertoire to initiate EAE.

The objective of the thesis was to evaluate the dynamics of MOG-specific B cells at the initiation of EAE in the secondary lymphoid organs and the brain. In this TCR^{1640} model in Lille, the EAE incidence was from 85% at 700 days of life. We checked the performance of a MOG tetramer (MOGtet) to detect and isolate MOG_{tet}^{+} B cells. This MOGtet allowed us to identify rare MOG_{tet}^{+} B cells primarily in CLNs and brains of diseased TCR^{1640} mice. Anti-MOG antibodies in serum were quantified by ELISA and detected in disease-free and diseased TCR^{1640} mice, without correlation with their age, delay of EAE and clinical score. However, serum transfer experiments showed that there was a difference in humoral activity between sera of diseased and disease-free TCR^{1640} mice, which aggravated incidence and severity of EAE in the 2D2 mouse (another EAE model). These results suggested the dynamics of the repertoire of MOG_{tet}^{+} or total B cells to a pathogenic repertoire for the EAE development. Induced germinal center B cells culture (iGB) and expansion (on 40LB fibroblasts) of MOG_{tet}^{+} or total B cells sorted from CLNs and brain of disease-free and diseased TCR^{1640} mice allowed to define some clonotypes for IgLK chains and IgHG chains considering the variable parts of the Ig chains.

Our findings highlight the potential pathogenicity supported by the repertoire of MOG-specific B cells in TCR^{1640} mice. The difficulty of the iGB single cell culture to expand effector cells will motivate to go furtherly to direct single cell sequencing of sorted CLNs-derived-MOG_{tet}^{+} B cells and CNS-derived (central nervous system) MOG_{tet}^{+} B cells from TCR^{1640} mice to complete the repertoire exploration .

I. Introduction.

A. Multiple sclerosis.

1. Epidemiology.

Multiple sclerosis (MS) is a chronical neuroinflammatory, demyelinating and degenerative disease of the CNS (central nervous system) including brain, spinal cord and optical nerve. MS affect 2,5 million of people in the world and induce physical disability (motor, sensory, urinary issues, visual, pain, fatigue and cognitive impairment) in young adult at a mean age of 30 years old and especially in women with a sex ratio closed to 3 women for 1 man [1].

During MS, lesions are disseminated in the CNS leading multiple disabilities. The different neurological functions (sensitive, motor, gait, bladder functions, cognition, cranial nerves, etc…) are transmitted in the form of nerve impulses carried by the nerve fibers of the white matter in brain or spinal cord. In the case of MS, the nerve impulse is interrupted in the lesions and is not transmitted to the rest of the body. This leads to the development of variable symptoms such as the temporal-spatial spread of lesions in the brain and bone marrow (Fig. 1) of MS patients.

Two forms of the disease are usually described: primary progressive (PPMS) form (15%) and relapsing-remitting (RRMS) form (85%). Relapsing-remitting form is characterized by relapses, corresponding to the development of new neurological signs followed by partial or total remissions. Inside the group of patients affected by the relapsing-remitting form, 50% will evolve into a secondary progressive (SPMS) form [2].

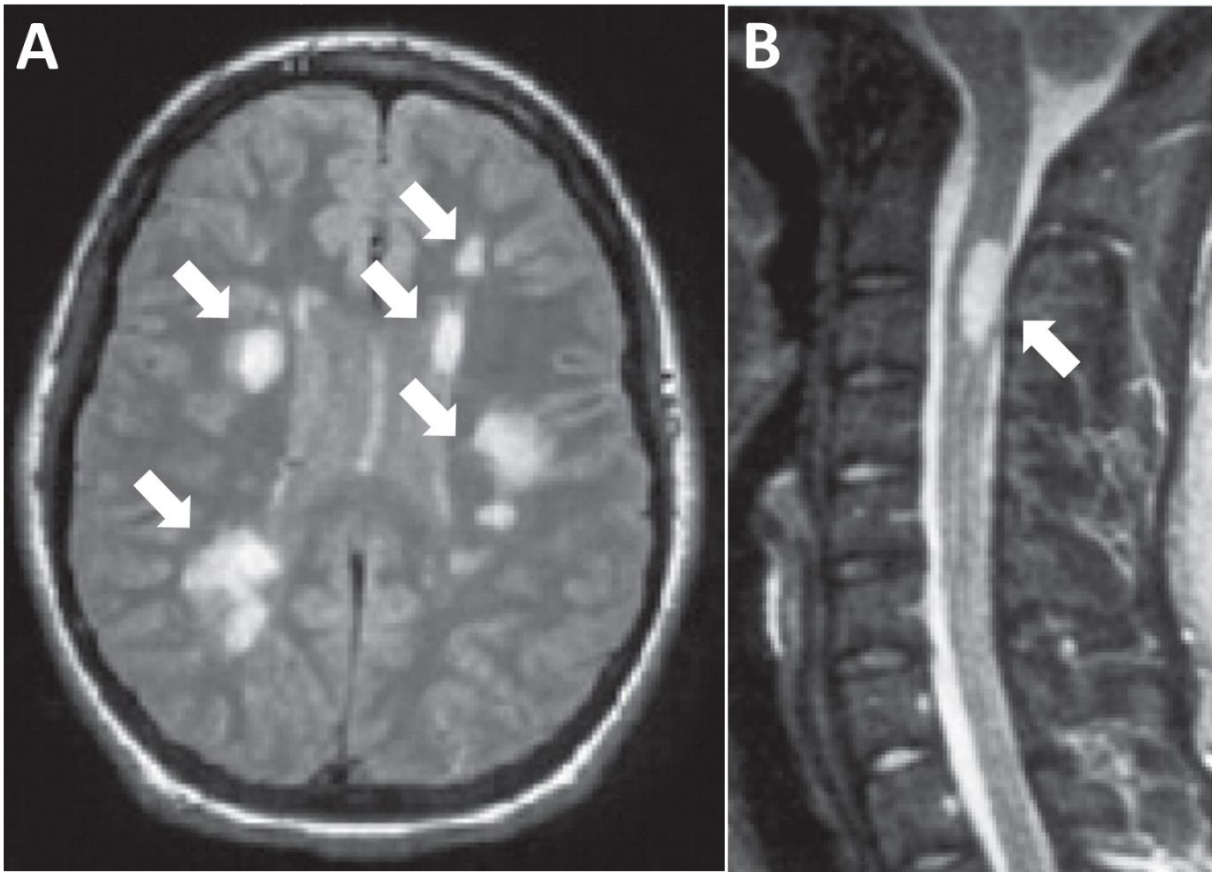

Figure 1 : Lesions in Multiple Sclerosis.
Detection of lesion using magnetic resonance imaging (MRI) in brain (A) and spinal cord (B) of MS patient. White arrows indicate T2-hypersignal lesions in white matter observed by MRI in MS patient. Adapted from Compston and Coles, 2008 [3].

2. Risk factor.

MS is a multifactorial disease within some factors were established like genetic predispositions supported by studies in twins [4]. In addition, the genetic predisposition associated with certain allele of the HLA-DR 2 locus has been known [5]. Moreover, screening of SNP (Single Nucleotide Polymorphisms) databases using Genome-Wide Association Studies data (GWAS) have identified many genetic variants linked to MS susceptibility and some of these variants are linked to the immune system and especially to the T cell response [6]. In addition, GWAS supports the hypothesis that MS is initially an immune disease with the human Leukocyte Antigen (HLA) like major susceptibility gene located on the locus of the human Major Histocompatibility Complex (MHC) [6]. However, many environmental factors have been

highlighted such as smoking [7], Epstein Barr virus exposition [8], obesity [9] and vitamin D deficit [10].

3. Diagnostic.

After observation of clinical symptoms, MS is diagnosed according to Mc Donald's criteria which have evolved from 2001 to 2017 and is characterized by definition of temporal and spatial dissemination of the lesions on MRI [11] (Fig. 2, A-B). Oligoclonal bands (OCB) can also be observed in cerebrospinal fluid (CSF) for 90% of MS patients [12] (Fig. 2, C). The detection of these intrathecal productions contributes to the diagnostic of MS in the last Mc Donald's 2017 criteria due to the prognosis factor of such findings for MS [13].

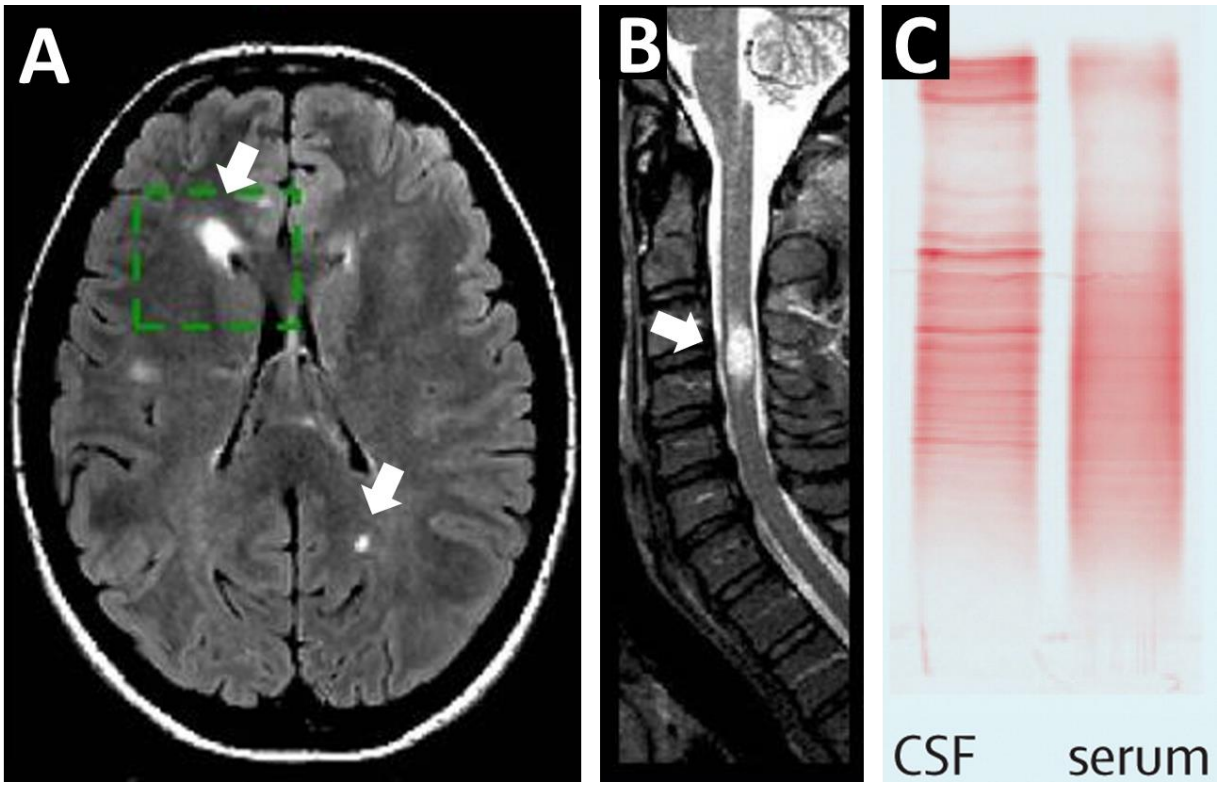

Figure 2 : Criteria of a diagnostic for MS.
Detection of lesion using magnetic resonance imaging (RMI) in brain (A) and spinal cord (B) of MS patient. White arrows indicate T2 hypersignal lesions observed on MRI in MS patient. Detection of oligoclonal bands after protein electrophoresis of the cerebrospinal fluid and the serum (C) of MS patient. More numerous oligocloclonal bands of IgG can be counted after isoelctrofocalisation of CSF proteins compared to serum of the same individual, showing intrathecal synthesis of Ig. A and B adapted from Filippi et al. 2019 [14]. C adapted from Compston and Coles, 2008 [3].

4. Mechanisms implicated in MS.

Pathologically, MS is characterized by inflammation, demyelination, reactive gliosis, and neuroaxonal damage. Indeed, MS is characterized by inflammatory reaction associated with demyelination in the CNS. In parallel with demyelination, a suffering of the axon can lead to axon ruptures and neurodegeneration [15]. During remissions, the inflammation is reduced and may disappear from the lesion site. This might allow an initiation of remyelination [16]. Remyelination partially restores nerve conduction and reduces clinical symptoms.

The hallmark of MS is the perivenular presence of focal immune cell infiltrates involving macrophages, CD4+ and CD8+ T cells [17], B cells, plasma cells, IgG antibodies and resident activated microglia cells [18]. Lesions are classified in active, inactive and shadow plaques [19]. Active lesions are characterized by the presence of activate macrophages containing myelin debris. Inactive lesions are characterized by the demyelination of the tissue and the absence of activated macrophages containing myelin debris. Shadow plaques are characterized by focal scar and low density of myelin on the surface of axons.

a) Inflammation

Concerning inflammation, early lesions present infiltrates of immune cells through the blood brain barrier (BBB). In these lesions, macrophages containing myelin debris dominate the infiltrate (Fig. 3), followed by CD8+ T cells, whereas lower numbers of CD4+ T cells (Fig. 3), B cells and plasma cells can also be found. When the disease is advanced and due to a chronical *in-situ* inflammation, tertiary lymphoid structures called ectopic lymphoid follicles were detected [20]. These ectopic lymphoid follicles would contribute to differentiation and

maturation of specific effector cells in CNS antigens. This will allow continued spread of inflammation effector cells to CNS antigen behind a closed BBB[21].

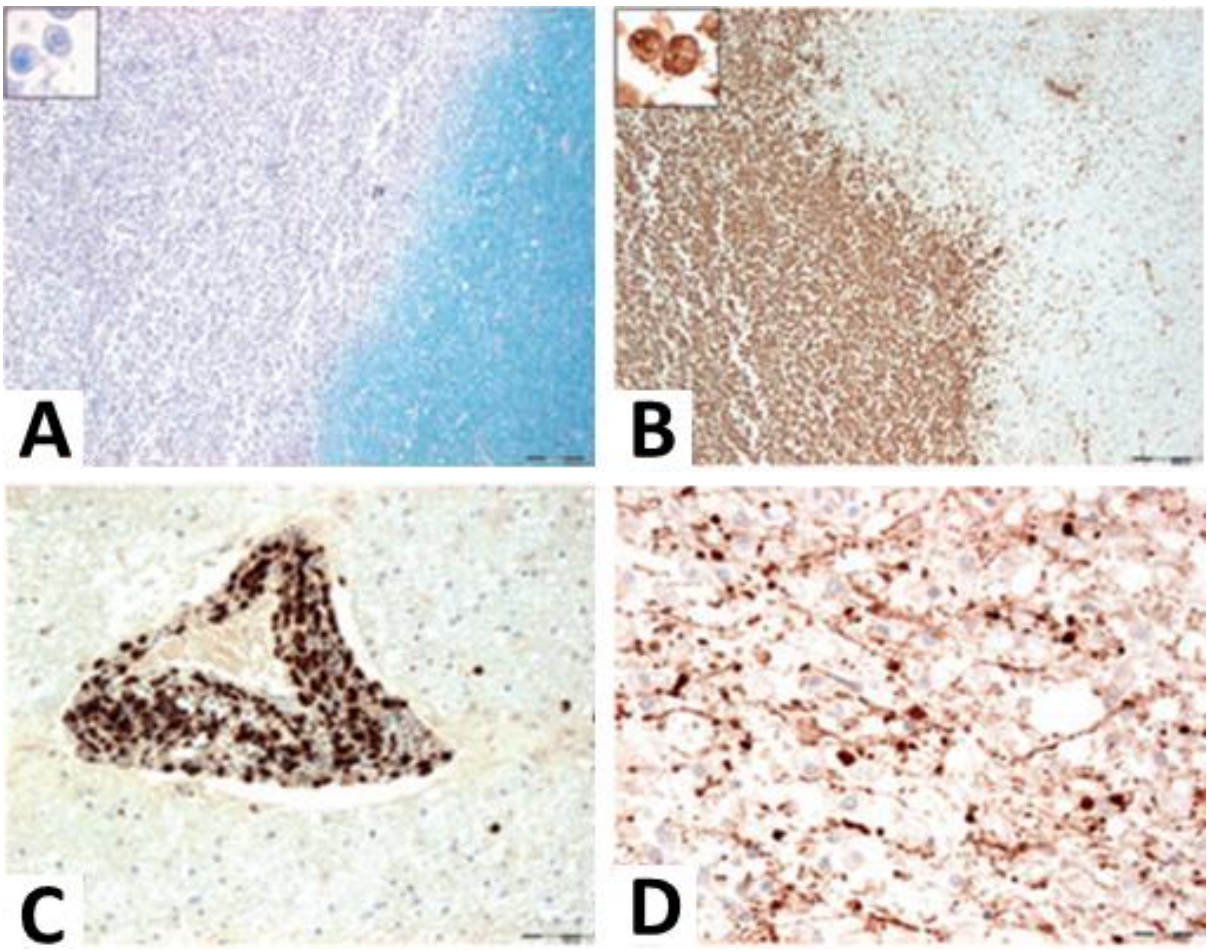

Figure 3 : Inflammation, demyelination and axonal injury in white matter active lesion of MS patient.
Different stainings show an active lesion from a patient with acute multiple sclerosis with active demyelination (A), profound macrophage (B) and T-cell infiltration (C) and extensive acute axonal injury (D). A, myelin staining in blue using Luxol fast blue. B, Macrophages and microglia staining using anti CD68 T cell staining using anti CD3 and axon staining using amyloid precursor protein. Adapted from Frischer et al 2009 [22].

Note that the lesions sites have variable compositions and were classified in four patterns [18]. Patterns I and II lesions were localized on small veins and venules and mainly associated with T cells and macrophages infiltration. In addition, the pattern II included Ig and complement deposits and would be the most prevalent lesion pattern in RRMS. Pattern III lesions were not localized on small veins and venules but were diffused and presented a decrease in myelin around inflamed vessels. Pattern IV lesions were diffused and was associated to ring of dead oligodendrocytes around the site of demyelination. The diversification of MS clinical symptom may reflect the complexity of the immune response invading CNS [23].

The infiltration of immune cells allows the recruitment of immune cells from the periphery to the CNS through the blood-brain barrier. Cells involved in inflammation can interact with each other in order to activate, differentiate and expand. Macrophages may have degraded antigens and present antigens on their surface to initiate activation of T-cells to CD8 T cells (cytotoxic) [24]. T cells allow the activation of B lymphocytes and then their differentiation and expansion into memory B cells and plasma cells producing antibodies. B cells can produce a specific response to antigens implicated in the inflammatory process. The B cell response will evolve by epitope spreading to target antigens on the inflammatory lesions site. Epitope spreading is defined by the diversification of epitope specificity from the initial focused. Epitope spreading applies to situations in which tissue damage from a primary inflammatory process causes the release and exposure of a previously “sequestered” antigen, leading to a secondary autoimmune response against the newly released antigen [25].

During inflammation, the assay of cytokines produced by immune cells show a predominantly pro-inflammatory cytokine production like IL-6 by macrophages, IL-17 (Th17) and IFNγ (Th1) by T cells [17] but also IL-12, IL-6, IL-15 and GM-CSF (granulocyte macrophage colony-stimulating factor) by activate B cells [26] [27]. In SPMS, BBB remains intact and the inflammatory response is compartmentalized in the CNS [2]. The anatomy of demyelinating lesions evolves with the appearance of lesions in the cortex. Demyelination occurs by expansion of existing lesions, with few *de novo* lesions appearing in the white substance. Chronic neuronal deterioration or neurodegeneration is important. In PPMS, lesions in the active tissue are mainly associated with the activation of the pro-inflammatory microglia and the recruitment of macrophages. Ectopic lymphoid follicles were detected and contribute to the differentiation and maturation of specific effector cells to CNS [20]. At this stage of the disease the inflammatory reaction is compartmentalized and works independently of the peripheral influx of immune cells.

In addition, lymphatic vessels have a key role for the circulation of lymphocytes in the immune system. In the CNS, CD4+ T cells, monocytes and dendritic cells can use cerebrospinal fluid to circulate from the arachnoid mater to the cervical lymph nodes (CLNs) [28] , allowing exchanges between CNS compartments and periphery.

b) Demyelination

As a result of inflammation, demyelination (Fig. 3,A) is initiated and characterized by the destruction of myelin oligodendrocytes (or myelin sheath), axons and neurons from CNS (Fig. 3,C). Myelin corresponds to the extensions of the plasma membrane of oligodendrocytes coiled around the axons. These structures are separated by bare axon spaces where ion channels are concentrated (called Ranvier nodes) and where the ion channels involved into nerve

impulse. This nerve impulse travels from Ranvier's node to another one. The function of this transit is to greatly increases the impulse speed (Fig. 4,A). Demyelination leads to a decrease in the rate of nerve impulses propagation and a redistribution of the different nerve channels (Fig. 4,B). This, accentuate the disorders of the conduction of the nervous message and then, the clinical signs. Following the attack of myelin, the myelin sheath thins and may disappear (Fig. 5), resulting in axonal loss [29] (Fig. 4,C).

Chronic inflammation would also produce inflammatory neurotoxic mediators such as metabolites oxygen and nitrogen reagents by microglia and resident astrocytes of the CNS. These inflammatory neurotoxic mediators cause deleterious mutations in mitochondrial DNA and metabolic stress accentuating neuronal degradation. This can lead to apoptosis or necrosis of pre- and post-synaptic neurons [15].

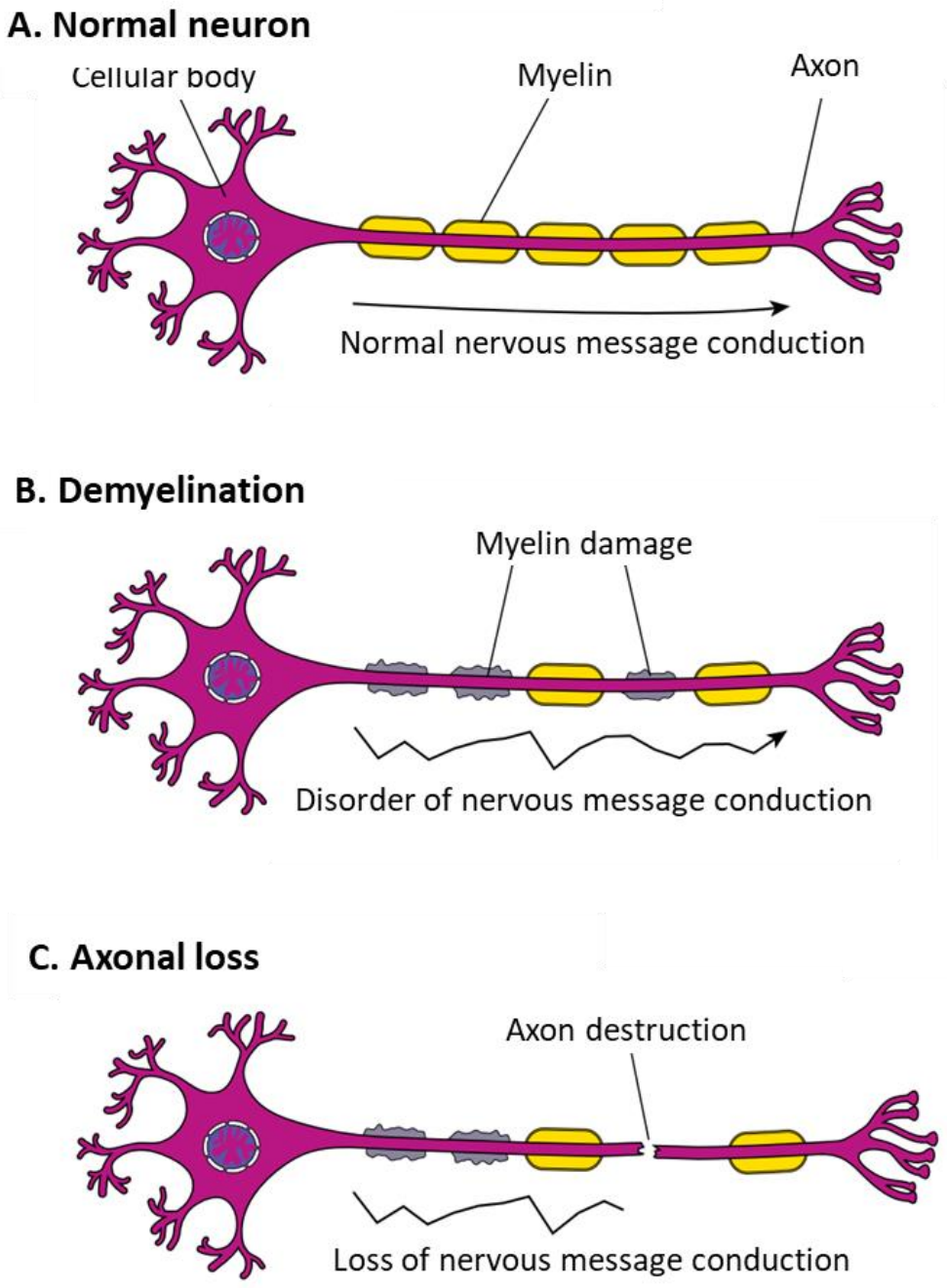

Figure 4 : Representation of axonal demyelination and axonal loss.
Representation of normal neuron (A), demyelination (B) and axonal loss (C) according to the nervous message conduction. Adapted from Florence Higue-van Steenbrugghe 2016 [30].

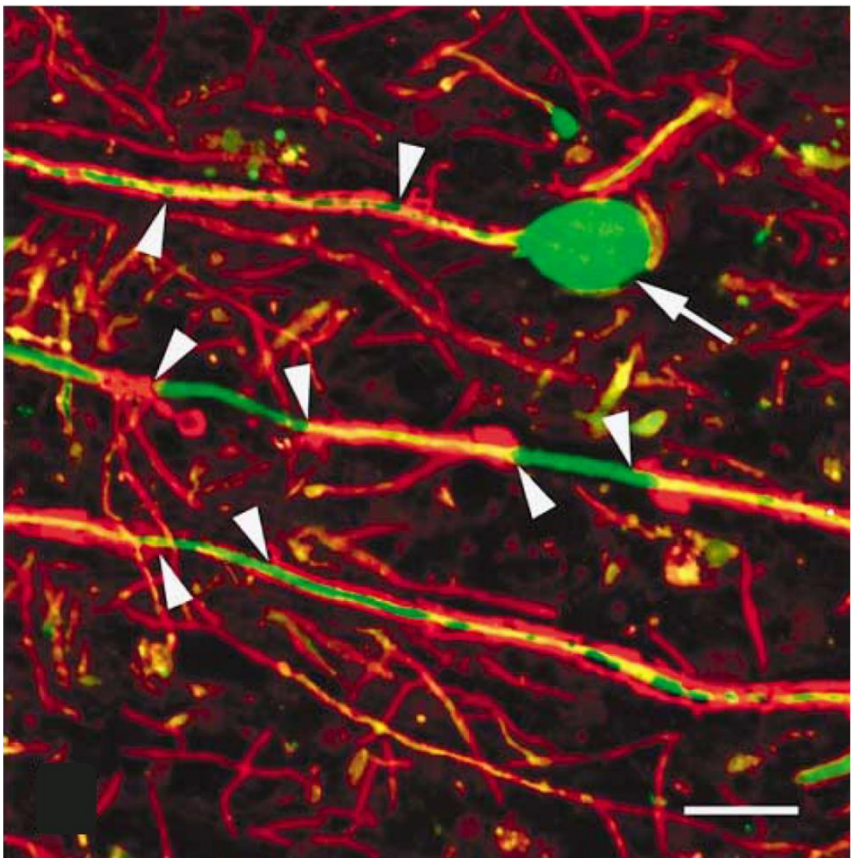

Figure 5 : Axonal demyelination in lesions of MS patient.
Non-phosphorylated neurofilaments staining in green and myelin staining in red show three large, non-phosphorylated-neurofilament–positive axons undergoing active demyelination (arrowheads) and one axon ends in a large terminal ovoid (full arrow). The scale bars represent 45 µm. Adapted from Trapp et al., 1998 [31].

5. Remyelination and/or neurodegeneration.

As a result of inflammation, demyelination is initiated remyelination and/or neurodegeneration. Oligodendrocyte progenitor cells participate to remyelination using their membrane to repair damages engaged by inflammation and immune cells in parallel to the clearance of debris realised by microglial cells and macrophages [32]. If the remyelination was not sufficiently efficient, the oxidative stress of neuron and the ion channel dysfunction can induce the axonal loss and neuron apoptosis [15]. With age the pathological processes are accentuated in parallel with reduced remyelination and reconstruction at the lesions sites [33].

B. Physio-pathological hypothesis in MS.

The current consensus is that the disease is initiated by peripheral activation of self-reactive lymphocytes targeting CNS autoantigens [17]. Molecular mimicry mechanisms may explain the development of the immune response in the periphery made on a genetic field predisposed to [34]. Many myelin antigens have been studied trying to track and define targets supporting this autoimmune disease [35]. However, to date, no studies have been able to formally explain the involvement of a specific antigen responsible for the MS disease, in myelin candidates as well as in myelin and oligodendrocytes [36].

In addition, the development of inflammation can lead to epitope spreading mechanisms that are characterized by the development of the immune response to other variable auto-antigens involved in the inflammatory mechanisms. Indeed, the degradation of CNS tissues during lesions reveals autoantigens normally inaccessible to the immune system [23]. This presentation of these autoantigens by immune cells will induce the formation of new specialized self-reactive cells.

Thus, the lesions observed are the result of the infiltration of macrophages, T and B cells through the blood-brain barrier or the cerebrospinal fluid barrier at the choroid plexus [18]. This cell infiltration of adaptive and innate immunity induces the triad "inflammation / demyelination / neurodegeneration" with an evolution of the antigenic targets of the CNS. Before the inflammation step, an unknow peripheral activation of self-reactive lymphocytes will begin to initiate the inflammatory reaction. The activation of self-reactive lymphocytes will induce the migration of these cells to the brain and the spinal cord. When the activated cells arrived in the brain and the spinal cord, a pro-inflammatory environment will be established. These pro-inflammatory environments will recruit other lymphocytes to complete the

inflammatory response. Macrophages, T cells and B cells cooperate leading to demyelination. This will induce the maturation of B cells into plasma cells and the secretion of anti-myelin specific antibodies. It was demonstrated an overlap of the cerebrospinal fluid IgG-H and Ig-L-chain proteomes with the Ig-transcriptomes from cerebrospinal fluid and from brain lesions [37]. This supposes that the antibody B cells repertoire present in the cerebrospinal fluid reflects Ig-transcripts of B cells populating and CSF-resident antibodies were produced by B cells at the lesion site and by CSF-resident B cells [37].

In parallel of direct cellular interactions, cells also produce cytokines participating to inflammation. It should be noted that many pro-inflammatory cytokines are found at the lesion level. For example, T cells (mostly Th1 and Th17) produce IFN gamma, TNF alpha, and IL-17 [38], macrophages produce IL-6 and B cells produce IL-12, IL-6, IL-15 and GM-CSF [26 27]. These soluble chemical mediators allow the recruitment of immune cells in the CNS. They also have a key role in the activation of cells and their maturation to generate a targeted response of inflammation.

These different conditions will lead to the demyelination of axons and the subsequent neurodegeneration. During the humoral response, some targets will evolve according to macrophage and microglia clearance of debris. [23].

C. Immunotherapy.

Immunomodulation and immunosuppression are used to slow the disease and reduce clinical progression without curing the disease [39]. These treatments allow controlling the inflammatory parameters (clinical relapses, accumulation of T2 lesions and gadolinium-enhanced lesion on MRI).

Interferons and copolymer-1 were the first immunomodulating drugs to be validated as modifying the disease course by controlling annualized relapses rates and cumulative lesions on MRI [40]. IFNβ performs several immuno-suppressive functions and induce inhibition of lymphocyte infiltration into the CNS [41]. Copolimer-1 is a synthetic copolymer identical in part to MBP known to be an encephalitogenic protein of myelin. This copolymer was able to bind with a strong affinity to MHC class II molecules carried by the APCs. This binding competition between the copolymer and myelin sheath proteins partially prevents the activation of the T response [42].

Some cytotoxic therapy as mitoxantrone, highly efficient in aggressive forms of MS were also used before biotherapies arrival [43]. Mitoxantrone is an anthracycline, initially prescribed in oncology for its cytotoxic properties (breast cancer, leukemia). This intercalating agent of DNA inhibits RNA and DNA synthesis by inhibiting type II topoisomerase. Its immunomodulatory capacity is made through inhibition of T cell and B cell proliferation and by induction of cell lysis or activation of programmed cell death [44].

Natalizumab was the first biotherapy and is a monoclonal antibody targeting integrins preventing activated lymphocytes to cross the BBB [45]. Teriflunomide is an immunostatic drug used as first line therapy in MS [46]. Dimethyl fumarate would act on the NRF2 (NF-E2-related

factor 2) pathway to be anti-inflammatory and can be considered as an immunosuppressant [47]. Fingolimod is an anti sphingosin-1-phosphate receptor preventing activated T cells to egress from lymphoid organ [48]. As for mitoxantrone, alemtuzumab (anti CD52) allow an induction therapy. Alemtuzumab largely deplete T cells [49]. The first clinical trials using B cell depletion in MS were supported by the animal studies showing that B cell depletion could influence EAE [50, 51]. Anti-CD20 therapies showed a high efficiency also on controlling inflammatory parameters of MS disease and is the first drug demonstrating a slowing capacity in primary progressive disease, supporting the inflammatory compound in the worsening and progressing mechanisms of MS. B cell depletion by rituximab remains the strongest evidence of the key role of B cells in pathology of MS [50].

D. Model of Experimental Autoimmune Encephalomyelitis (EAE).

In order to better understand MS, animal models have been developed. Each of these models has benefits and issues that give to each model a study target.

Initially, EAE models were based on rabbit and monkey brain by repeated injection of normal brain tissues in rabbits and monkey [52]. Then, it was shown the involvement of encephalitogenic peptides characteristics. Myelin basic protein (MBP) in this model as well as other myelin proteins such as protheolipoprotein (PLP) or myelin oligodendrocytes glycoprotein (MOG) in active immunization using Freund adjuvant (CFA) and pertussis toxin to break down the BBB. Many models have been developed to respond to specific hypotheses considering inflammation and/or demyelination processes of the autoimmune experimental disease induced. There are 4 types of EAE model: the induced model, the passive model, the adoptive model and the spontaneous model.

1. Induced model of EAE.

Active EAE is induced by animal immunization using CNS protein homogenates, myelin peptides, emulsified in a complete Freund adjuvant (CFA) of virus. The key component of CFA is the inactivated heated *Mycobacterium tuberculosis bacterium* [53]. The peptide-adjuvant solution induces the presentation of the antigen by the MHC class II to CD4 T cells in a highly inflammatory context. The highly inflammatory context is necessary for the activation of specific auto-reactive T cells. These self-reactive T cells activated at the peripheral level in the draining lymph nodes (Th1 and Th17 T cells) then migrate into the CNS with activated B cells and inflammatory monocytes. This leads to a high incidence of the disease in susceptible animals with clinical signs induction 9 to 12 days after immunization. Active immunization using CNS protein homogenates or myelin peptides and CFA emulsified is one of the most commonly used protocols to induce EAE because it is easily executable and generally reproducible. For example, two monophasic models of EAE: C57BL/6 mouse after immunization with MOG_{35-55} (myelin oligodendrocyte glycoprotein) and CFA [54]; rat after immunization with MBP_{63-81} and CFA. These EAE models usually lead to a monophasic experimented disease. Other models more resembling to MS have also been developed such as SJL/J mice immunized once with $PLP_{139-151}$ and CFA that develops multiphase EAE with relapses and remissions characterized by the evolution of the epitope spreading, due to the $I\text{-}A^s$ background [25].

2. Passive and adoptive model of EAE.

Passive or adoptive EAE can also be induced in recipient animal by the transfer of specific pathogenic myelin-specific CD4 T cells generated by active immunization of the donor animal [55]. Passive EAE established the key role of T cells directed against CNS proteins in the pathogenicity of the disease.

3. Spontaneous model of EAE.

Trying to avoid artificial peripheral increase inflammation and polyclonal inflammation, transgenic models called "spontaneous model of EAE" have been generated. These models are transgenic mice for myelin-specific TCRs or/and BCRs. They spontaneously develop neurological disorders with a broad variety of clinical incidence and phenotype [56, 57].

Spontaneous EAE is based on genetic modification usually associated with specific targeting of myelin proteins by immune cells such as T and B lymphocytes For example, in the 2D2 mice model which are transgenic C57BL/6 mice for the expression of a specific TCR for the peptide MOG_{35-55}, 50% of mice develop an EAE [58]. Moreover, 35% of 2D2 mice develop optic neuritis with similar but restricted lesions to the optic nerve and no progression to clinical EAE. This preferential phenotype of optic neuritis reflects the differential expression of MOG which is 2-fold more represented in optical nerve compared to spinal cord.

Another mice model called OSE mouse was developed on C57BL/6 transgenic mouse which expresses TCR specific for the peptide MOG_{35-55} and B cells producing antibodies with the heavy chain of a demyelinating MOG-specific antibody (8.18C5) [59]. In this model, mice developed inflammatory and demyelinating lesions located in the optic nerve and spinal cord, sparing brain and cerebellum. In comparison, in the IgH^{MOG} model, mice were only transgenic to produce B cells producing antibodies with the heavy chain of a demyelinating antibody specific for MOG (8.18C5); mice do not develop inflammatory and demyelinating lesions. But the presence of the transgene accelerates and exacerbates experimental autoimmune encephalitis [60]. These models suggest that a recruitment of myelin protein-specific B cells by myelin protein-specific T cells may lead to an autoimmune disease in CNS.

TCR^{1640} mice model aims to be closer to the pathophysiology of MS. The TCR^{1640} mice are TCR^{1640} (specific for MOG$_{92\text{-}106}$) transgenic SJL/J mice. It was obtained by Hartmut Wekerle's team in the Max Planck Institute in Martinsried [61]. Most of female TCR^{1640} mice developed relapsing form of EAE versus only half male TCR^{1640} mice. Remaining mice developed chronical form of EAE. At least 70% of TCR of TCR^{1640} mice were transgenic. The T cell response would recruit MOG-specific B cells from the endogenous repertoire to initiate EAE. In this model, the hypothesis is that B cells response is essential in the disease process because it has been shown that MOG-deficient mice and B cell depleted mice (Fig. 6,A) are protected from EAE [61]. Note that in this model, mice in EAE have a cellular infiltrate and demyelination similar to that of MS patient. Mice with ataxic form displayed large inflammatory and demyelinated lesions in cerebellum and brain stem. Mice affected by the conventional EAE displayed lesions distributed throughout the spinal cord, brain stem, and optic nerve [61]. In the CNS of diseased-TCR^{1640} mice were found macrophages, activated CD4 T cells (Th1 and Th17), CD8 T cells and B cells and Ig deposits [61]. Inflammatory infiltrates were embedded in large areas of demyelination and axon destruction. Moreover, as with MS patients, the microbiota is involved in the development of EAE in the TCR^{1640} mice model [62] (Fig. 6,B). The characteristics of this model make this model a unique model to study the natural evolution of the B cells repertoire in an EAE model.

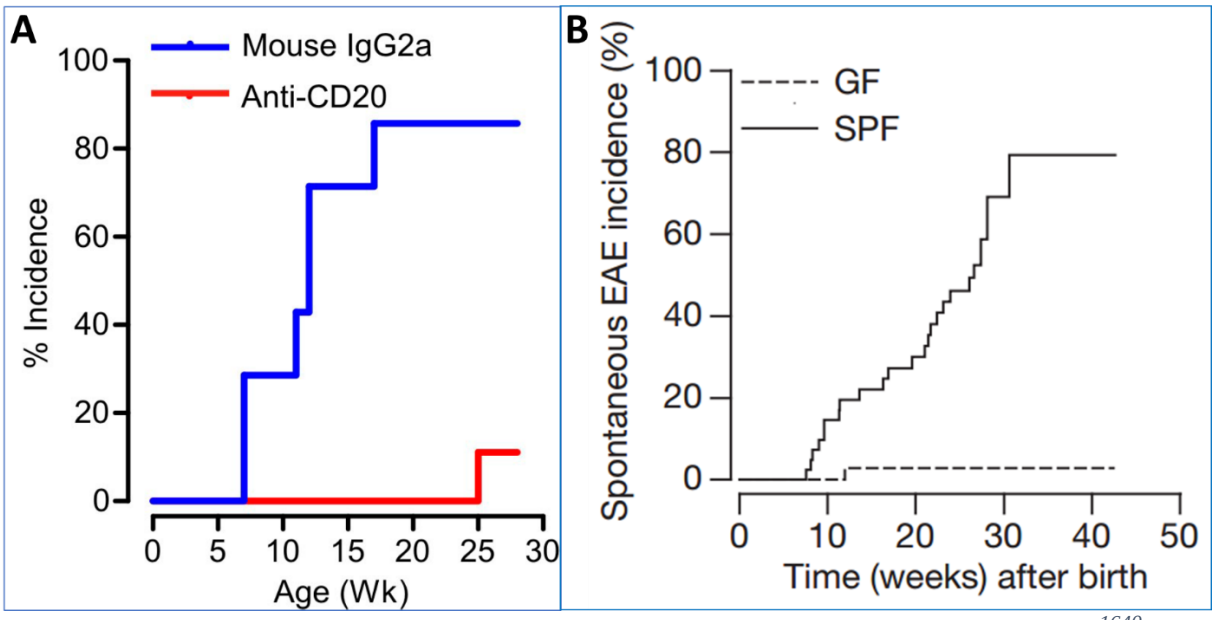

Figure 6 : Protection to EAE using anti-CD20 antibodies or germ-free food in TCR^{1640} mice model.

A, cell depletion protects TCR^{1640} mice from spontaneous EAE. B cells were depleted from TCR^{1640} mice by twice weekly injections of anti-CD20 antibodies from day 3 after birth (in red), and control mice received mouse IgG2a control isotype antibodies (in blue). Adapted from Pöllinger et al., 2009. B, Mice with germ-free food were protected from spontaneous EAE. Incidence (in percent) of TCR^{1640} mice housed in germ-free food (in dashed lines) or specific pathogen-free food (in full line). Adapted from Berer et al., 2011 [58].

E. B cells.

B lymphocytes are actors of lot of mechanisms of immunity like antibodies production, T cell activation and inflammation regulation using cytokine secretion. Ig deposits, B cells localization at the inflammatory lesion and the efficacity of treatment anti-B cells demonstrate the key role of B cells in MS.

1. Ontogeny and role of B cells in human.

The origin of B cell is found in the bone marrow (Fig. 7). In the bone marrow, pro-B cells are formed from hematopoietic stem cells. These pro-B cells (CD19+, CD38+) have the ability to recognize the native form of antigen using B cell receptor (BCR) which is a transmembrane immunoglobulin (Ig). The Ig is a protein heterodimer (Fig. 8) consisting of two identical heavy (H) chains and two identical light chains (L). Each H or L chain includes a constant region (C) and variable region (V), the combination of variable domains defining the antigen binding site. The formation of the H and L chains is the result of the combination of several gene segments organized in different chromosomes. The locus of heavy chain genes is located on the Humans chromosome 14. Variability (V), diversity (D) and Junction (J) genes encoding for the variable domain are present in this locus (Fig. 7).

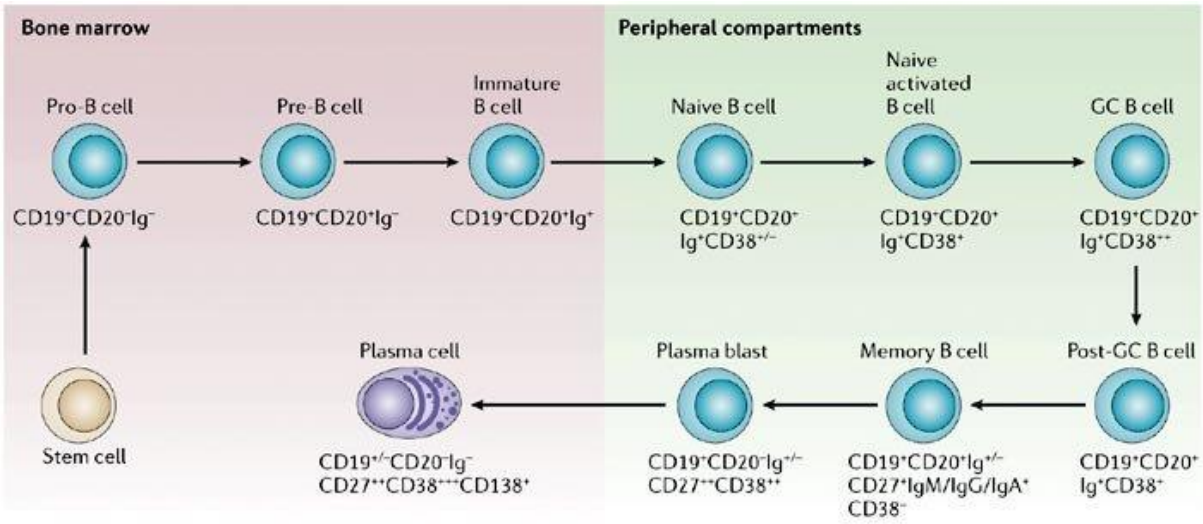

Figure 7: Ontogeny of B cells
Ontology of B cells and maturation in from bone marrow to peripheral compartment. Adapted from MedicoAID on http://www.medicoaid.com/qod-618-b-cell-maturation/

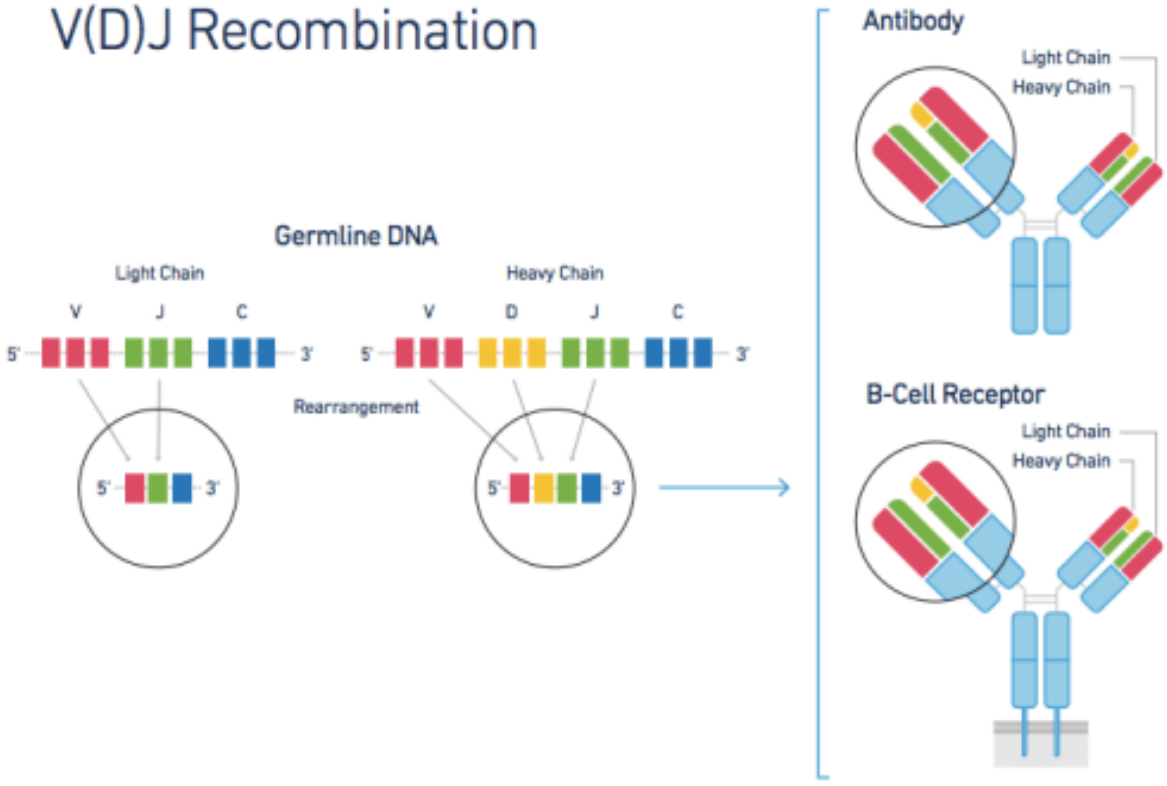

Figure 8 : VDJ recombination and formation of BCR
BCR structure and construction of the BCR specificity using the VDJ recombination. Adapted from https://www.10xgenomics.com/blog/immune-repertoire-profiling-at-single-cell-resolution

Pro-B cells were selected by negative selection leading to the elimination of immature B cells expressing specific self-IgMs. After this step, immature B cells (CD19+, CD138-, GL7-, FAS-, PNA-, IgM+, CD38-) migrate to spleen, where a second negative selection start. Then, immature LB begin mature naïve LB (CD19+, CD138-, IgM+, CD38+/-) and migrate to follicles of secondary lymphoid organs and will start T-dependent immune responses [63]. Following the recognition of the antigen by the BCR, signal transduction results in antigen endocytosis followed by its degradation and presentation in the MHC class II/peptide complex. Cell cooperation between B cells and helper follicular T cells permit B cell activation and clonal amplification (Fig. 9)

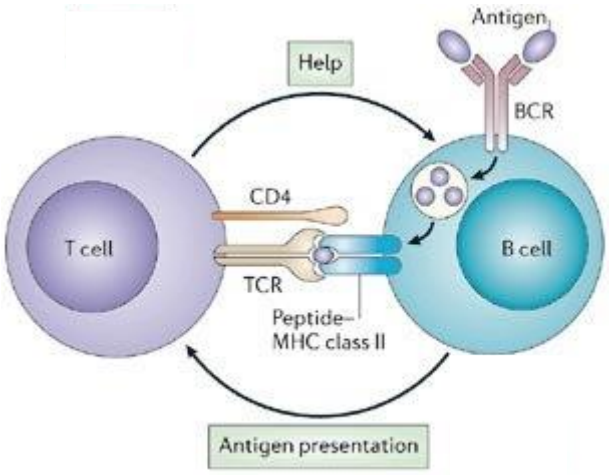

Figure 9 : Activation of B cells by T cells.
B cell was activated by cross presentation of antigen on her MHC class II to the TCR of a T cell. Adapted from http://molbiol4masters.masters.grkraj.org/html/Cell_And_Molecular_Immunology2-Innate_Humoral_And_Cell_Mediated_Immunity.htm

Then, some activated B cells differentiate to plasma cells (CD38-, CD19+, CD138+) or follicular B cells (Fig. 7). Follicular B cells migrate to an area of the follicle, forming a transient structure called the germinal center (GC) expressing GL7, FAS, PNA markers on surface. Within GC, B cells are subjected to somatic hypermutation (SHM) and class switch recombination (CSR) to increase the diversification of B cells and generate more refined receptors for antigen. SHM consists of point mutations in variable segments and adjacent sequences of heavy and light chains. SHM contribute to increase the BCR's affinity for its

target. CSR consists on secretion of Ig whose isotype is most suited to the antigen encountered. If the antigenic specificity of Ig is determined by the variable regions of the H and L chains, the effector functions depend on the constant regions of the heavy chains and vary according to the isotypes.

Somatic hypermutation and class switching depend on the expression of the Activation Induced Cytosine Deaminase (AID) enzyme during the transcription mechanism [64] (Fig. 10). These steps are essential in order to initiate a specific immune-response with a high specificity for the Ig target.

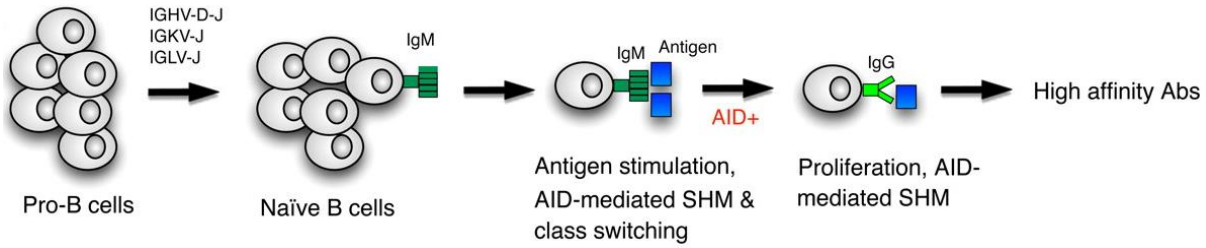

Figure 10 : Hypermutation somatic of B cells
Adapted from Bowers et al. 2011 [65]

After these steps, B cells evolve to plasma cells and memory B cells (Fig. 7). Plasma cells ($CD19^+$, $CD138^+$, $GL7^+$, FAS^+, PNA^+, IgM^-, $CD38^-$) will produce specific antibodies targeting antigen initially recognized by the BCR and mediate the humoral response in correlation with the complement. Memory B cells ($CD19^+$, $CD38^+$, IgM^-, PNA^-) migrate to lymphoid organs and await a second contact to the antigen target to speedily initiate the plasma cells amplification and the humoral response highly specific for again the antigen target. During these steps of maturation, activation, amplification and antibody production, B cells secrete cytokines modulating inflammation [66]. For example, after antigenic presentation of Ig target on MCH class II to helper follicular T cell, activated B cells can secrete pro-inflammatory

cytokines like IL-12, Il-6, IL-15 and GM-SCF but also anti-inflammatory cytokines like IL-35, IL-10 and TGFβ [67].

2. B cells in Multiple sclerosis.

B cells roles are (i) secreting injuring auto-antibodies, (ii) transporting antigens, (iii) to present antigens to T cells, (iv) producing cytokines.

Oligoclonal bands in MS. Normal CSF is devoid of Ig and other plasma proteins. OCB in CSF are a valuable biomarker in MS with a temporal invariance and clonal uniformity demonstrated for a long time [68]. OCB are one of the key feature of the MS diagnosis [69]. Their cellular origin is now well established. The transcriptomic analysis of Ig repertoire of individual CSF B cells and the protemic sequencing of isolated OCB proved that most of OCB were the product of local CSF or parenchyma resident B cells [37]. The persistency of the OCB over time in MS argues for appropriate survival conditions for B cells in CNS or CSF. Moreover, it was shown that astrocytes which are a major plurifonctional CNS glia lineage produce B cell growth factors including BAFF, CXCL 10, CXCL13 to support B cell survival [70]. Interestingly deep sequencing analysis identifyed similar gene pedigrees in CSF as well as in the periphery suggesting exchanges between CNS and peripheral B cell populations [71].

B cell auto-antigens. Lucchinetti et al [18] described that in the major form of MS (RRMS), CNS lesions involved activated C9neo indicating an antibody reaction. Moreover, plasmatic exchanges could improve neurological disabilities in a cohort of patient presenting pattern II lesions [72]. Leptomeningeal B cells aggregates are furtherly shown associated with demyelination and neuronal degeneration with arguments for humoral factors and antibodies diffusion in tissues [73]. Lastly B cell depletion is a powerful therapy in MS [50] and contribute to think that B cells in MS play a key role in the cumulative lesion processes. However, the target

antigens still remain a debate. Today no demyelinating candidates can be found an no myelin or other glia autoantigen are identified [74]. Some conflicting results were published considering ion channels on synaptic structures [75, 76]. The most intriguing target remain MOG, a major encephalitogen in rodent EAE, MOG is a protein on the surface of myelin, directly accessible to humoral antibody. Anti-MOG can be transient found in childhood MS and acute demyelinating encephalitis and is now considered in human associated with a new entity in between MS and neuromyelitis optical (NMO), the MOG autoimmune disease (MOGAD) [77, 78, 79]. It is interesting to highlight that human anti-MOG antibodies are species-specific recognizing conformational epitopes on Human not on rodent MOG [80].

Cytokines. B cells act as a source of both pro- and anti-inflammatory cytokines [81, 82]. Naïve and activated B cells are potent producers of protective and pathogenic cytokines. B cells are involved in regulating other immune cells that affect inflammatory responses. B cells can produce IL-6, enhance Th17 cells differentiation, and prevent the production of regulatory T cells [24]. In EAE, deficiency of IL-6 producing B cells reduce the experimental disease as in MS [83]. Peripheral B cells can increase the secretion of many inflammatory factors such as IL6, TNF alpha and lymphotoxin alpha. B cells facilitate pro-inflammatory B cell responses such as polyclonal stimulation in MS [83]. In the same way increase of IL17 and IFN gamma worsen MS severity [84]. Inflammatory B cells are also represented by GM-CSF-producing B cells which facilitate IL-6 and TNF expressions. Deletion of those GM-SCF-producing B cells lead to decrease myeloid cells and pathogenic immune responses [83]. Anti-inflammatory cytokines are usually represented by TFGbeta-1, IL-35 and IL-10 cytokines. B cells are able to produce a large amount of IL-10, compromising the action of various antigen presenting cells and inhibiting the process of TH1 and TH17 cells [85]. Mice deficient in IL-35 and IL-10 producing B cells may not recover from auto-immune attacks. Production of IL-10 is conferred to naïve

B cells [84]. Recent animal studies revealed that antigen experienced B cells affect plasma cells differentiation and the production of IL-10, IL-35 and regulatory B cells cytokines [86, 87].

These results are linked to the critical role of B cells in regulating immunopathological synapses and T cell production. Questions remained on which functions may be exploited and targeted to improve MS conditions.

B cell treatment. The most successful therapy targeting B cells are anti-CD20 therapies. CD20 is a broad marker of B cell differential from B cell to mature B cell but no plasma cell. The mechanism of rituximab is however not fully understanding and is not linked to the antibody-dependent B cell properties, but probably more to the antigen-presenting cell properties or cytokines properties. It is interesting to highlight that neutralization of B cell activation factor (BAFF) which is essential for B cell survival factor , is inefficient in MS, but exacerbates MS [82].

Mechanisms that lead to recruitment of autoimmune B cells in a developing CNS brain autoimmune disease and their function in the pathogenesis of MS remain to be clarified.

EAE. Classical induced EAE models are of limited values because of the artificial methods of use of adjuvants, immunisation, or cell transfer. Spontaneous model of EAE may give some clues in initiation of autoimmune conditions leading to develop the disease.

In OSE mouse model which is a double transgenic C57BL/6 model with MOG specific T cells expressing a MOG specific TCR along with a knocked-in MOG-specific H chain in its B cells, B cells capture soluble MOG antigen to cognate T cells to amplify the autoimmune response [61]. In TCR^{1640} mouse model, B cell have a non-manipulated BCR and are recruited from the endogenous repertoire by transgenic TCR, to produce anti-MOG antibodies. That EAE model

need availability of MOG and does not develop in germ-free condition (no anti-MOG antibody in germ-free condition) [62]. The recruitment of MOG-specific B cells seems to condition in that model the expansion and activation of autoimmune B cells and to lead to initiation and development of the autoimmune processes in CNS.

II. Objective.

As the TCR^{1640} model can contribute to explore initiating mechanisms in autoimmune processes by through the recruitment of MOG-specific B cells, we propose to track these cells in time and location and describe how their BCR repertoire can be changed and evolve towards a pathogenic process.

This project, in collaboration with the Ludwig-Maximilians-University of Munich, aims to analyze the evolution of B cell repertoire in TCR^{1640} mice. MOG-specific B cells were sequentially collected during the initiation and development of the disease in lymphoid organs and CNS of TCR^{1640} mice. It could identify new markers and potential therapeutic targets.

For the realization of the project, TCR^{1640} mice model has been implanted in the animal facilty of Lille and chararacterized. MOG-specific B cells will be searched in different lymphoid organs and CNS of TCR^{1640} mice.

The objective of the PhD was to confirm the role of MOG-B cell repertoire changing in the dynamics of EAE development through TCR^{1640} model.

III. Materials and Methods.

A. Mice.

TCR^{1640} mice were TCR^{1640} transgenic SJL/J mice generated by the Max Planck Institute of Neurobiology (Martinsried, Germany) and imported in Lille in 2016 according to an MTA [61]. Nontransgenic littermate (NTL) mice were obtained by crossing of TCR^{1640} transgenic mice and SJL/J mice. IgH^{MOG} mice were transgenic mice with Jh locus of the immunoglobulin heavy chain replaced by the VDJ gene segment of the monoclonal antibody 8-18C5. Homozygous mice were used for breeding of IgH^{MOG} mice [60]. Phenotype of IgH^{MOG} mice was performed by immuno-staining of splenocytes using 7AAD viability (BioLegend, San Diego, CA), anti-B220 antibody coupled to PerCP-Cy5.5 (BD Biosciences, San Jose, CA), anti-IgM^{a} coupled to PE (BD Biosciences, San Jose, CA) and anti-IgM^{b} coupled to FITC (BioLegend, San Diego, CA) presented in table 1. Homozygous IgH^{MOG} mice presented an IgM^{a} detection of more than 95% of B cells (Fig. 11). 2D2 mice were C57BL/6 mice transgenic for a TCR with specificity for the peptide MOG$_{35–55}$ [58]. All mouse strains were bred and experimented in the specific pathogen free (SPF) animal facilities of the University of Lille according to the authorization number (APAFIS#5157-201611 101 1562655 v3) for the animal experimentation.

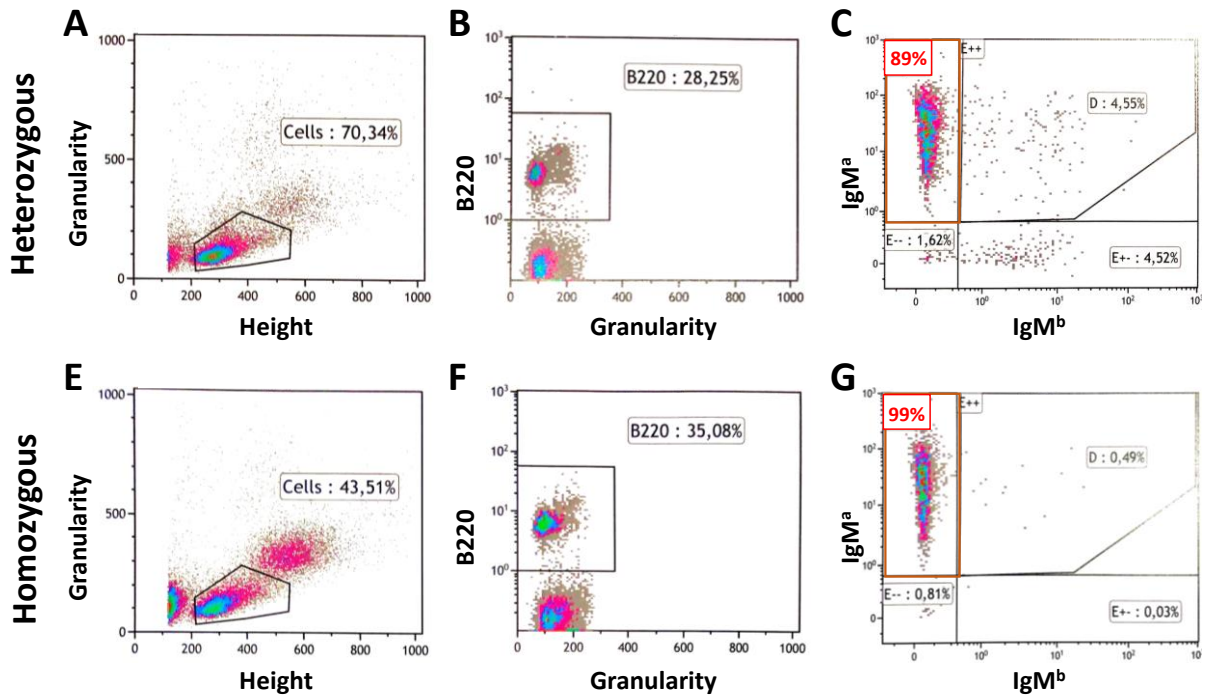

Figure 11 : B cell phenotype of IgH^{MOG} mice determined by flow-cytometry.
Splenocytes from IgH^{MOG} mice were stained with 7AAD (viability dye), anti-B220, anti-IgM^{a} and anti-IgM^{b} antibodies. A and E, selection of lymphocyte population. B and F, selection of B cells marked by B220 marker (B cell marker for mice). C and G, detection of IgM^{a} positive B cell. A, B and C show phenotype of heterozygous IgH^{MOG} mouse. E, F and G show phenotype of homozygous IgH^{MOG} mouse. Homozygous IgH^{MOG} mice were considered when more than 95% of B cells were positive for IgM^{a}.IgM $^{+}$ B cells are transgenic MOG-specific B cells.

	Staining	Fluorochrome	Isotype	Source	Dilution	clone	Supplier	Reference
Panel "IgH-MOG genotypage"	B220	PerCP-Cy5	IgG2a, κ	Rat	1/200	RA3-6B2	BD Biosciences	561101
	IgMa	PE	IgG1, κ	Mouse	1/200	DS-1	BD Biosciences	553517
	IgMb	FITC	IgG1, κ	Mouse	1/200	AF6-78	BioLegend	406206
Panel "Efficiency MOG tetramer staining"	**Panel "Efficiency MOG tetrame**	**Fluorochrome**	**Isotype**	**Source**	**Dilution**	**clone**	**Supplier**	**Reference**
	7AAD Viability				1/100		BioLegend	420404
	CD19	PE-Cy5	IgG2a, κ	Rat	1/200	6D5	BioLegend	115510
	CD45.1	APC	IgG2a, κ	Mouse	1/200	A20	BioLegend	110714
	CD45.2	PE	IgG2a, κ	Mouse	1/200	104	BioLegend	109808
	mMOG tetramer	FITC			1/100			
Panel "MOG specific B cells"	**Staining**	**Fluorochrome**	**Isotype**	**Source**	**Dilution**	**clone**	**Supplier**	**Reference**
	7AAD Viability				1/100		BioLegend	420404
	CD19	Pacific Blue	IgG2a, κ	Rat	1/200	6D5	BioLegend	115523
	B220	PerCP-Cy5	IgG2a, κ	Rat	1/200	RA3-6B2	BD Biosciences	561101
	CD4	APC-Cy7	IgG2a, κ	Rat	1/200	RM4-5	BioLegend	100526
	mMOG tetramer	FITC & PE			1/100			
Panel "CD40LB"	**Staining**	**Fluorochrome**	**Isotype**	**Source**	**Dilution**	**clone**	**Supplier**	**Reference**
	7AAD Viability				1/100		BioLegend	420404
	Streptavidin	PE			1/200		BioLegend	405204
	Biotinylated CD40L (CD154)		IgG	Arm Ham	1/200	MR1	BioLegend	106503
Panel "FACS sorting"	**Staining**	**Fluorochrome**	**Isotype**	**Source**	**Dilution**	**clone**	**Supplier**	**Reference**
	7AAD Viability				1/100		BioLegend	420404
	CD19	PE-Cy5	IgG2a, κ	Rat	1/200	6D5	BioLegend	115510
	CD4	BV786	IgG2a, κ	Rat	1/200	RM4-5	BioLegend	100552
	mMOG tetramer	FITC & PE			1/100			
Panel "iGB cells activation"	**Staining**	**Fluorochrome**	**Isotype**	**Source**	**Dilution**	**clone**	**Supplier**	**Reference**
	7AAD Viability				1/100		BioLegend	420404
	Biotinylated peanut aglutinin				1/100		Vector	B-1075
	Streptavidin	FITC			1/200		BioLegend	405202
	FAS	PE-Cy7	IgG2 l2	Arm Ham	1/200	Jo2	BD Biosciences	557653
	GL-7	Alexa Fluor 647	IgM, κ	Rat	1/200	GL7	BioLegend	144606
	CD38	Pacific Blue	IgG2a, κ	Rat	1/200	6D5	BioLegend	102720
	CD138	PE	IgG2a, κ	Rat	1/200	281-2	BioLegend	142504
	CD138	APC	IgG2a, κ	Rat	1/200	281-2	BioLegend	142505
	IgG1	FITC	IgG1, κ	Rat	1/200	A85-1	BD Biosciences	553443
	IgM	PE	IgG1, κ	Mouse	1/200	DS-1	BD Biosciences	553517
	CD19	Brilliant Violet 605	IgG2a, κ	Rat	1/200	1D3	BD Biosciences	563148

Table 1 : Antibodies used in flow cytometry experiments.

B. Scoring.

Clinical scoring of EAE was performed as follows: score 0, for disease-free; 1 for atony of the tail; 2 for delayed rightening; 2.5 for one hind leg paralyzed; 3 for paralysis of the hind limbs; 4 for paralysis of the anterior limbs; and 5 for complete paralysis or death of the animal. Mice were scored by Florent Salvador (level 1 animal experimentation accreditation since 2017/12/22) every 1 to 2 days.

C. Serum transfer experiment.

After sedation using isofluorane, 2D2 mice were injected by retro-orbital infusion with 200ng of pertussis toxin (List Biological Laboratories, Campbell, CA) at day 0. At days 2, mice were injected by retro-orbital injection with 200ng of pertussis toxin associated with 50µL of PBS or serum from NTL mice, IgH^{MOG} mice, disease-free or diseased TCR^{1640} mice. These injections were performed with Dr Nathalie Journiac.

D. Samples collection.

For the detection of anti-MOG antibodies in serum, mice were sacrificed by cervical dislocation or terminal anaesthesia by injection of sodium barbital. Blood was collected in the heart. Serum was extracted after blood centrifugation (1000g) à 4°C and stored at -20°C. To determine the localisation of MOG-specific B cells and to perform iGB culture, mice were sacrificed by cervical dislocation or terminal anaesthesia by injection of ketamine/xylazine. Spleen, CLN (cervical lymph nodes), Payer patches (PP), axillary lymph nodes (ALN), inguinal lymph nodes (ILN) and mesenteric lymph nodes (MLN) were collected and stored on ice. Cells were dissociated using cell strainer of 40µm and stored on ice. Cells from brains were collected after dissociation, digestion using collagenase D (Roche, Basel, Switzerland) and ultracentrifugation on Percoll /RPMI gradient. Cells were stored on ice waiting for the step for

counting and FACS (Fluorescence-activated cell sorting) staining. Cell counting was performed using COVA slide after 1/10 dilution in trypan blue solution.

E. Cell culture.

Table 2 presents the composition of medium used for different cell culture. HEK (human embryonic kidney) cell culture were cultured in freestyle medium (Thermo Fisher Scientific, Waltham, MA) under antibiotic selection (Thermo Fisher Scientific, Waltham, MA) at 37°C, 0% CO_2. 40LB cell culture was realized with 40LB medium (Thermo Fisher Scientific, Waltham, MA) with G-418 antibiotic selection (Thermo Fisher Scientific, Waltham, MA) at 37°C, 5% CO_2. 40LB feeder cells were supplied by the MPI and approved by an MTA with its inventor Professor Kitamura. For iGB single cell culture, one single total B cell or single MOG-specific B cell from spleen, CLNs or brain was sorted by FACS sorter and seeded in 96-well plate precoated with 600 live 40LB feeder cells [88, 89]. The iGB medium was supplemented with IL-4 (R&D Systems, Minneapolis, MN) [2ng/mL] and IL-21 (R&D Systems, Minneapolis, MN) [10ng/mL] at day 0, 2 to the end of the culture. iGB culture lasted 8-12 days at 37°C, 5% CO_2. 40LB cells viability of more than 90% was obtain after 2 weeks of culture. The expression of CD40 ligand on the surface of 40LB was checked using 7AAD viability (BioLegend, San Diego, CA), biotinylated anti-CD40L antibody (BioLegend, San Diego, CA) and streptavidin coupled to PE (BioLegend, San Diego, CA) presented in table 1 by FACS staining (Fig. 12).

iGB medium	Informations	Supplier	Reference
Fetal Bovine Serum	10%	Gibco	10270-098
L-Glutamin	2mM	Gibco	25030-081
Non Essential Amino Acid	0,1mM	Gibco	11140-035
Sodium pyruvate	1mM	Gibco	11360-070
HEPES	10mM	Sigma	H0887
Penicillin-Streptomycin	1%	Gibco	15140-122
B mercaptohetanol	50µM	SIGMA	M-7154
RMPI 1640	450mL	Gibco	61870-010
40LB medium	**Informations**	**Supplier**	**Reference**
Fetal Bovine Serum	10%	Gibco	10270-098
L-Glutamin	2mM	Gibco	25030-081
Non Essential Amino Acid	0,1mM	Gibco	11140-035
Sodium pyruvate	1mM	Gibco	11360-070
Penicillin-Streptomycin	1%	Gibco	15140-122
B mercaptohetanol	50nM	SIGMA	M-7154
DMEM	450mL	Merck	D5796
HEK medium	**Informations**	**Supplier**	**Reference**
Freestyle medium	450mL	Fisher Scientific	11550426

Table 2 : Composition of iGB medium, 40LB medium and HEK medium.

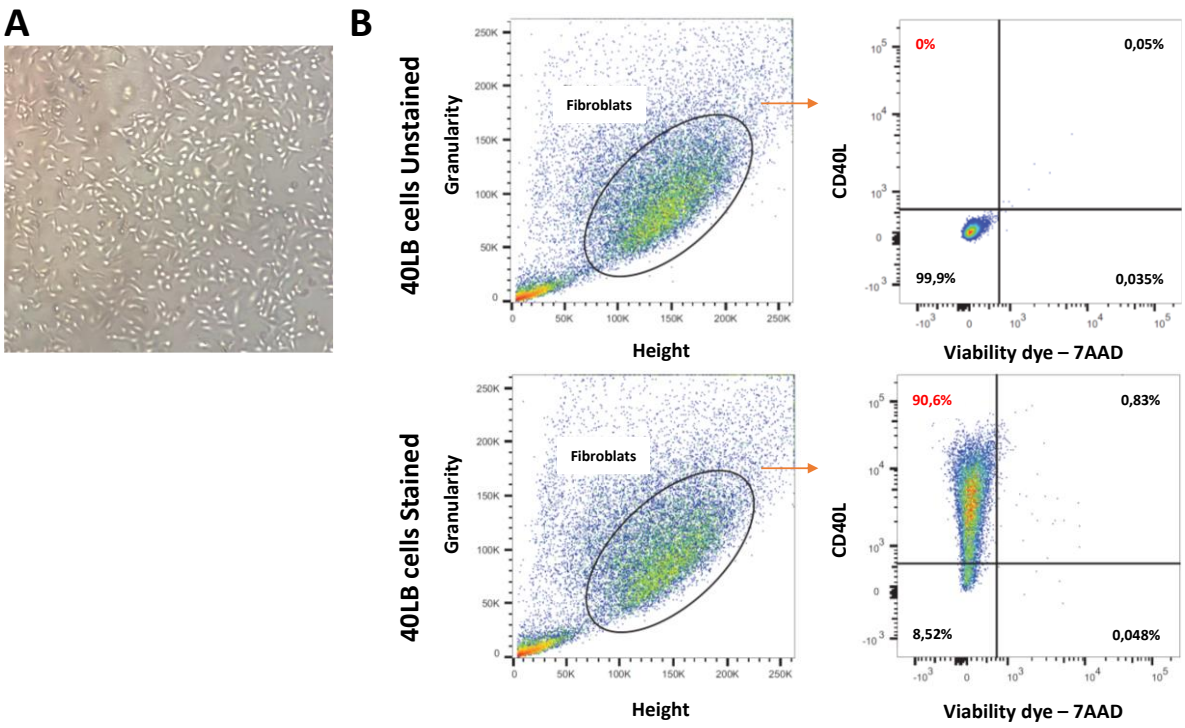

Figure 12 : 40LB cells and control of CD40 ligand expression.
A, Photography of cells. B, 40LB cells were stained with 7AAD (viability dye) and anti-CD40 ligand (CD40L) coupled with PE. 90,6% of CD40L cells were live CD40L positive cells.

F. Anti-MOG and anti-total IgG1 antibodies quantification by ELISA.

Serially diluted serum (1/100 to 1/1 000) or iGB supernatant (1/100 to 1/1 000) collected from transgenic mice were transferred to 96-well ELISA plates (Thermo Fisher Scientific, Waltham, MA) precoated with recombinant MOG protein (produced in the laboratory) or purified anti-IgG1 antibodies (BD Biosciences, San Jose, CA). Detection used biotinylated anti-IgG1 for primary antibody (BD Biosciences, San Jose, CA) and a streptavidin-HRP complex (BD Biosciences, San Jose, CA) for the detection. TMB solutions (BioLegend, San Diego, CA) were used to reveal substrate reaction and stopped the reaction with hydrochloric acid (BioLegend, San Diego, CA). Measurements at 450 nm on FLUOstar Omega. Two standards were used for these quantifications: purified 8.18C5 antibodies produced in the laboratory by Dr. Mathide Bas and Dr. Nathalie Journiac to quantify anti-MOG antibodies in AU (Arbitrary Unit) and purified IgG1 (BD Biosciences, San Jose, CA) antibodies to quantify total IgG1 antibodies in ng/mL.

G. MOG monomer and tetramer production.

HEK cells at more than 90% of viability were transfected with a ratio of 1/2 of MOG_{1-125} plasmid (Fig. 14) /Polyethylenimine linear (CliniSciences, Nanterre, France). The efficiency of transfection was evaluated with a ratio of 1/2 of plasmid control GFP (pSUPER.retro.neo+gfp, OligoEngine, in figure 13)/Polyethylenimine linear in OptiPro solution (Thermo Fisher Scientific, Waltham, MA). After 24h, GFP expression was analysed by fluorescence microscopy using a Leica DMI8 at objective X40 (Fig. 15) and analysed by flow cytometry (Fig. 16). More than 21% of transfected cell express GFP using cytometric analysis. On day 2, the medium was supplemented with lactalbumin (Merck KGaA, Darmstadt, Germany). On day 9, the MOGm (MOG monomer) was eluted using an imidazole gradient ranging from 20 to 500mMol (Merck KGaA, Darmstadt, Germany) and purification column

(Cytivia, Marlborough, MA). To control the presence of MOGm in elution fractions, Western blotting was performed to identify MOG protein band at the expected size of 20KDa (Fig. 17). Western blotting was performed using anti-MOG antibodies at 1µg/mL (clone 8-18C5, Merck KGaA, Darmstadt, Germany) detected using anti-IgG (Heavy + Light chain) antibodies coupled to peroxidase at 1/10 000 (Jackson ImmunoResearch, Sacramento, CA). ECL solution (Thermo Fisher Scientific, Waltham, MA) was used for the revelation. MOGm proteins were purified by dialyse using tube (Merck KGaA, Darmstadt, Germany) in PBS (Thermo Fisher Scientific, Waltham, MA) and stored at 4°C. Biotinylated MOG monomer (MOGbiot) was built using the BirA kit (Avidity, Aurora, CO) and purified by dialyse using tube in PBS. To produce recombinant murin myelin oligodendrocyte glycoprotein tetramerized (MOGtet), MOGbiot previously produced was conjugated with a ratio of 4 mol of MOGbiot for 1 mol of streptavidin-FITC (BioLegend, San Diego, CA) or streptavidin-PE (BioLegend, San Diego, CA) coated microbeads. The quality of each production was monitored with splenocytes from IgH^{MOG} mice. Cells were stained with MOG_{tet}, 7AAD viability (BioLegend, San Diego, CA), and an anti-CD19 antibody coupled to Pacific Blue (BioLegend, San Diego, CA). To determine the efficiency of MOGtet to detect rare MOG-B cell specificity, B cells were purified using the EasySep™ Mouse B Cell Isolation Kit (StemCell, Cologne, Germany). Several known cell mix starting from mix equivalent to 1 B cell from IgH^{MOG} mouse inside 100000 B cells from C57BL/6 mouse and finishing at 1 B cell from IgH^{MOG} mouse inside 1 B cells from C57BL/6 mouse. Cells were labelled using extracellular and intracellular staining (Table 1). Extracellular staining was made using 7AAD viability (BioLegend, San Diego, CA), anti-CD19 antibody coupled to BV605 (BD Biosciences, San Jose, CA), Biotinylated peanut agglutinin (cat. Bektop, Koltsovo, Russia), Streptavidin coupled to FITC (BioLegend, San Diego, CA), anti-FAS coupled to PE-Cy7 (BD Biosciences, San Jose, CA), anti-GL-7 coupled to Alexa Fluor 647 (BioLegend, San Diego, CA), anti-CD38 coupled to Pacific Blue (BioLegend, San Diego,

CA) and anti-CD138 coupled to PE (BioLegend, San Diego, CA) presented in table 1. Intracellular staining was made using anti-CD19 antibody coupled to BV605 (BD Biosciences, San Jose, CA), anti-CD138 coupled to APC (BioLegend, San Diego, CA), anti-IgM coupled to PE (BD Biosciences, San Jose, CA) and anti-IgG1coupled to FITC (BD Biosciences, San Jose,

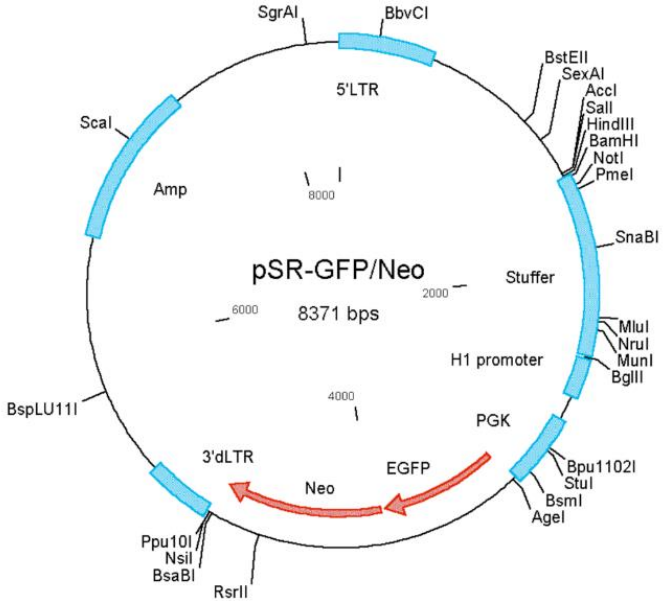

Figure 13 : Map of pSUPER.retro.neo+gfp vector.

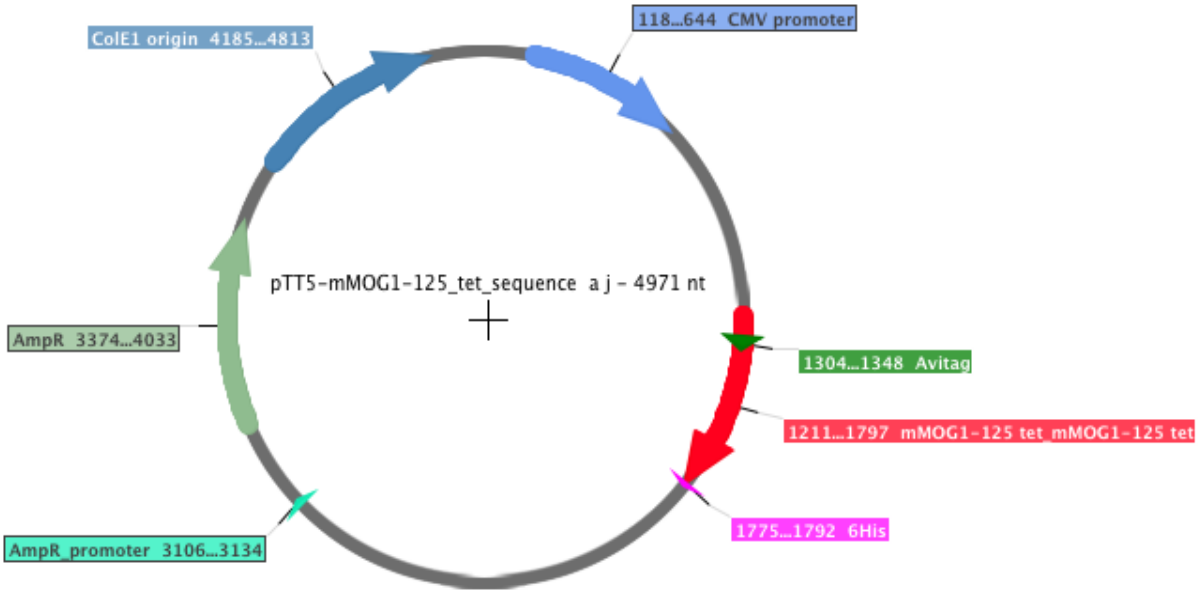

Figure 14 : Map of the constructed MOG^{1-125} vector used to synthesize the extracellular part of MOG^{1-125}.
AmpR promoter is the promoter of the AmpR gene. AmpR encodes the β-Lactamase which is involved in resistance to ampicillin. ColE1 origin is the origine of replication. CMV promoter is a strong promoter of transcription. Avitag is a short sequence implicate in the biotinylation of MOG protein. MOG_{1-125} is the coding sequence of the extracellular part of MOG. 6His is a tag histidin used for purify the MOG_{1-125} protein.

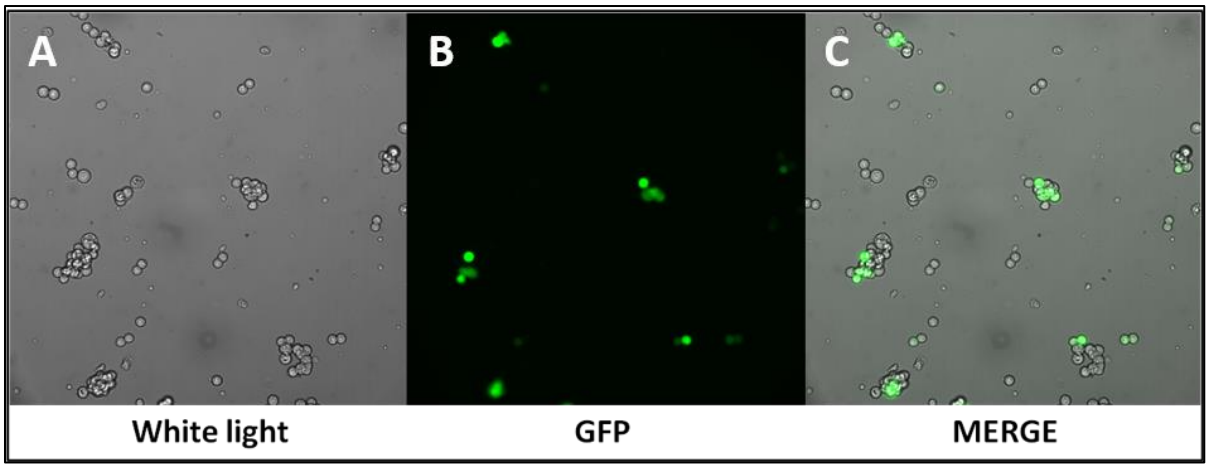

Figure 15 : Control of HEK cells transfection efficiency by microscopy.
Transfection test on HEK cells with the GFP control vector. Cells observed at 24h post-transfection by fluorescence microscopy. A, Transfected cells were observed with white light. B, GFP fluorescence was observed on transfected cells. C, Merge of white light and GFP observations to confirm the expression of GFP by transfected cells.

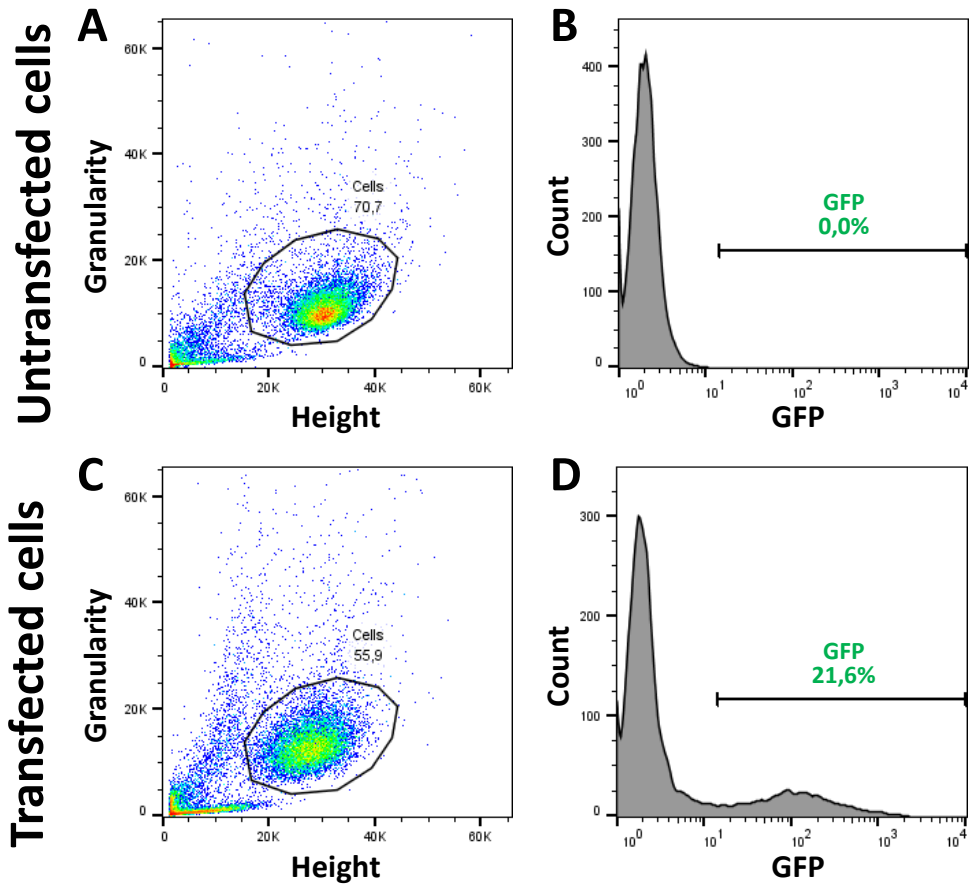

Figure 16 : Control of HEK cells transfection efficiency by cytometry.
Transfection test on HEK cells with the GFP control vector. Cells observed at 24h post-transfection by cytometry. A and B, untransfected cells. C and D, transfected cells. A and C, selection of cells at expected granularity and height. B and D, GFP fluorescence signal was researched. 21,6% of transfected HEK cells expressed GFP.

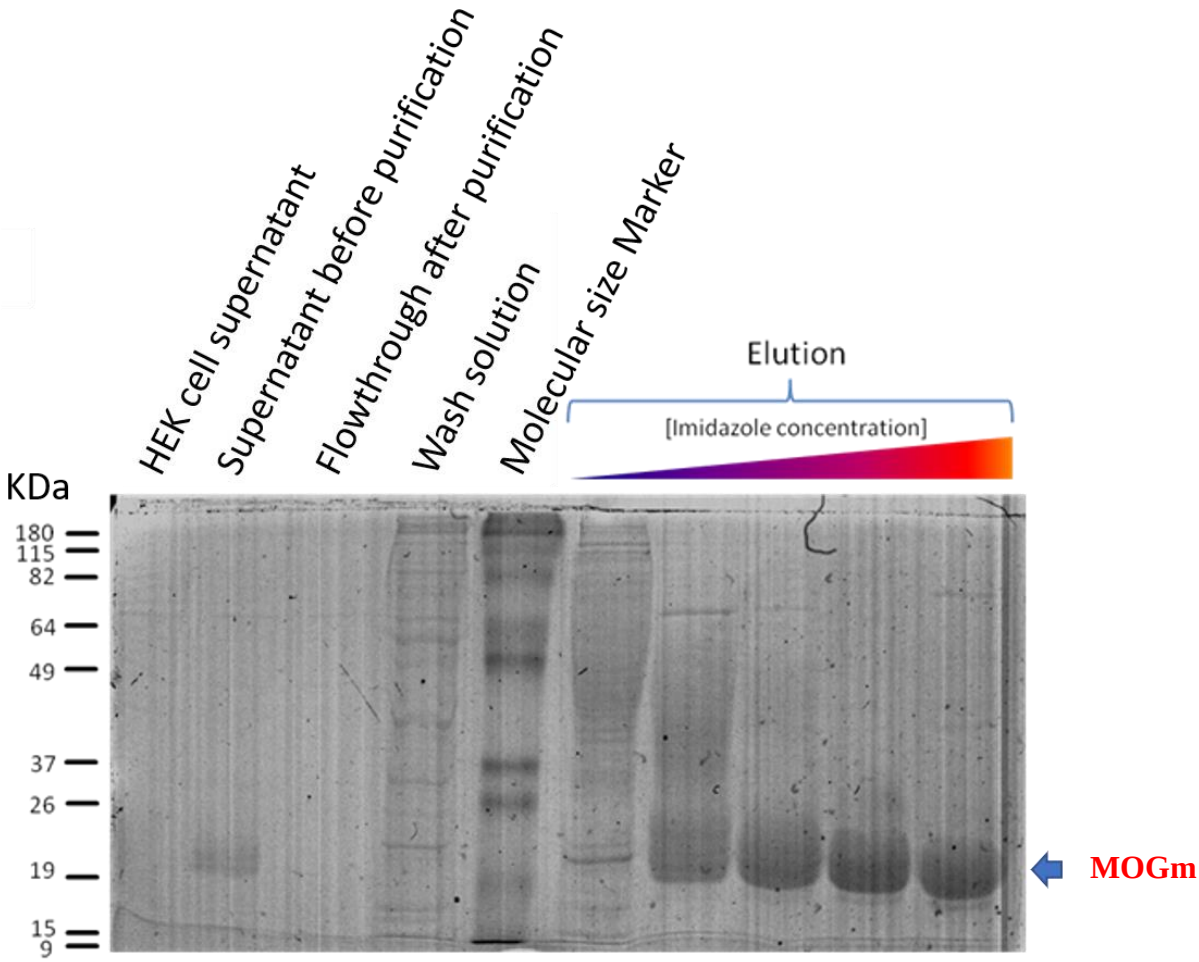

Figure 17 : Western blot showing the productions of mMOGr.
Production of MOGm proteins using HEK cells and purification using gradient of imidazole. Detection of MOGm production using anti-MOG antibodies at 1µg/mL (clone 8-18C5) and anti-IgG (H+L) antibodies coupled to peroxidase at 1/10 000 and detection by ECL solution. MOGm proteins were detected in supernatant of transfected cells and in elution fraction.

H. RNA extraction.

After iGB culture, amplified cells and 40LB feeder cells were collected using Tris-EDTA solution. RNAs were extracted using Trizol/chlorophorm process (TRI Reagent® Merck KGaA, Darmstadt, Germany) or the RNeasy Mini Kit (Qiagen, Courtaboeuf, France).

I. RT and PCRs.

RNA was retrotranscribed into cDNA using the kit (Thermo Fisher Scientific, Waltham, MA). cDNA was used to amplify target sequences of IgHG and IgLK primers (Table 3) using PCR programs presented in table 4 and validated in figure 18. To control the efficiency of primers, RNA extracted of B cells from spleen of C57BL/6 mice, SJL/J mice were retrotranscribed. cDNA were amplified using couples of primers IgH forward /IgHG reverse and IgLK forward/IgHK reverse designed by Dr Anneli Peters (2015), Taq DNA Polymerase (Qiagen, Courtaboeuf, France) and on thermocycler (Eppendorf, Hamburg, Germany). Migration of PCR products was made on 4% agarose gel (Thermo Fisher Scientific, Waltham, MA). After revelation of bands on UV machine, bands at the expected sizes were collected by cutting the gel. PCR products were purified using the kit QIAquick Gel extraction (Qiagen, Courtaboeuf, France).

Target	Degenerate sequences (5'->3')
IgH forward	SAGGTSCAGCTGCAGSAGTGTGG
IgHG reverse	CTCAGGGGAARTAVCCYTTGAC
IgLK forward	GAYATTGTGMTSACMCARWCTMCA
IgLK reverse	GATGGTGGGAAGATGGATACAGTT

Table 3 : Degenerate sequences of primers used for IgHG and IgLKappa (IgLK) target sequences.

IgHG	94°C	94°C	67°C	72°C	94°C	57°C	72°C	72°C
	3min	10sec	20sec	20sec	30sec	30sec	1min	10min
	X1	X20 -0,5°C/cycle			X35			X1
IgHK	94°C	94°C	68°C	72°C	94°C	58°C	72°C	72°C
	3min	10sec	10sec	20sec	30sec	30sec	1min	10min
	X1	X20 -0,5°C/cycle			X35			X1

Table 4 : Programs used for IgHG and IgLK PCRs.

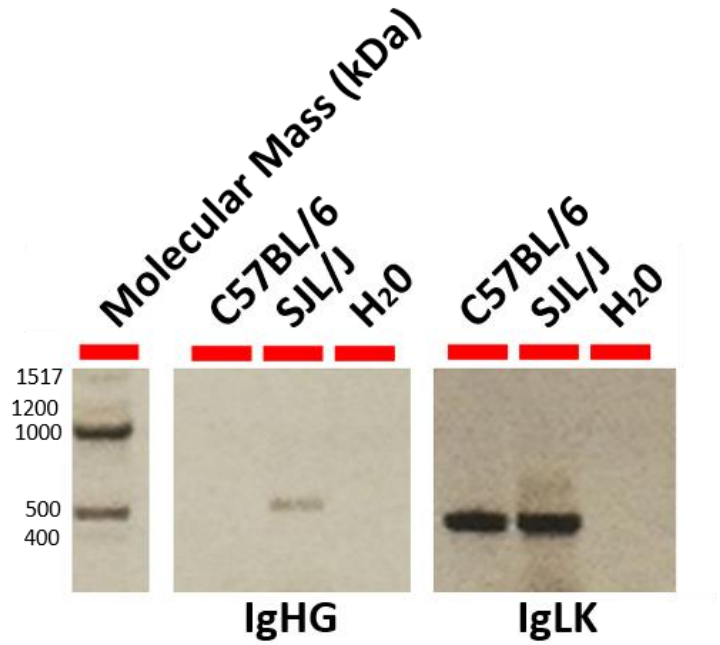

Figure 18 : Validation of IgHG and IgLK primers. PCR performed on H_2O and DNA extracted from B cells of spleen collected from C57BL/6, SJL/J. Bands were detected for the amplification of IgHG sequences (expected size at 500kDa) of SJL/J mice. Bands were detected for the amplification of IgLK sequences (expected size at 400 kDa) of C57BL/6 and SJL/J mice.

J. Flow cytometric analysis.

Table 4 presents panels of antibodies used to determine the genotype of IgH^{MOG} mice, the efficiency of MOG tetramer to detect MOG-specific B cells, the localization of MOG-specific B cells in TCR^{1640} mice, to control the expression of CD40L by 40LB feeder cells, to seed total and MOG-specific B cells for iGB single cell culture and to determine the phenotype of cells obtained after iGB culture. To determine the genotype of IgH^{MOG} mice, Navios cytometer (Beckman Coulter) was used according the software (Kaluza®). LSR Fortessa™ X-20 (BD) according the software (DiVa®) was used to determine the efficiency of MOGtet to detect MOG-specific B cells, the localisation of MOG-specific B cells, the expression of CD40L by 40LB feeder cells, the phenotype of cells obtained after iGB culture and the phenotype of cells obtained after iGB single cell culture. To sort total B cells and MOG-specific B cells, FACS ARIA (BD) was used according the software (DiVa® V7). Data obtained with Navios and Fortessa X-20 cytometers were respectively analysed using (Kaluza® software V2) and FlowJo® software V10.5.3.

K. Sequencing.

Samples sequencing by SANGER technology at the sequencing platform of GENOSCREEN (Lille, France).

L. Analyses of sequences.

Sequences obtained for IgLK and IgHG chains were submitted to IMGT/V quest and tools (http://www.imgt.org/) to define junction decryptions for each sequences and corresponding amino-acid sequences to find out the different clonotypes.

M. Statistical analyses.

GraphPad PRISM version 9 (CA, USA) was used for statistical analyses and graphs. EAE incidence was analyzed by Kaplan-Meier plots and statistical significance was calculated using the logrank test. Two-way ANOVA allowed to compare the clinical score evolution of 2D2 mice receiving passive transfer of serum. Simple linear regression evaluated correlations between EAE scores, age and measurements of antibodies in serum, and between EAE score and delay after EAE onset and percentage of MOG_{tet}^{+} B cells in CLN or CNS. T-tests were used for comparing means of measurements of antibodies in supernatants from cell cultures. p-values < 0.05 were considered significant.

IV. Results.

A. Characterization of TCR^{1640} mice model in the LIRIC animal facility.

A cohort of 180 TCR^{1640} mice (82 females and 98 males) was followed during a mean of 236±113 days. In this cohort, the total incidence of EAE was at last follow up of 93.9% (n=169 TCR^{1640} mice) (Fig. 19). The total incidence in female subgroup at last follow up was of 96.7% in the female subgroup and of 90.2% in the male subgroup without significant difference (p=0.06).

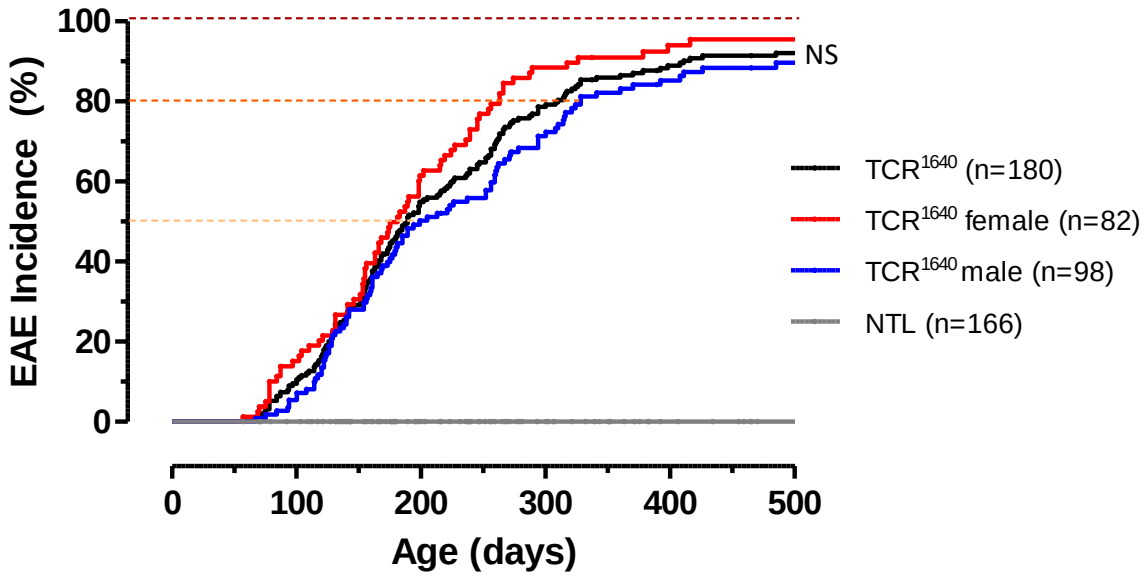

Figure 19: EAE incidence of TCR^{1640} mice.
TCR^{1640} mice are shown in black, female mice in red, male mice in blue and NTL mice in grey. Percentage of EAE incidence in TCR^{1640} mice and NTL mice according to the number of post-natal days at the University of Lille.

EAE started at a mean age of 197±87 days. In the female subgroup (n=74), EAE started at a mean age of 184±79 days and at 207±92 days in the male subgroup (n=95) without significant difference (p=0.2). In female TCR^{1640} mice, 25% mice started EAE at 131 days and 75% at 239 days. In male TCR^{1640} mice, 25% mice started EAE at 129 days and 75% at 271 days.

Concerning the mortality, in this cohort 76.7% (n=138) of TCR^{1640} mice died because of EAE, 4.4% (n=8) died due to other disease or for old age and 18.9% (n=34) were sacrificed for experimentation. TCR^{1640} mice death due to EAE occurred at a mean delay of 45±61 days after EAE onset or a median delay of 27 days [1÷295] after EAE onset (Fig. 20). Death due to EAE occurred at a mean of 53±67 days after EAE onset in the female subgroup (n=61) and 37±54 days in the male subgroup (n=77) without significant difference (p=0.23). In the female TCR^{1640} mice subgroup, 25% of the mice died due to EAE at 10 days after EAE onset and 75% at 70 days after EAE onset. Concerning male TCR^{1640} mice, 25% of the mice died due to EAE at 10 days after EAE onset and 75% at 40 days after EAE onset.

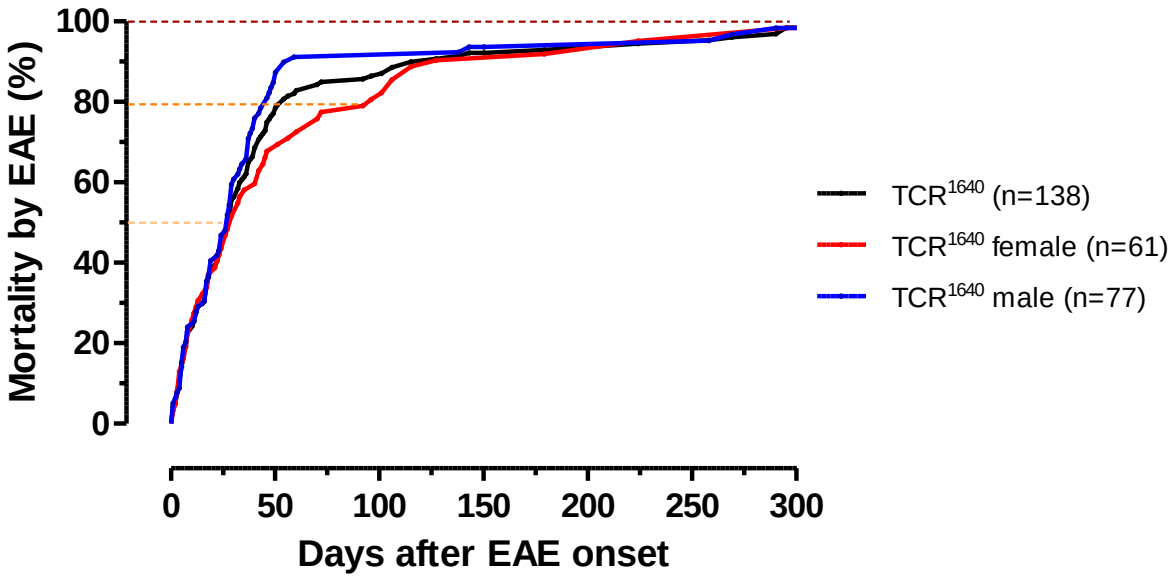

Figure 20: Mortality of TCR^{1640} mice due to EAE.
TCR^{1640} mice are shown in black, female mice in red and male mice in blue. Percentage of TCR^{1640} mice died by EAE according to the number of days after EAE onset at the University of Lille.

In the TCR^{1640} model, there is no difference between the gender of the mice and the incidence of the disease, the time to onset EAE and the mortality according to the age and the number of days after EAE onset.

Within the all cohort, a small cohort of 8 females and 13 males were followed just after weaning to be more accurately scored and examined daily during a mean of 264±105 days. In this subgroup, EAE incidence at last follow up was 90.5% (n=19) of TCR^{1640} mice. EAE started at a mean age of 221±84 days (Fig. 21).

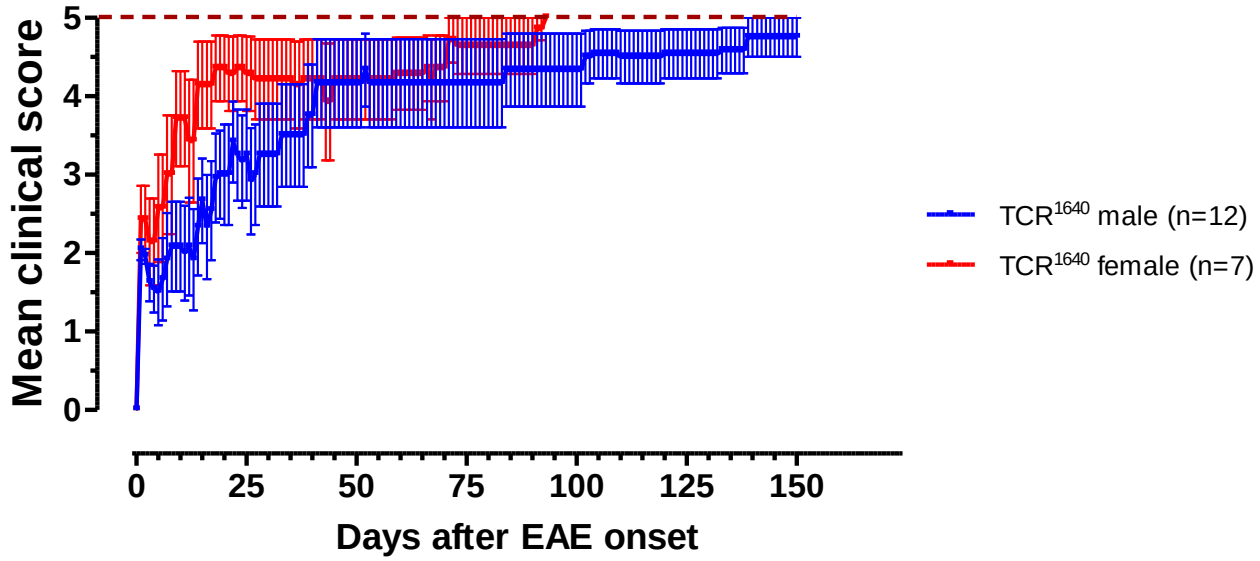

Figure 21: Clinical evolution of EAE in TCR^{1640} mice.
Female TCR^{1640} mice are shown in red and male mice in blue. Mean clinical score of TCR^{1640} mice according to the number of days after EAE onset at the University of Lille.

Figure 22 illustrates the average of EAE evolution in the female and male groups. We observed two clinical forms of the disease: 47.7% presented a single inflammatory event leading quickly to death (Fig. 22 A-C); 52.6% of TCR^{1640} mice developed more than one relapse with a mean of 2.8±0.8 relapses at last follow up (Fig. 22 B-D).

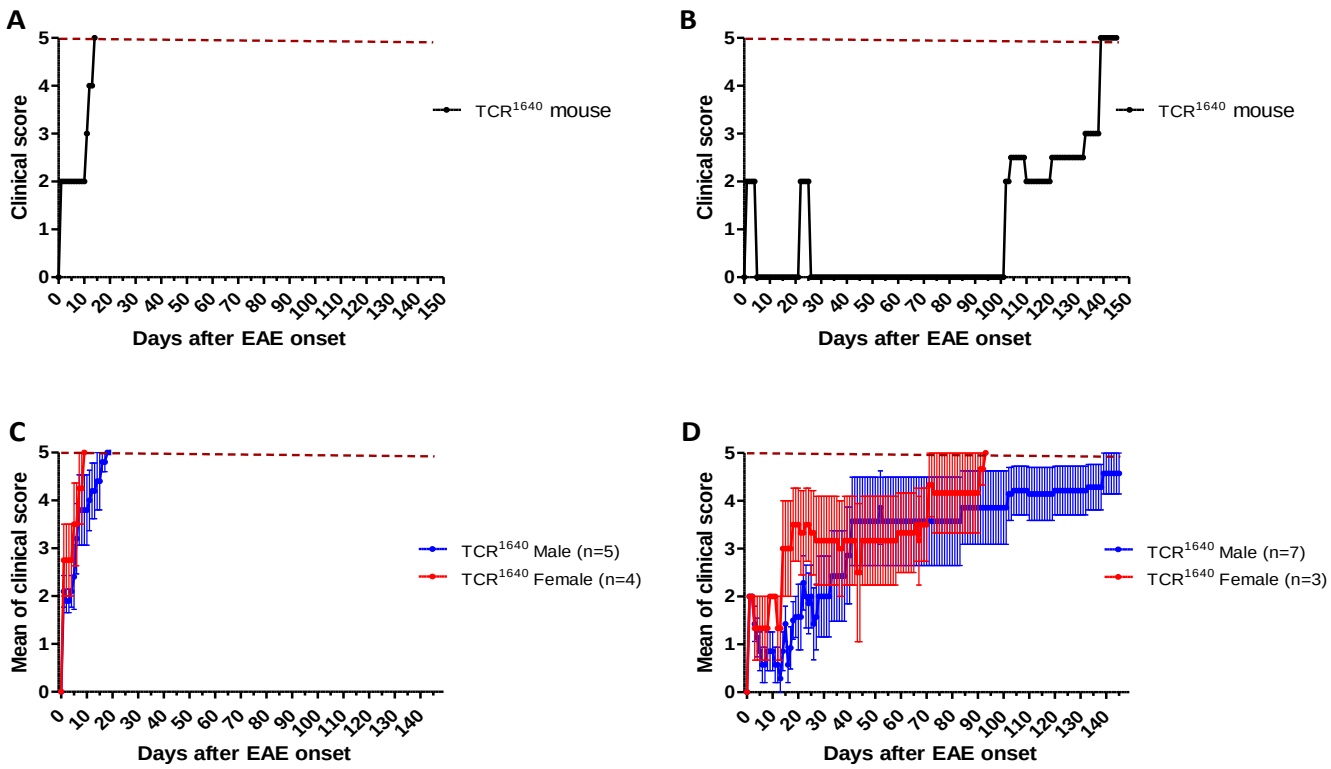

Figure 22: Clinical evolution of EAE in TCR^{1640} mice depending to the form of the disease. Representative TCR^{1640} mouse are shown in black, Female TCR^{1640} mice in red and male TCR^{1640} mice in blue. Clinical score of a representative TCR^{1640} mouse in aggressiveness form of the EAE (A) or relapsing-remitting form of EAE (B) are shown according to the number of days after EAE onset at the University of Lille. Mean clinical score of TCR^{1640} mice in aggressiveness form of the EAE (C) or relapsing-remitting form of EAE (D) are shown according to the number of days after EAE onset at the University of Lille.

Concerning the mice affected by the relapsing-remitting form of EAE, the mean of maximal clinical was of 2.2±0.4 during the first relapse, 3.2±1.5 during the second relapse, 4±1.4 during the third relapse and 5±0 during the fourth relapse (Fig. 23).

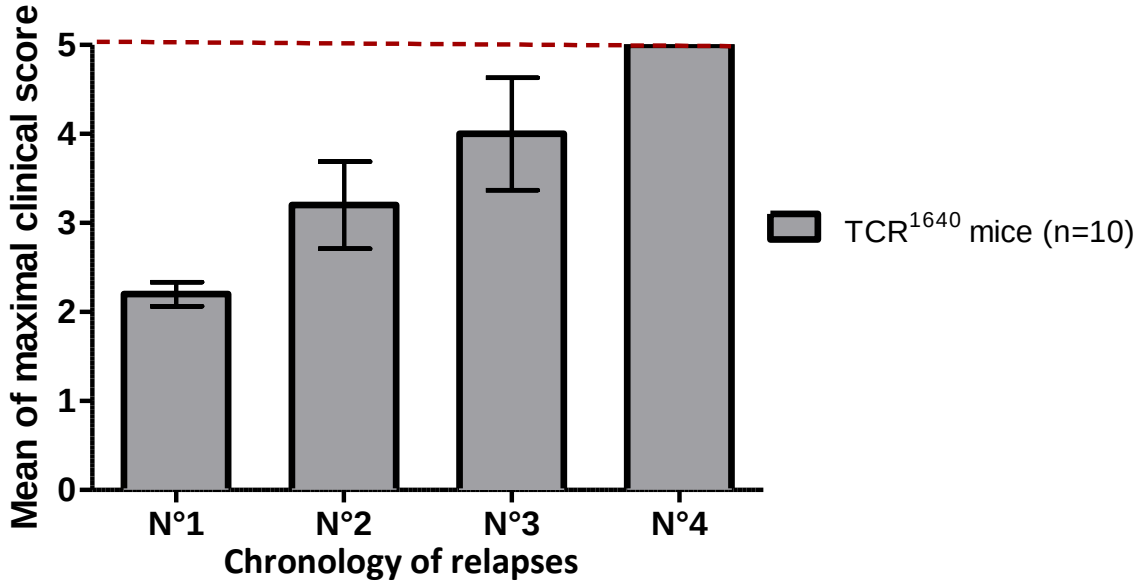

Figure 23: Clinical evolution of EAE in TCR^{1640} mice depending to the number of relapses. Mean clinical score of TCR^{1640} mice affected by the relapsing-remitting form of EAE are show according to the number of relapses.

In conclusion, these results show a delay in the development of spontaneous EAE in TCR^{1640} mice, variation in the form of the disease with an aggressive form and a relapsing remitting form with no significant difference between male and female.

B. Anti-MOG response in the TCR1640 mice model.

Sera from IgH^{MOG} mice (n=13), NTL mice (n=21), disease-free (n=15) and diseased TCR^{1640} mice (n=28) were collected in order to determine the presence of total IgG1 and IgG1 anti-MOG antibodies by ELISA assay (Fig. 24).

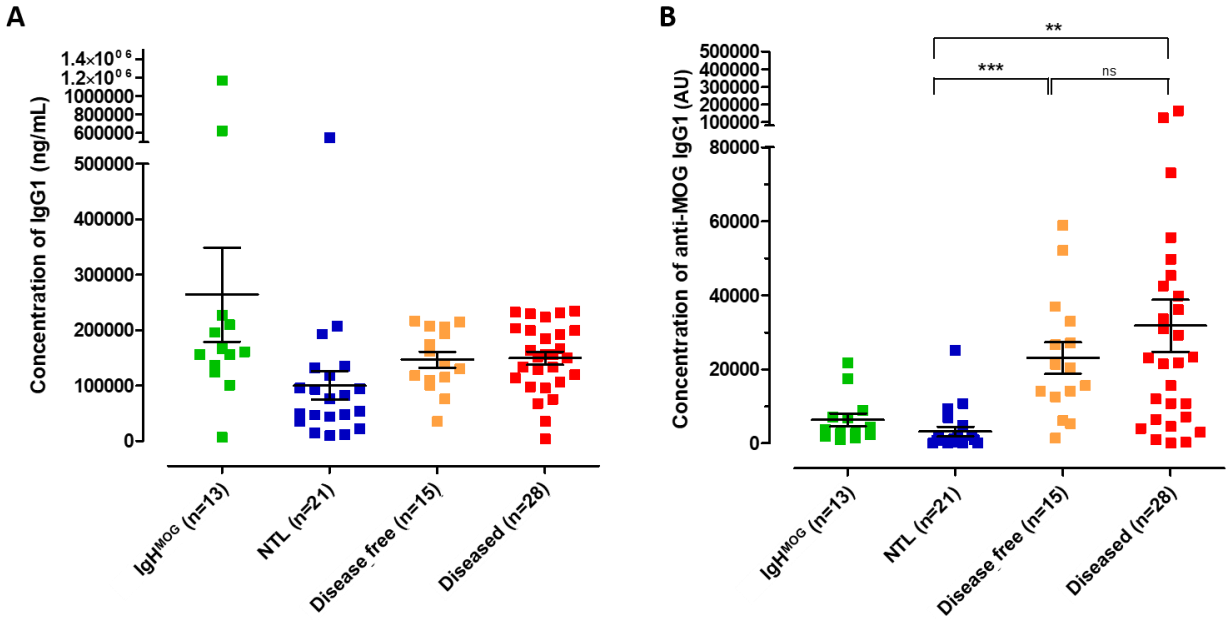

*Figure 24 : Quantification of total IgG1 and anti-MOG IgG1 antibodies in serum. Total IgG1 in ng/mL (A) and anti-MOG IgG1 antibodies in AU (B) in serum using ELISA assay. **=p<0.001 and ***=p<0.0001.*

Total IgG1 were observed in all groups of mice without significant difference. Anti-MOG IgG1 were only observed in sera from disease-free TCR^{1640} mice (23078±4281UA) and diseased TCR^{1640} mice (31780±7039AU) without significant difference between both TCR^{1640} mice group. Disease-free and diseased TCR^{1640} mice presented significantly higher concentration of anti-MOG IgG1 antibodies compared to NTL control mice, with respectively p value of p<0.0001 and p=0.001. The same observation was made for disease-free and diseased TCR^{1640} mice compared to IgH^{MOG} mice (data not showed).

Figure 25 shows the total IgG1 and anti-MOG IgG1 antibodies concentration in sera from diseased TCR^{1640} mice according to the clinical score (A and B), the number of days after EAE onset (C and D) and the age of mice (E and F). Concerning the clinical score, no

correlation was observed between both parameters with respectively r^2=0.03; p=0.35 for total IgG1 and r^2=0.01; p=0.54 for IgG1 anti-MOG. Concerning the number of days after EAE onset, no correlation was observed between both parameters with respectively r^2=0.05; p=0.27 for total IgG1 and r^2=0.02; p=0.47 for IgG1 anti-MOG. Concerning the age of mice in days, no correlation was observed between both parameters with respectively r^2=0.06; p=0.09 for total IgG1 and r^2=0.003; p=0.73 for IgG1 anti-MOG.

These findings show that anti-MOG antibodies are a biomarker in TCR^{1640} mice model without any correlation with the clinical status, the delay after EAE onset or the age of mice.

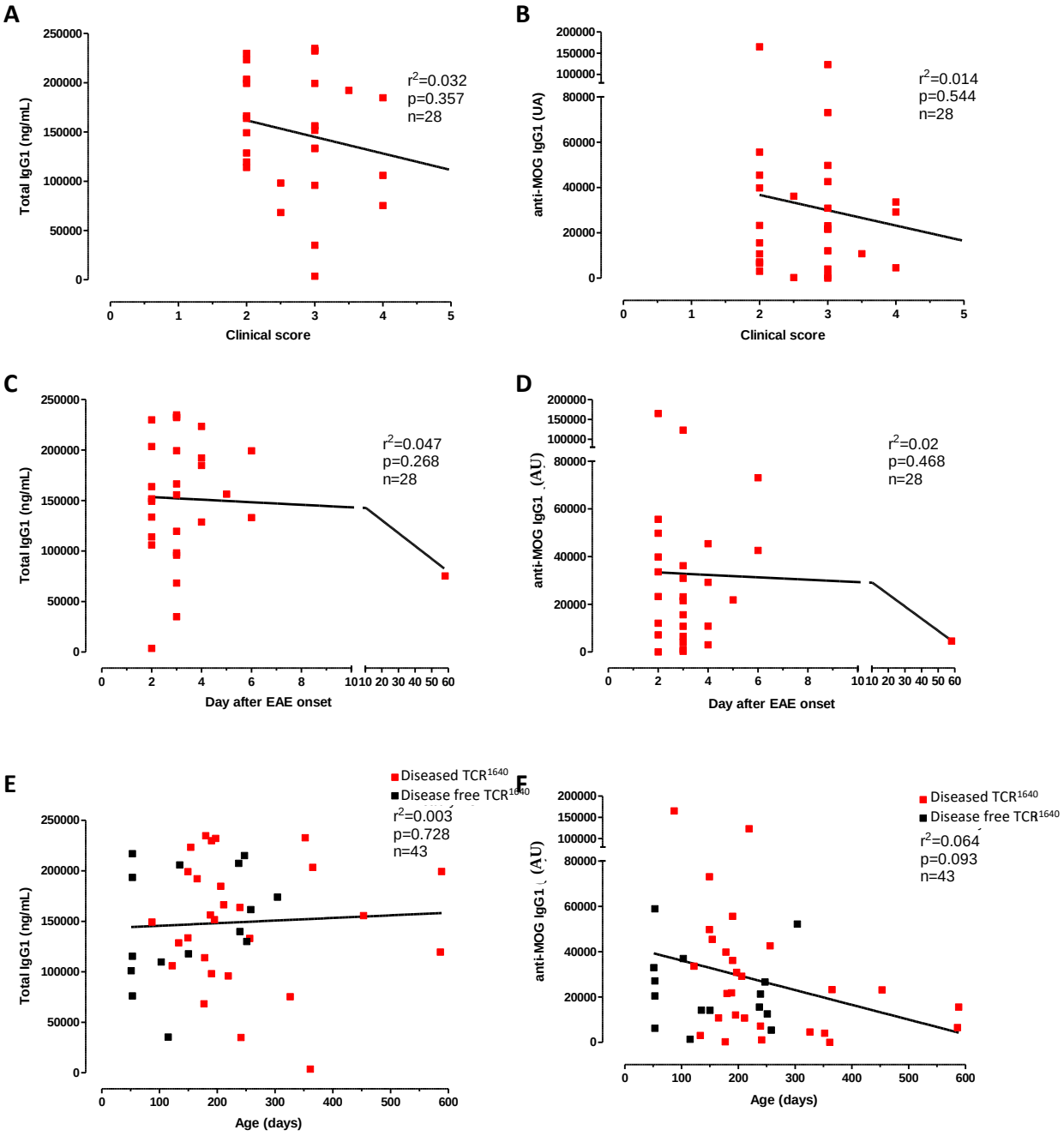

Figure 25 : Correlation between concentration of total IgG1, anti-MOG IgG1 antibodies and clinical score (A & B) or days after EAE onset (C & D) or age in days (E & F).
A-C and E show the total IgG1 concentration (ng/mL). B-D and F, show the anti-MOG IgG1 concentration (AU).

Figure 26 shows how serum from IgH^{MOG} mice, NTL mice, disease-free TCR^{1640} mice and diseased TCR^{1640} mice influence the EAE incidence and the EAE clinical score of 2D2 mice. Serum from diseased TCR^{1640} mice (A) increases significantly the incidence (p=0.03) and the severity (p<0.001) of EAE in 2D2 mice. Other serum did not have any influence on the incidence or the severity of EAE in 2D2 mice in our animal facility.

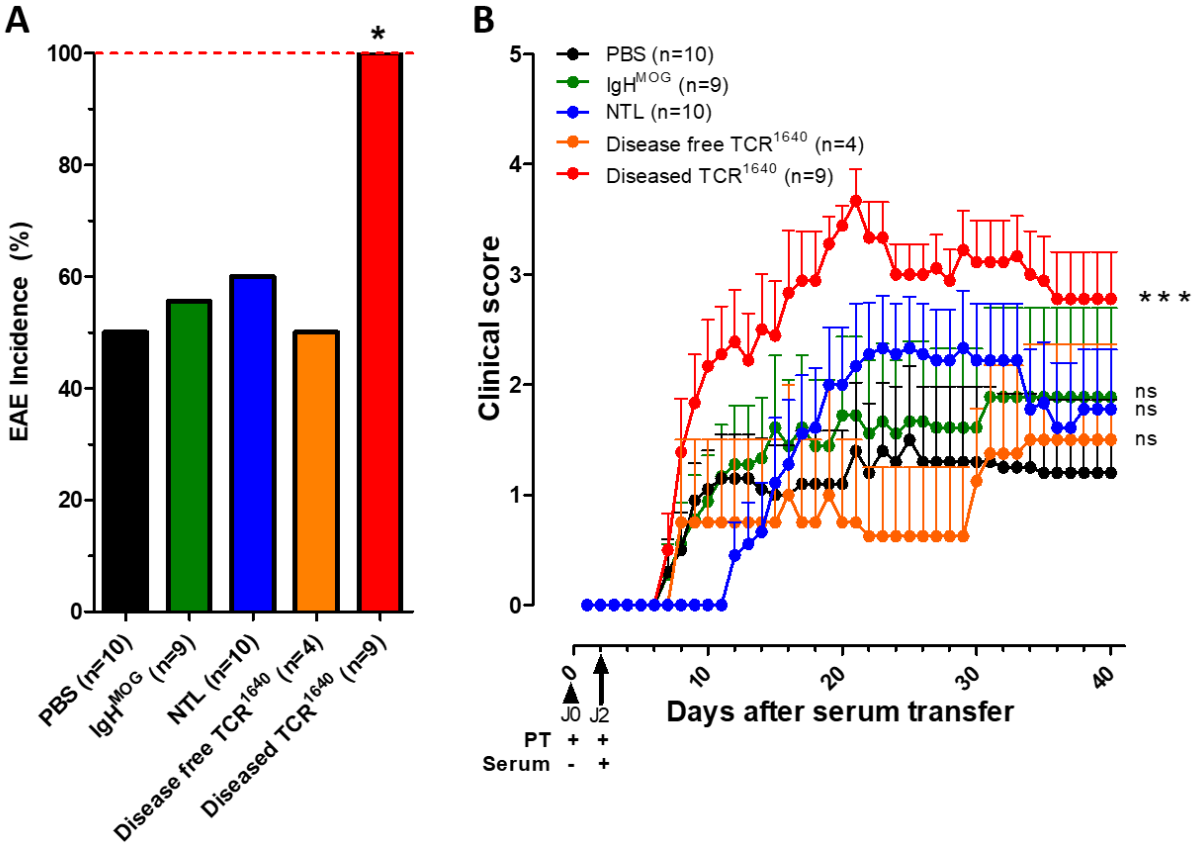

*Figure 26 : Incidence (A) and clinical evolution (B) in 2D2 mice after injection of PBS or serum from IgH MOG mice, disease-free TCR^{1640} mice or diseased TCR^{1640} mice. ***=p<0.001.*

These data support the role of a humoral factor present in serum of diseased TCR^{1640} mice which contributes to a higher incidence and to the severity of EAE in 2D2 mice.

C. Localisation of MOG tetramer positive B cells in TCR^{1640} mice model.

1. MOG monomer staining compare to MOG tetramer staining to track MOG-specific B cells.

An IgH^{MOG} mouse was sacrificed and spleen was collected to purified B cells which are in this mice MOG-specific B cells. Cells were stained using the MOG monomer and revelled by the Streptavidin coupled to a dye or stained using the MOG tetramer. Figure 27 shows the percentage of MOG-specific-B cells stained by MOG monomer and MOG tetramer. The MOG monomer detected 58.3% of MOG specific B cells and the MOG tetramer detected 83% of MOG-specific B cells. These results show that, the MOG tetramer are more sensitive to detect MOG-specific B cells compare to MOG monomer. It is explained by a higher avidity of the MOG tetramer due to its ability to simultaneously engage its binding on three BCRs

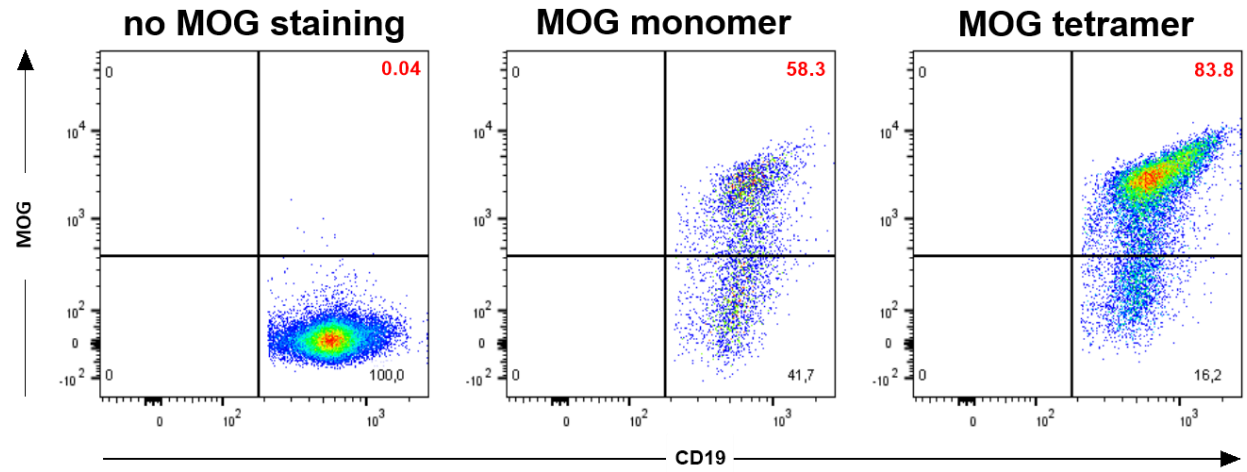

Figure 27 : Detection of MOG specific B cells by MOG monomer and MOG tetramer production. B cells purified from spleen of Homozygous IgH^{MOG} mouse were labelled with 7AAD, anti-CD19, MOG monomer or MOG tetramer.

2. Efficiency of MOG tetramer staining to track MOG-specific B cells.

An IgH^{MOG} mouse with CD45.2 leucocytes and an C57-BL/6 mouse with CD45.1 mice were sacrificed and spleens were collected. B cells were purified and several known mix of B cells from IgH^{MOG} mouse and WT mouse were realized for respectively 50%, 10%, 5%, 4%, 2%, 1%, 0.1%, 0.01% and 0.001% B cells from IgH^{MOG} mice with respective detection of IgH^{MOG} B cells (CD45.2 B cells) equal to 33.1%, 4.7%, 2.8%, 1.9%, 1.2%, 0.65%, 0.057%, 0.0048% and 0.0022% in B cells. Figure 28 shows the percentage of MOG-specific-B cells stained by MOG_{tet} in different mix of CD45.2+ MOG-specific B cells / CD45.1+ B cells. In a cell suspension containing 100% of MOG-specific-B cells (Fig. 28-A) MOGtet detected closed to 70% of MOG-specific B cells. In preparation containing 33.1% of MOG-specific B cells detectable, MOGtet detected 23% of MOG-specific-B cells (Fig. 28-B). In preparation containing 4.7% of MOG-specific B cells detectable, MOG_{tet} detected 3,47% of MOG-specific B cells (Fig. 28-C). In preparation containing 0.058% of MOG-specific B cells detectable, MOGtet detected 0,05% of MOG-specific B cells (Fig. 28-D). In preparation containing 0.004% of MOG-specific B cells detectable, MOGtet did not allow to detect precisely MOG-specific B cells (Fig. 28-E). In a cell suspension containing only WT CD45.1 cells (Fig. 28-A) MOG_{tet} did not allow to detect any B cells with high affinity for MOG (Fig. 28-F). These results are graphically projected in Figure 29 and show that under a ratio of 1/3000, MOGtet staining became unspecific.

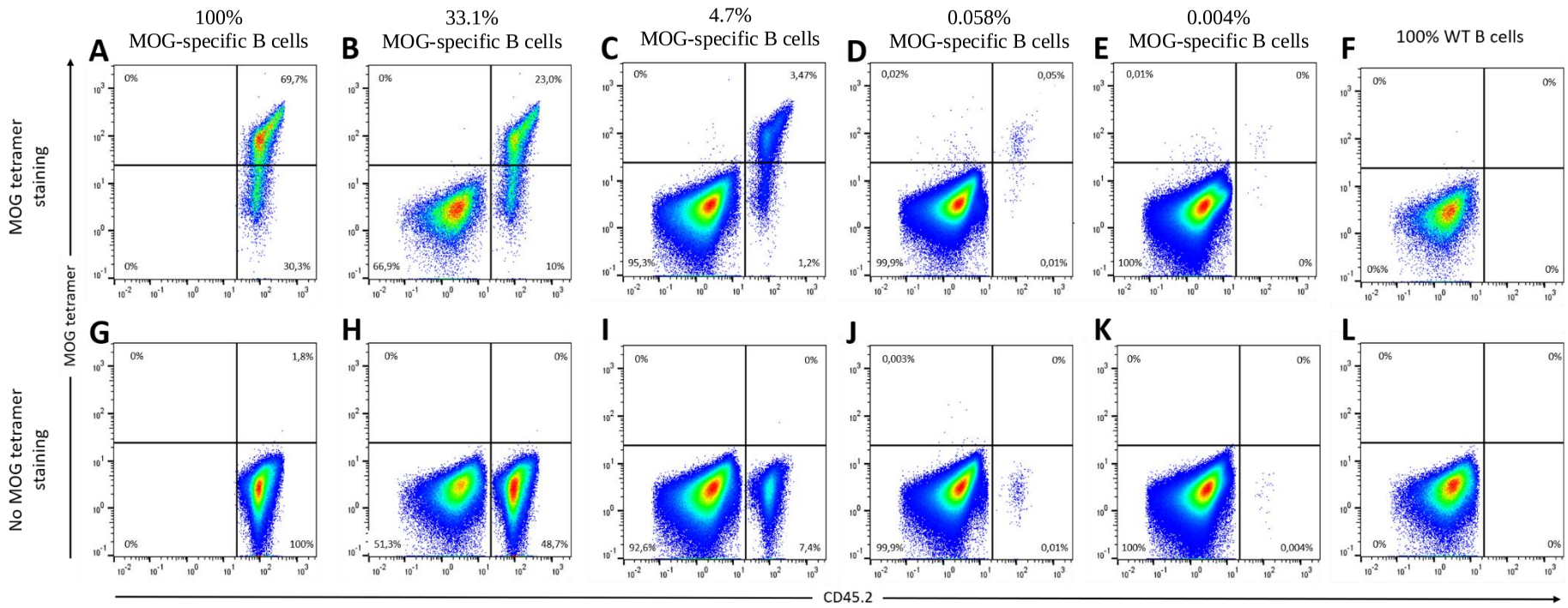

Figure 28 : FACS immuno-staining defining the efficiency of MOGtet to detect MOG-specific B cells.
Data showed the percentage of MOG-specific B cells stained by MOGtet (A, B, C, D, E and F) or without MOGtet (G, H, I, J, K and L) in a known mix of CD45.2+ MOG-specific B cells with CD45.1+ cells. Mix of cells composed of 100% CD45.2+ MOG-specific B cells (A and G) and observed 33.1%% CD45.2+ MOG-specific B cells (B and H), 4.7% CD45.2+ MOG-specific B cells (C and I), 0.058% CD45.2+ MOG-specific B cells (D and J), 0.0048% CD45.2+ MOG-specific B cells (E and K) and 100% CD45.1+ B cells (F and L). Cells were labelled with 7AAD, anti-CD19, anti-CD45.1, anti-CD45.2 and or not MOG tetramer.

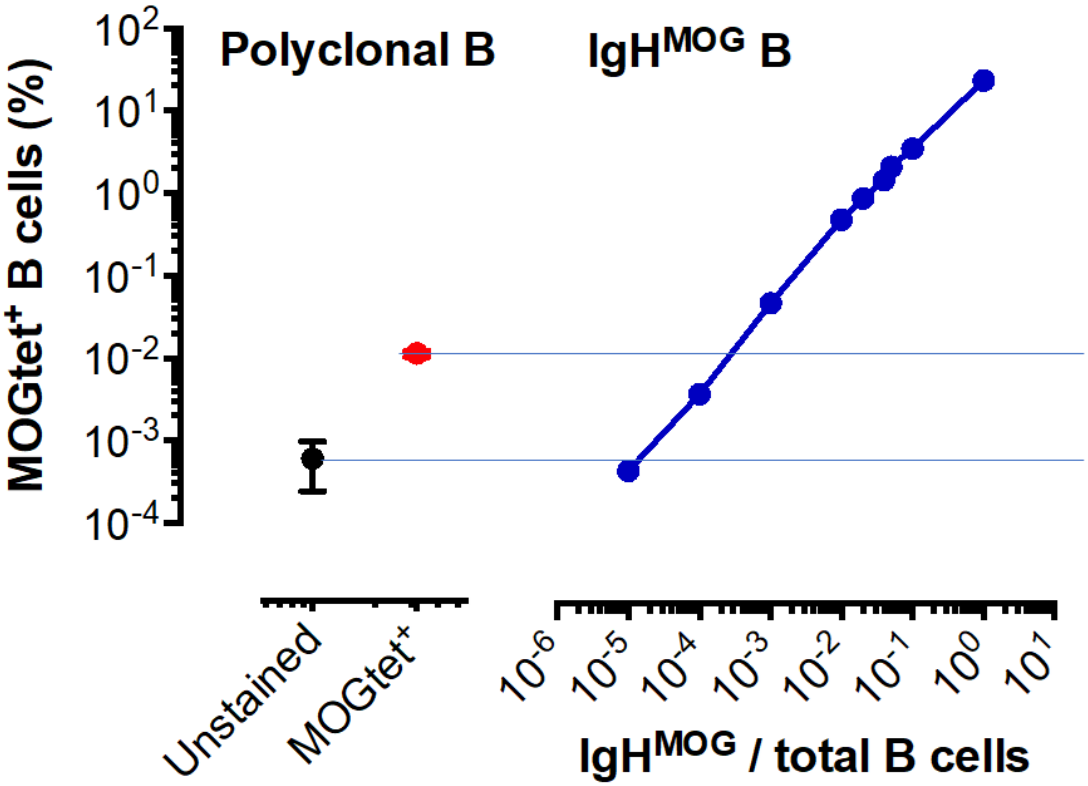

Figure 29 : Detection of MOG specific B cells in a known mix of B cells. B cells purified from spleen of Homozygous IgH^{MOG} mouse (CD45.2) and WT mouse (CD45.1) were mixed in known proportion. Cells were labelled with 7AAD, anti-CD19, anti-CD45.1, anti-CD45.2 with MOG tetramer. Experimental background and possible endogenous MOG-specific B cells were represented in black and red by the $CD45.2^{-}MOG_{tet}^{+}$ population in WT B cells stained or not with the MOG tetramer. Percentages of $CD45.2^{+}MOG_{tet}^{+}$ B cells (in blue) were quantified in several mix of B cells. Under a ratio of 1/3000, MOGtet staining became unspecific.

3. Search of MOG tetramer positive B cells in different organs.

A cohort of 14 TCR^{1640} mice (10 females and 4 males) were sacrificed at different time points before and after onset of symptoms: 2 TCR^{1640} mice were sacrificed before EAE onset at an age of 234±91 days; 12 TCR^{1640} mice (9 females and 3 males) were sacrificed after EAE onset at respectively a mean age of 157±59 days and a mean of 24±25 (median=21[1;70]) days after EAE onset with a mean clinical score of 2.75±0.5. MOG$_{tet}^{+}$ B cells were quantified in spleen, Payer plate (PP), axillary lymph nodes (ALN), inguinal lymph nodes (ILN) and mesenteric lymph nodes (MLN), CLN (cervical lymph nodes) and brain according to the procedure presented in Figure 30.

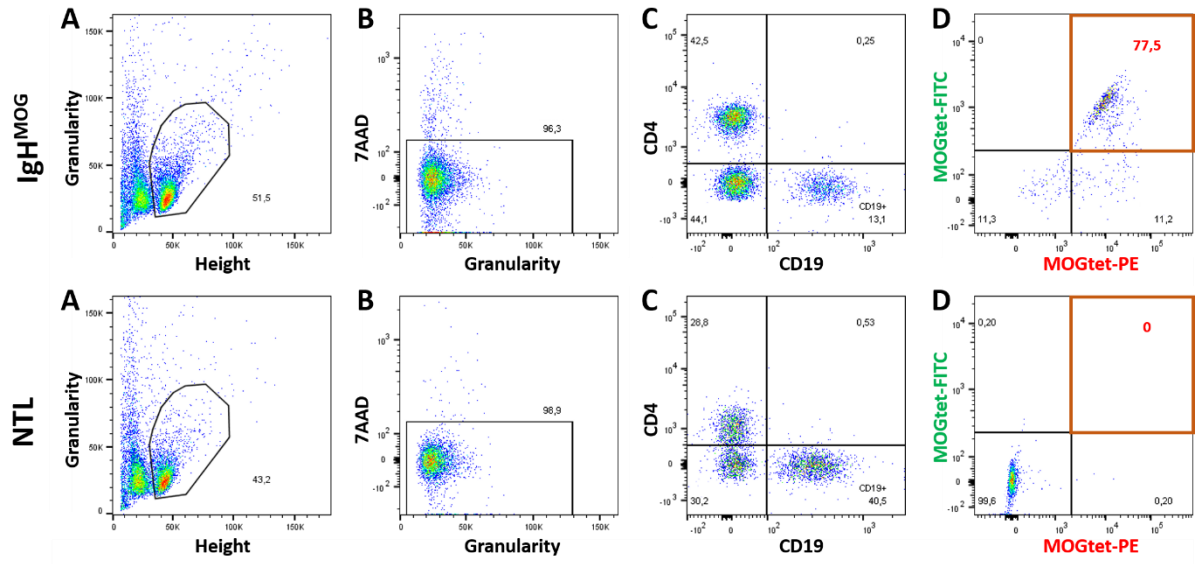

Figure 30 : Selection of live MOG$_{tet}^{+}$ B cells in lymphoid organs. Selection pathway for MOG$_{tet}^{+}$ B cells. Here, cells come from the deep cervical lymph nodes of IgH^{MOG} mouse and NTL mouse. A, selection of cells corresponding to B cells sizes. B, selection of live cells. C, selection of the B cell population. D, selection of MOG$_{tet}^{+}$ B cells in total B cells. MOG$_{tet}^{+}$ specific B cells were detected only in CLNs from IgH^{MOG} mice and not in NTL mice.

Figure 31 shows the absolute number of total B cells in the different lymphoid organs (data not shown for PP, ALN, ILN and MLN) and brain of each group of mice. As expected, B cells were detected in spleen and CLNs for each group of mice without significant difference between the groups of mice. B cells were present in brain for diseased TCR^{1640} mice but also in heathy TCR^{1640} mice. No B cells were present in the brain for NTL and IgH^{MOG} mice. B cells were significantly more numerous in brain of diseased TCR^{1640} mice compared to NTL and IgH^{MOG} mice.

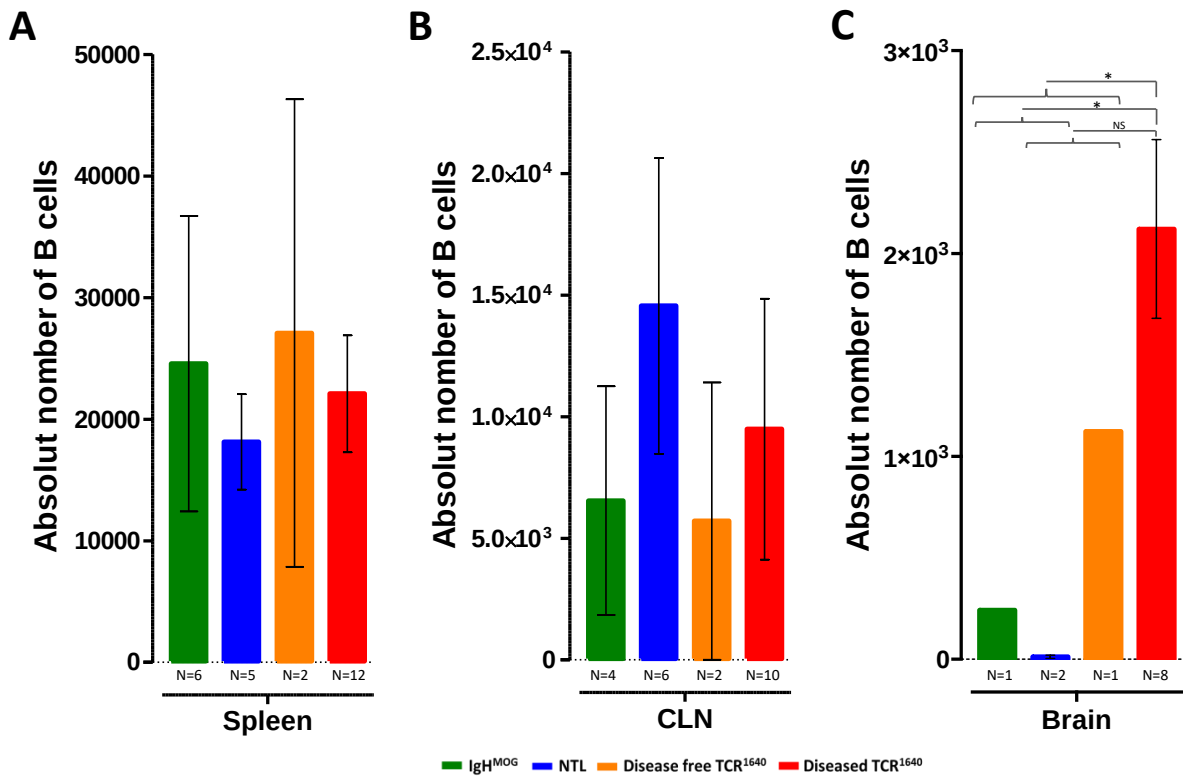

Figure 31 : Absolut number of B cells counted in spleen, CLN and brain.
Quantification of B cells counted in spleen (A), CLN (B) and brain (C) of TCR^{1640} mice before and after EAE onset, NTL mice and IgH^{MOG} mice. (= p<0.05).*

Figure 32 shows the proportion of T cells and B cells in the different lymphoid organs (data not shown for PP, ALN, ILN and MLN) and brain of each group of mice. As expected, T (24±12%) cells and B cells (38±20) were detected in spleen for each group of mice. In CLN and moreover in brain, it was difficult to detect proportion of T cells and B cells similar to cells detected in spleen. In CLN, proportions of T cells and B cells were respectively equal to 27±25% and 24±21. In brain, proportions of T cells and B cells were respectively equal to 7±6% and 12±14.

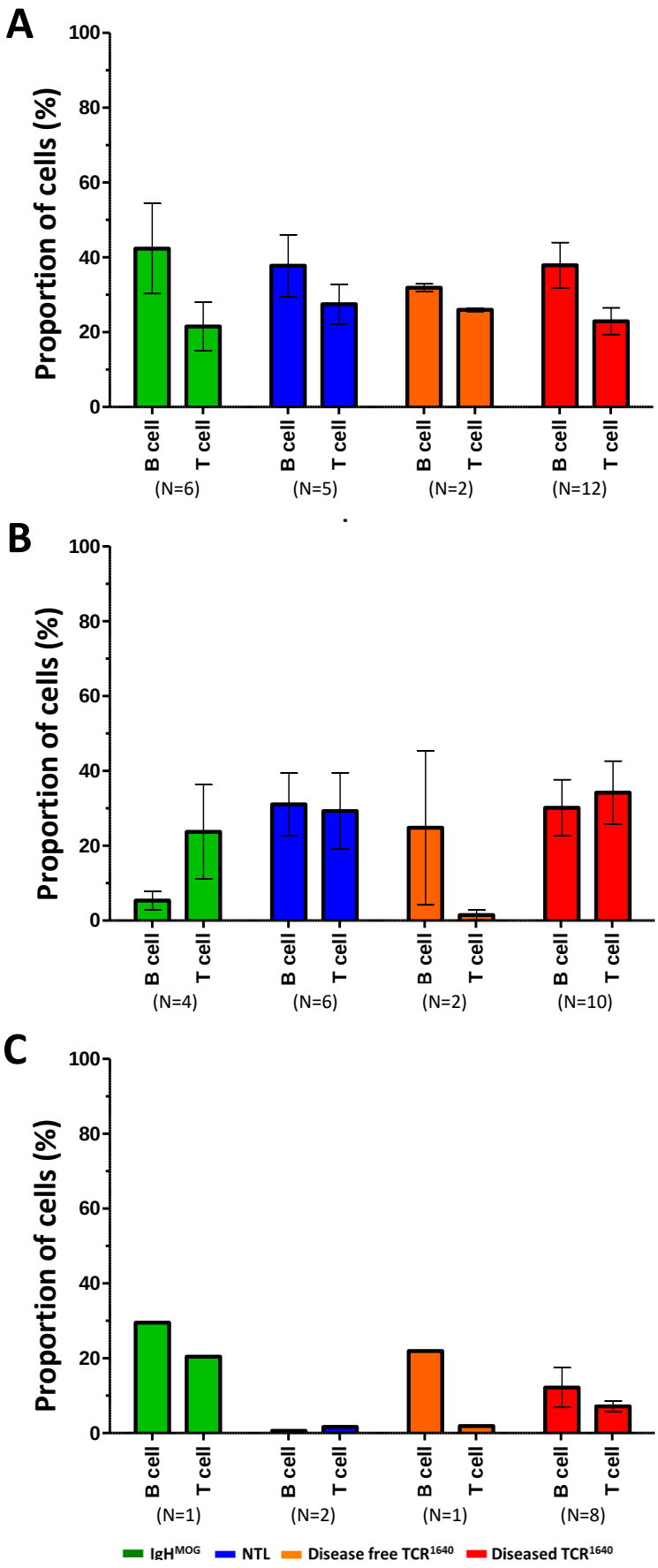

Figure 32 : Proportion of T cells and B cells counted in spleen CLN and brain. Percentage of T cells and B cells counted in spleen (A), CLN (B) and brain (C) of TCR^{1640} mice before and after EAE onset, NTL mice and IgH^{MOG} mice.

Figure 33 illustrates MOG_{tet}^{+} B cells quantification into total B cells in different lymphoid organs and brain (data in ALN, ILN, MLN and PP are not shown). As expected MOG_{tet}+ B cells were detected in all lymphoid organs for IgH^{MOG} mice. No MOG_{tet}^{+} B cells were detected in brain for these former mice. No MOG_{tet}^{+} B cells were detected in lymphoid organs or brain for NTL and disease-free TCR^{1640} mice. MOG_{tet}^{+} B cells were detected at a low proportion in CLN only considering the lymphoid organs and in brain of diseased TCR^{1640} mice.

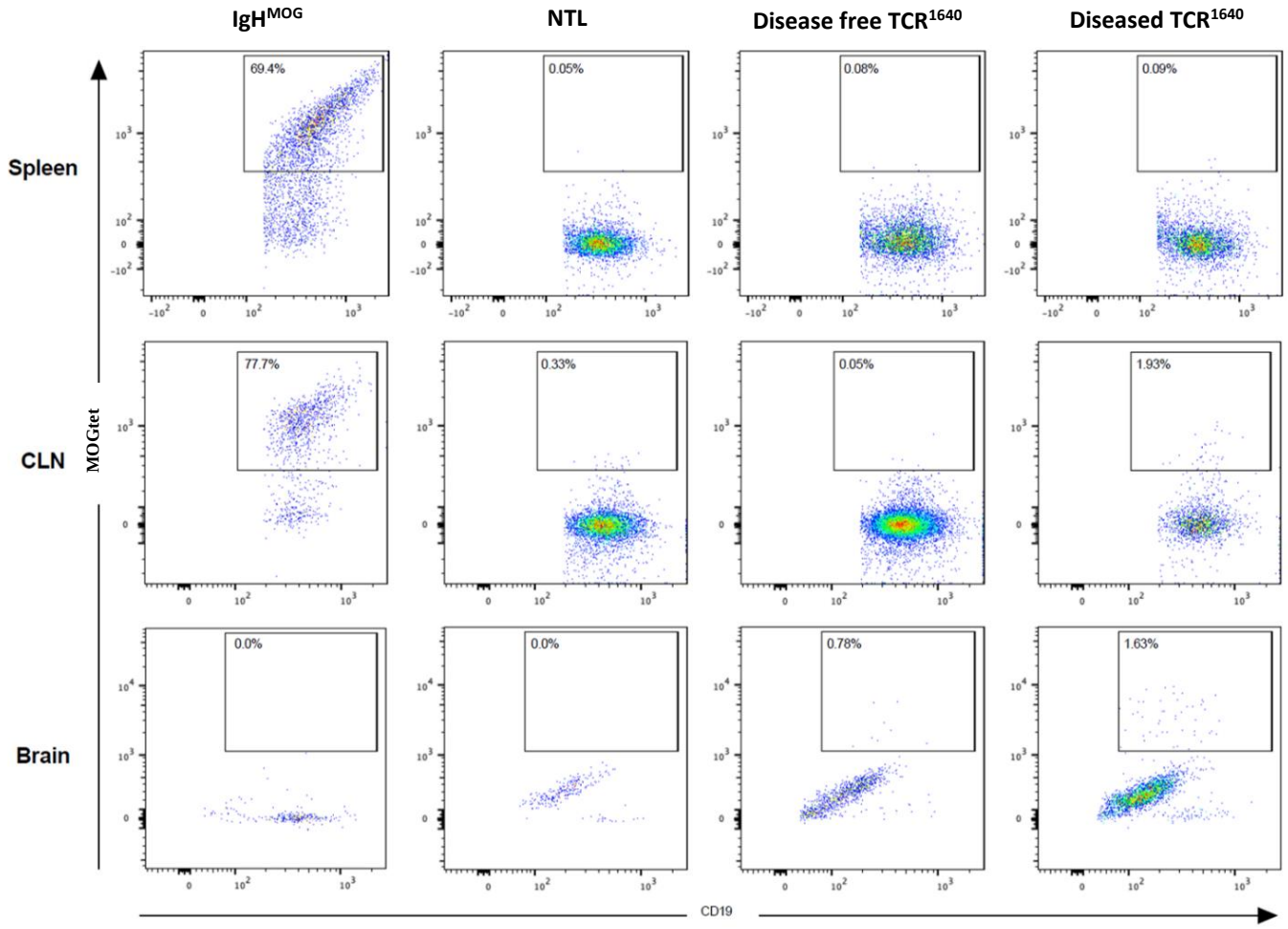

Figure 33 : Selection of live MOG_{tet}+ B cells in different type of organs. Example of the MOG_{tet}^{+} B cells quantification in total B cells. Here, cells come from spleen, PP, ALN, ILN, MLN, CLN and brain of IgH^{MOG} mice, NTL mice and TCR^{1640} mice before and after EAE onset.

Figure 34 shows the percentage data of MOG_{tet}^{+} B cells into total B cells in mice in the different organs (data in ALN, ILN, MLN and PP are not shown). In spleen, as expected, MOG_{tet}^{+} B cells were observed in IgH^{MOG} mice (43.3± 9.8%); no MOG_{tet}^{+} B cells were

observed in NTL, disease-free and diseased TCR^{1640} mice. In CLN, as expected, MOG$_{tet}^{+}$ B cells were observed in IgH^{MOG} mice (27.67±16.8%) but also in diseased TCR^{1640} mice at a low proportion (0.84±0.27%); no MOG$_{tet}^{+}$ B cells were observed in NTL and disease-free TCR^{1640} mice. In CLN, a significant high proportion of MOG$_{tet}^{+}$ B cells (p=0.03) were observed in diseased TCR^{1640} mice compared to control mice (NTL and disease-free TCR^{1640} mice). In brain, MOG$_{tet}^{+}$ B cells were observed in diseased TCR^{1640} mice at a low proportion (0.73 ± 0.19%) but at a significatively higher proportion (p=0.03) compared to control mice (IgH^{MOG}, NTL and disease-free TCR^{1640} mice); no MOG$_{tet}^{+}$ B cells were observed in IgH^{MOG} and NTL mice).

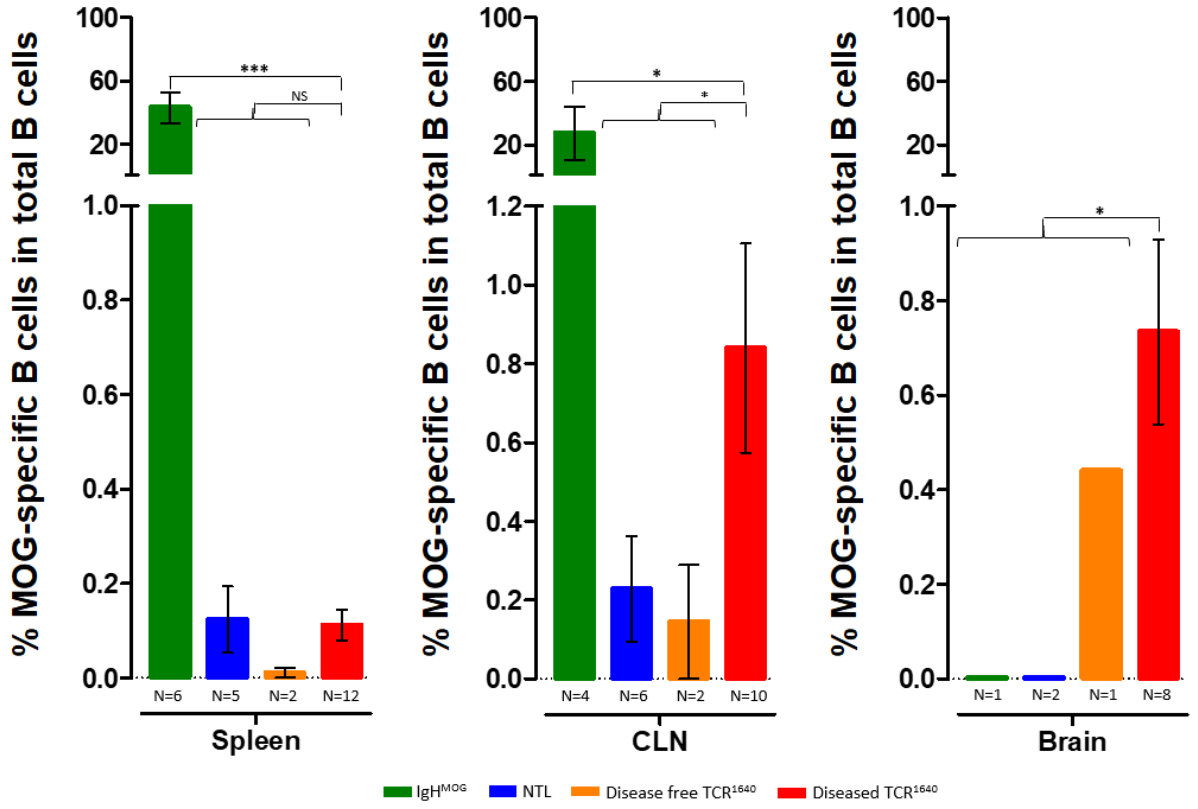

Figure 34 : Proportion of MOG$_{tet}^{+}$ B cells in the total B cells. Data from several experiments were pooled. Cell populations representing fewer than 200 total B cells were excluded. The labelled cells came from spleen (A), CLN (B) and brain (C) of TCR^{1640} mice before and after EAE onset, NTL mice and IgH^{MOG} mice. (=p<0.05, ***=p<0.0001).*

Figure 35 shows the percentage of MOG-specific B cells in CLN and brain according to the delay after EAE onset. No correlation was observed between both parameters (CLN R^2=0.009; p=0.793 and brain R^2=0.235; p=0.2).

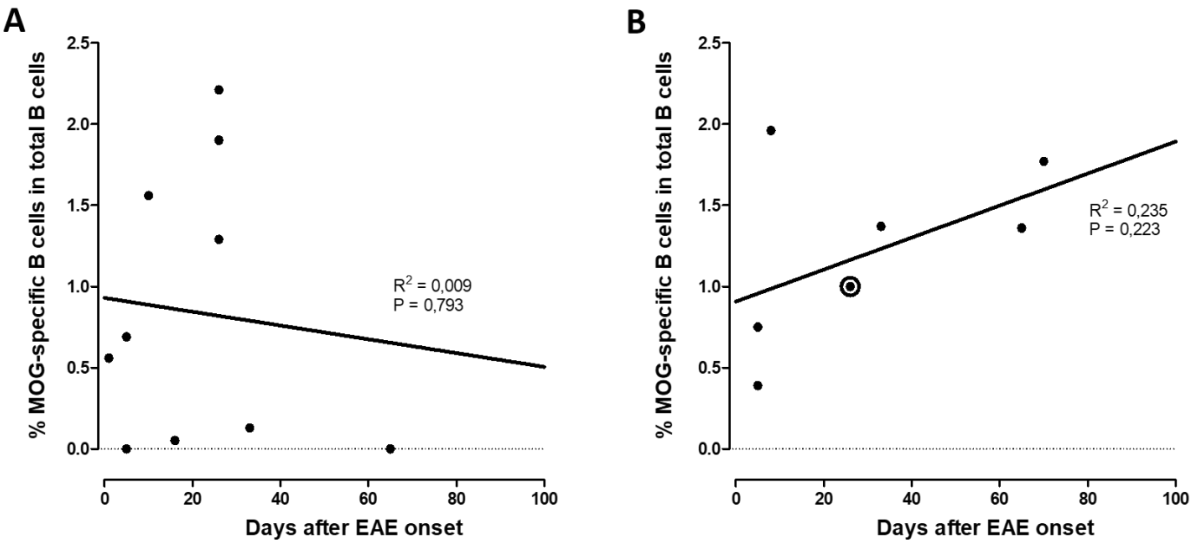

Figure 35 : Correlation between live MOG_{tet}^+ B cells and number of days after EAE onset. Percentages of live MOG_{tet}^+ B cells into total B cells were represented according to the number of days after EAE onset for CLN (A) and brain (B) of diseased TCR^{1640} mice.

These results highlight the presence of MOG_{tet}^+ B cells in diseased TCR^{1640} mice after EAE onset in brain and CLN without correlation between the proportion of MOG_{tet}^+ B cells and the delay of EAE.

D. iGB single cell culture and construction of sequences bank.

To initiate iGB culture, a cohort of 9 TCR^{1640} mice (4 females and 8 males) were sacrificed at different time points before and after onset of symptoms: 3 disease-free TCR^{1640} mice (2 females and 1 male) were sacrificed at mean age of 104±31 days; 9 TCR^{1640} mice (2 females and 7 males) were sacrificed after EAE onset at a mean age of 228±113 days and a mean of 4±1 days after EAE onset with a mean clinical score of 2.6±0.6.

Table 5 reports information concerning groups of mice sacrificed for iGB single cell culture from spleens, CLNs and brains. Details concerning number of cells counted before sorting and concerning the number of seeded vials after sorting are given on Table 5. A maximum of one 96-well plate was used for B cells from 5 spleen. We used the maximum of sorted B cells from CLN and brain.

	n=	ages		Day after EAE onset		clinical score		Nomber of cells before sorting (10^6)						Mean of total B cells sorted by cytometry						Mean of MOG specific B cells sorted by cytometry					
								SPLEEN		CLN		Brain		SPLEEN		CLN		Brain		SPLEEN		CLN		Brain	
		Mean	SD	Mean	SD	Mean	SD	Mean	SD	Mean	SD	Mean	SD	Mean	SD	Mean	SD	Mean	SD	Mean	SD	Mean	SD	Mean	SD
NTL	1	385.00						21.50						94.00											
IgH^{MOG}	3	202.00	69.00					31.13	13.38	3.00	1.27	0.40	0.42					93.00		126.67	54.85	125.00	91.92	29.00	
Disease free TCR^{1640}	3	103.67	31.01							2.89	0.30	1.35	0.35			95.00	0.00	93.00	3.46			70.33	19.35	34.67	39.27
Diseased TCR^{1640}	9	228.00	113.07	3.56	1.13	2.60	0.60	19.49	0.02	2.33	2.30	0.66	0.21	94.00	1.00	118.75	47.5	95.00	0.00			67.5	38.89	22.75	4.27

Table 5 : Compilation of data generated for the iGB culture of spleen, CLN and brain B cells and MOG specific B cells from NTL (n=1), IgH^{MOG} (n=3), disease-free (n=3), diseased TCR^{1640} mice (n=9). It was reported the mean age of mice at sacrifice, the delay of EAE, the number of cells collected per organs before cytometry sorting and the mean B cells and MOG$_{tet}^{+}$ B cells sorted in single cells by cytometry per experiment.

Table 6 reports information concerning the efficiency of the iGB single cell culture and the number of ELISA assay of supernatants from iGB culture. A little less of 50% and 15% of the B cells seeded for single cell culture from spleen of respectively NTL mice and MOG-specific B cells from spleen of IgH^{MOG} mice led to cluster after 9 days. Concerning total B cells from spleen of diseased TCR^{1640} mice, we observed about 40% of clusters after 8 days of iGB single cell culture. Total B cells and MOG_{tet}^{+} B cells from CLNs of disease-free TCR^{1640} mice led to about 40% of cluster after 9 days of single cell culture. Total B cells sorted from CLNs of disease-free and diseased TCR^{1640} mice led also to about 40% of clusters after 9 days of iGB single cell culture. This efficiency of single cell culture dropped to about 15% and less for MOG_{tet}^{+} B cell from CLNs of diseased TCR^{1640} mice and for total B cells and MOG_{tet}^{+} B cells from CLNs and brain of disease-free and diseased TCR^{1640} mice. Notice that, some total B cells could be sorted from brain of disease-free TCR^{1640} mice for single cell culture but no MOG_{tet}^{+} B cell was sorted from these mice. Single cell culture of total B cells and MOG_{tet}^{+} B cell from spleen, CLNs and brain of IgH^{MOG} mice gave very low percentage of clusters.

Concerning supernatants of iGB culture analysed by ELISA (Fig. 35), higher concentration of total IgG1 was observed in supernatants of single cell culture with MOG_{tet}^{+} B cell from CLNs of disease-free and diseased TCR^{1640} mice compared to supernatants of single cell culture with total B cells from these same mice ($p<0.0001$). Anti-MOG activity was detected only in supernatants from single cell culture with MOG_{tet}^{+} B cells in CLN from disease-free and diseased TCR^{1640} mice ($p<0.0001$).

NTL (n=1)		Spleen				CLN				Brain			
		Total B cell		MOG_{tet}+		Total B cell		MOG_{tet}+		Total B cell		MOG_{tet}+	
		Mean	SD	Mean	SD	Mean	SD	Mean	SD	Mean	SD	Mean	SD
Single cell sorted by cytometry		94											
Mean of single cell sorted by cytometry per mouse													
Delay of iGB culture (days)		9											
Number of iGB cluster		42											
Mean of iGB cluster per mouse													
Percentage of well giving cluster		44.7%											
Mean of amplification per cluster		6810											
Number of iGB cluster supernatant collected (%)		41 (98)											
Number of PCR (%)	IgHG												
	IgLKappa												
Number of PCR amplification bands collected (%)	IgHG												
	IgLKappa												
Analysable sequences (%)	IgHG												
	IgLKappa												

IgH^{MOG} (n=3)		Spleen				CLN				Brain			
		Total B cell		MOG_{tet}+		Total B cell		MOG_{tet}+		Total B cell		MOG_{tet}+	
		Mean	SD	Mean	SD	Mean	SD	Mean	SD	Mean	SD	Mean	SD
Single cell sorted by cytometry				380				250		93		29	
Mean of single cell sorted by cytometry per mouse				127	55			125	92				
Delay of iGB culture (days ± SD)		11.50 ± 2.12											
Number of iGB cluster				47				1		12		0	
Mean of iGB cluster per mouse				16	20			1	1				
Percentage of well giving cluster				12.4%				0.4%		12.9%		0,0%	
Mean of amplification per cluster				3100	3204			875	1237	1300			
Number of iGB cluster supernatant collected (%)				47 (100)				1 (100)		12 (100)			
Number of PCR (%)	IgHG			9 (19)				1 (100)		12 (100)		.	
	IgLKappa			9 (19)				1 (100)		12 (100)			
Number of PCR amplification bands collected (%)	IgHG			7 (78)				1 (100)		8 (67)			
	IgLKappa			14 (156)				2 (200)		11 (92)			
Analysable sequences (%)	IgHG			7 (100)				0 (0)		3 (38)			
	IgLKappa			4 (57)				1 (50)		5 (45)			

Table 6 : Compilation of data generated during the iGB culture of spleen, CLN and brain B cells and MOG_{tet}+ B cells from NTL (n=1), IgH^{MOG} (n=3), disease-free TCR^{1640} mice (n=3) and diseasedTCR^{1640} mice (n=9). It was reported the number of B cells and MOG_{tet}+ B cells sorted as single cells by cytometry, the number of cells sorted by single cell cytometry, the delay of iGB culture, the number of iGB cluster observed. The mean of iGB cluster observed per experiment, the percentage of well giving iGB cluster, the mean of amplification counted per iGB cluster, the number of iGB supernatants collected for ELISA assay (percentage of iGB supernatants collected into the number of cluster observed), the number of PCRs realized with target IgHG and IgKappa (percentage of PCR realized into the number of cluster observed), the number of PCRs realized with target IgHG and IgKappa giving amplification bands (percentage of PCRs realized giving amplification band into the number of PCRs realized) and the number of analysable sequences after sequencing of PCR application bands (percentage of analysable sequences into the number of PCR amplification bands collected).

Disease free TCR^{1640} (n=3)		Spleen				CLN				Brain			
		Total B cell		MOG$_{tet}$+		Total B cell		MOG$_{tet}$+		Total B cell		MOG$_{tet}$+	
		Mean	SD	Mean	SD	Mean	SD	Mean	SD	Mean	SD	Mean	SD
Single cell sorted by cytometry						285		211		279		104	
Mean of single cell sorted by cytometry per mouse						95	0	70	19	93	3	35	39
Delay of iGB culture (days ± SD)		9.3 ± 2.5											
Number of iGB cluster						132		84		10		0	
Mean of iGB cluster per mouse						44	15	28	19	3	6	0	0
Percentage of well giving cluster						46.3%		39.8%		3.6%		0,0%	
Mean of amplification per cluster						6300	984.9	5167	1079	1217	2107	0	0
Number of iGB cluster supernatant collected (%)						53 (40)		78 (93)		10 (100)		0 (0)	
Number of PCR (%)	IgHG					42 (32)		29 (35)		0 (0)			
	IgLKappa					42 (32)		29 (35)		0 (0)			
Number of PCR amplification bands collected (%)	IgHG					20 (48)		4 (14)					
	IgLKappa					23 (55)		2 (7)					
Analysable sequences (%)	IgHG					5 (25)		0 (0)					
	IgLKappa					6 (26)		1 (50)					

Diseased TCR^{1640} (n=9)		Spleen				CLN				Brain			
		Total B cell		MOG$_{tet}$+		Total B cell		MOG$_{tet}$+		Total B cell		MOG$_{tet}$+	
		Mean	SD	Mean	SD	Mean	SD	Mean	SD	Mean	SD	Mean	SD
Single cell sorted by cytometry		283				475		135		475		91	
Mean of single cell sorted by cytometry per mouse		94	1			119	48	68	39	95	0	23	4
Delay of iGB culture (days ± SD)		8.6 ± 2.3											
Number of iGB cluster		105				184		20		62		4	
Mean of iGB cluster per mouse		35	34			17	17	5	5	12	15	1	2
Percentage of well giving cluster		37.1%				38.7%		14.8%		13.1%		4.4%	
Mean of amplification per cluster		2878	4069			4588	2835	3233	3412	2686	2799.55	NC	NC
Number of iGB cluster supernatant collected (%)		48 (46)				154 (84)		20 (100)		61 (98)		4 (100)	
Number of PCR (%)	IgHG					151 (82)		14 (100)		57 (92)		0 (0)	
	IgLKappa					151 (82)		14 (100)		57 (92)		0 (0)	
Number of PCR amplification bands collected (%)	IgHG					57 (38)		11 (79)		11 (19)			
	IgLKappa					64 (42)		8 (57)		14 (25)			
Analysable sequences (%)	IgHG					17 (30)		0 (0)		1 (9)			
	IgLKappa					11 (17)		0 (0)		7 (50)			

Table 6 : Compilation of data generated during the iGB culture of spleen, CLN and brain B cells and MOG$_{tet}$+ B cells from NTL (n=1), IgH^{MOG} (n=3), disease-free TCR^{1640} mice (n=3) and diseased TCR^{1640} mice (n=9). It was reported the number of B cells and MOG$_{tet}$+ B cells sorted as single cells by cytometry, the number of cells sorted by single cell cytometry, the delay of iGB culture, the number of iGB cluster observed. The mean of iGB cluster observed per experiment, the percentage of well giving iGB cluster, the mean of amplification counted per iGB cluster, the number of iGB supernatants collected for ELISA assay (percentage of iGB supernatants collected into the number of cluster observed), the number of PCRs realized with target IgHG and IgKappa (percentage of PCR realized into the number of cluster observed), the number of PCRs realized with target IgHG and IgKappa giving amplification bands (percentage of PCRs realized giving amplification band into the number of PCRs realized) and the number of analysable sequences after sequencing of PCR application bands (percentage of analysable sequences into the number of PCR amplification bands collected).

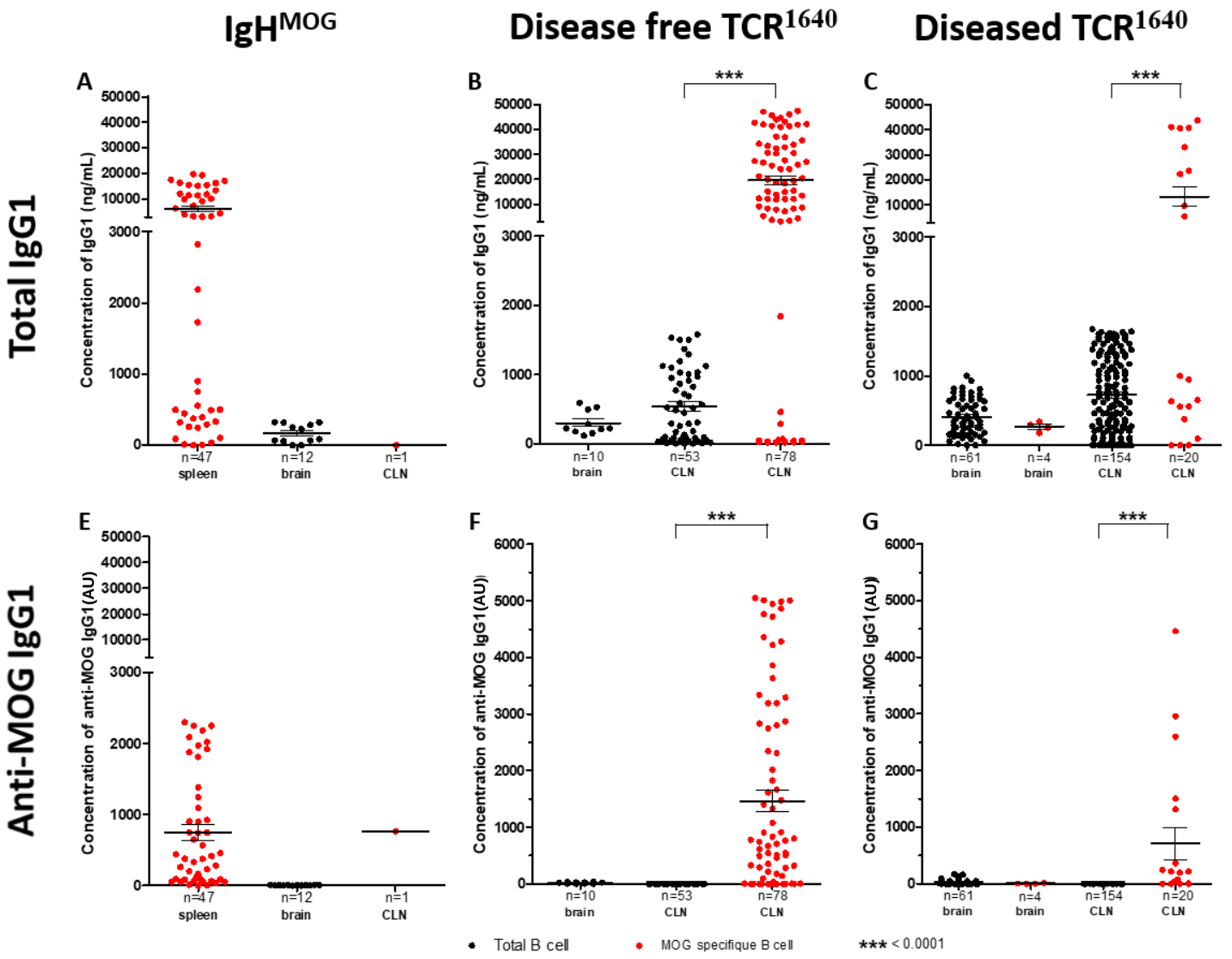

Figure 36 : Quantification of anti-MOG antibodies by ELISA in supernatants of iGB culture. Quantification of total IgG1 (A, B and C) and anti-MOG IgG1(D, E and F) antibodies in supernatants of iGB culture from spleen, CLN and brain cells. IgH^{MOG} (A and B) samples, disease-free TCR^{1640} mice (B and E) samples and diseased TCR^{1640} mice (C and F) samples represent respectively 1, 3 and 7 experiments. Quantification of total IgG1 in ng/mL and anti-MOG IgG1 antibodies in AU

Figure 37 illustrates cluster development of total B cell and MOG_{tet}^{+} B cells sorted from CLNs and brains. Figure 38 and 39 show the phenotype of cells obtained after 8 days of iGB single cell culture from CLN and brain of diseased TCR^{1640} mice at 4 days after EAE onset and clinical score equal to 3,5. In cell obtained from CLN and brain, plasma cells (CD138) and B cells (CD19) were identified. The expression of FAS, GL7, PNA and IgG1 were detected without detection of CD38 and IgM. The phenotype of these cells corresponded to plasma cells and activated B cells.

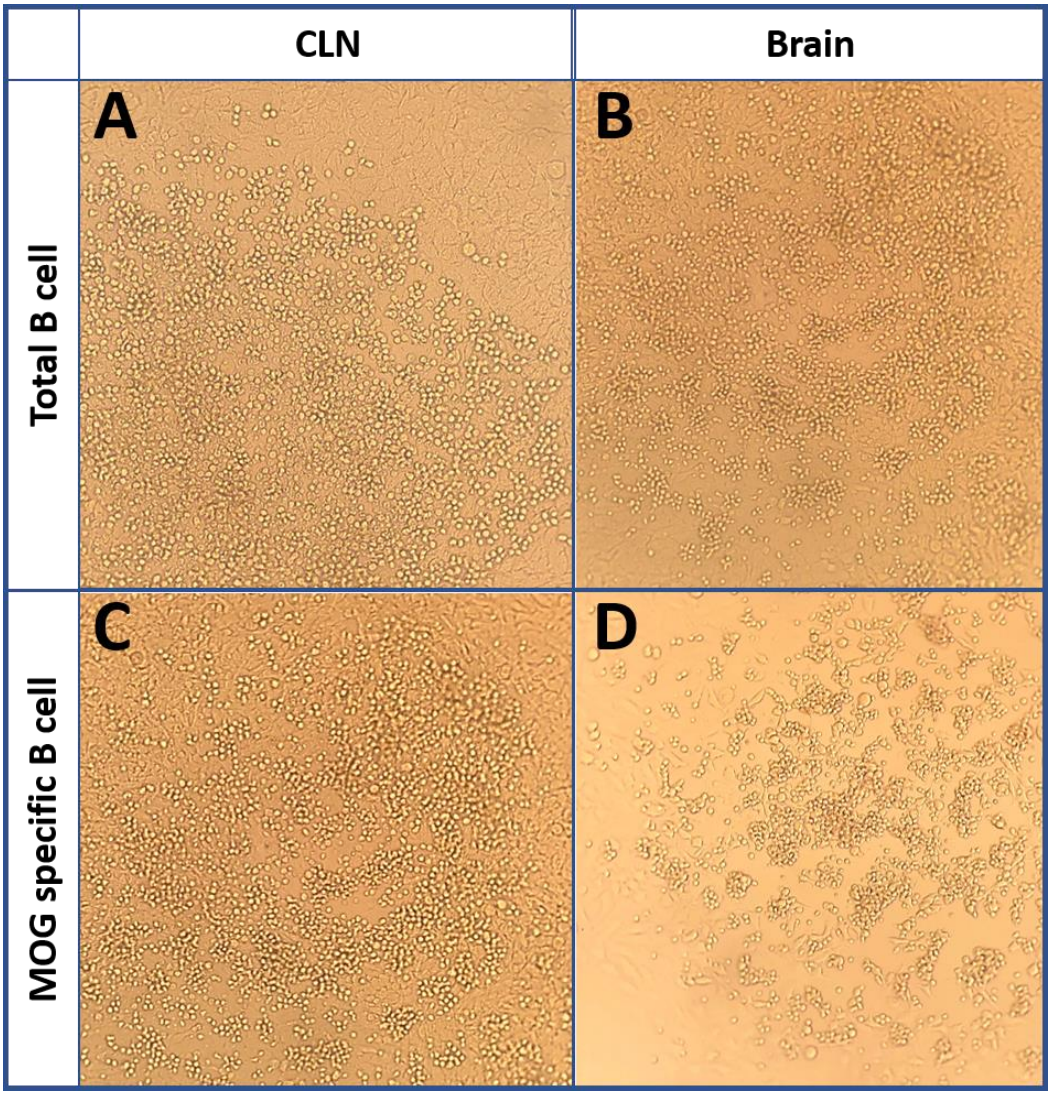

Figure 37 : Photographs of clusters obtained after iGB single culture of CLN and brain total B cell and MOG_{tet}^{+} B cell after 8-12 days of culture. Total B cells and MOG_{tet}^{+} B cells extracted from CLN and brain of disease-free and diseased TCR^{1640} mice. A, iGB cluster of total B cell from CLN of diseased TCR^{1640} mice. B, iGB cluster of total B cell from brain of disease-free TCR^{1640} mice. C, iGB cluster of MOG_{tet}^{+} B cell from CLN of diseased TCR^{1640} mice. D, iGB cluster of MOG_{tet}^{+} B cell from brain of diseased TCR^{1640} mice.

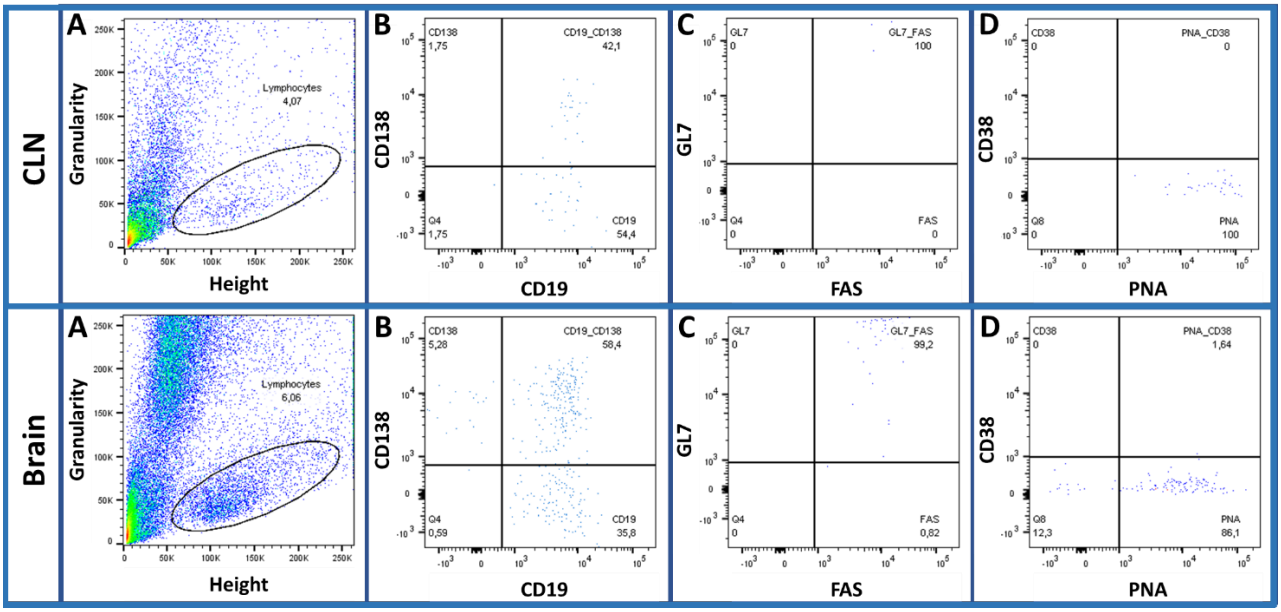

Figure 38 : Extracellular phenotype of 10 cells amplified using iGB culture.
Cells obtained after 8 days of iGB culture from 10 B cells from CLN or brain of diseased TCR^{1640} mice at 4 days after EAE onset, clinical score 3.5. A, selection of cells corresponding to B cells sizes. B, selection of B cells (CD19) and plasma cells (CD138). C, in B cells population, quantification of GL7 and FAS expression. D, in B cells population, quantification of CD38 and PNA expression.

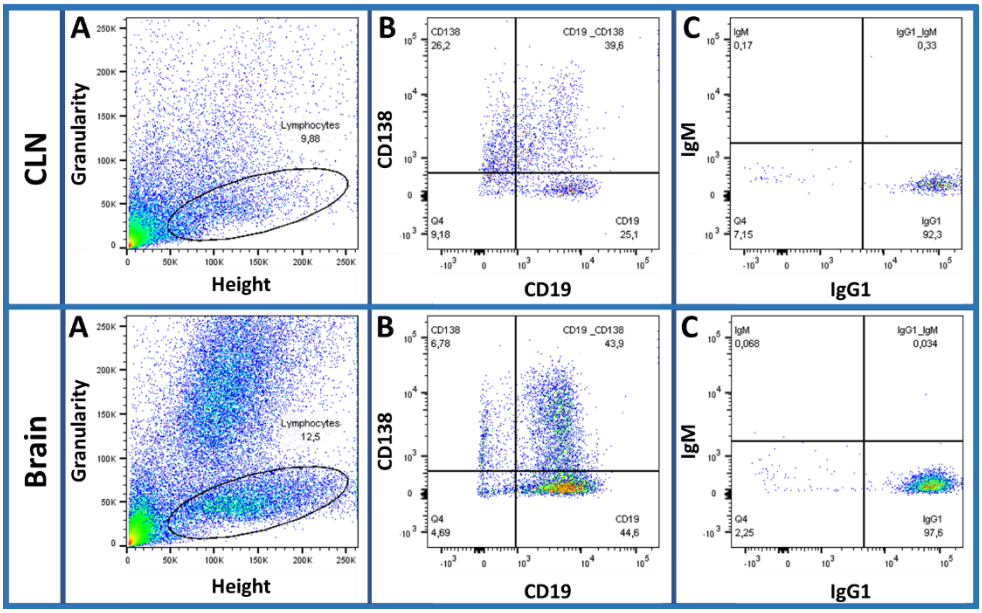

Figure 39 : Intracellular phenotype of 10 cells amplified using iGB culture.
Cells obtained after 8 days of iGB culture from 10 B cells from CLN or brain of diseased TCR^{1640} mice at 4 days after EAE onset, clinical score 3.5. A, selection of cells corresponding to B cells sizes. B, selection of B cells (CD19) and plasma cells (CD138). C, in B cells, population, quantification of IgM and IgG1 expression.

E. PCR products and bank construction.

Figure 40 illustrates PCRs realised after RNA extraction from cluster obtained after single cell culture. Bands at the expected sizes of 500kDa for IgHG and 400kDa for IgLK were collected. Purified PCRs products were sequencing by SANGER technology at the sequencing platform of GENOSCREEN (Lille, France). Table 6 presents the number of PCRs performed, the PCR efficiency and the number of analysable sequences obtained. Readable sequences represented a low percentage of samples sequenced (less than 50%) for each sequence obtained.

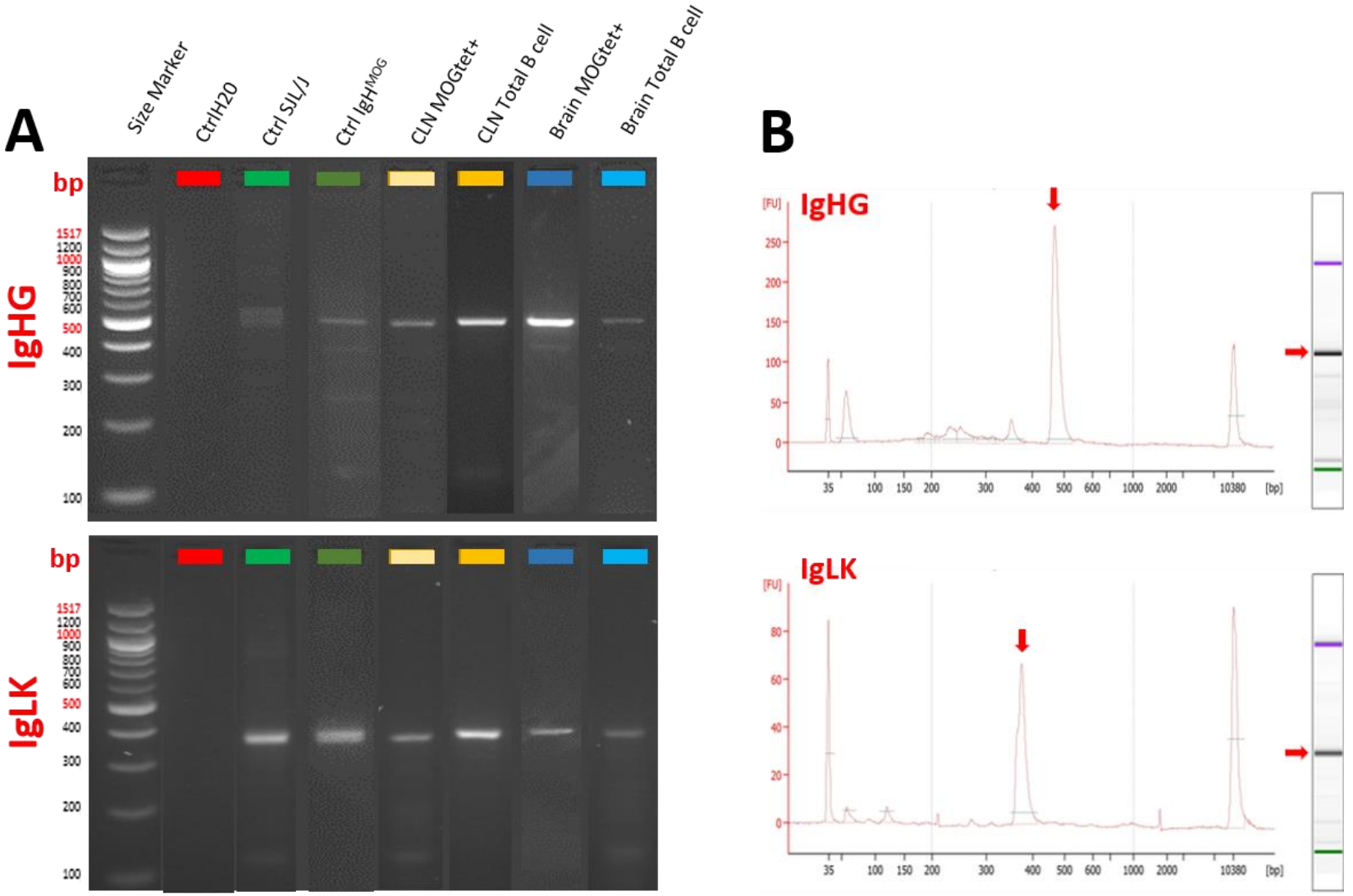

Figure 40 : Migration of IgHG and IgLK cDNA from clusters of single cell culture. A, expected migration bands are observed at 500bp for IgHG and 400bp for IgLK B, the Bioanalyzer shows the presence of the majority band at 500bp for IgHG and 400bp for IgLK.

F. Transcriptomic analysis.

Table 7 shows the results of the different sequences obtained and analyzed within the IMGT tool (http://www.imgt.org). All the genomic sequences and amino-acid sequences obtained for IgHG chains were different and no genomic clonotype was found twice. For IgLK chains, 13 different genomic clonotypes were identified and 3 of them were found 3 times and in different organs and concerning total B cells as well as MOG_{tet}^{+} B cells. No IgHG sequence could be paired to any corresponding IgLK sequence. A consensual amino-acid sequence was found for the different genomic clonotypes found for IgLK. Submitted to the protein BLAST tool from NCBI with *mus musculus* (taxid:10090) as targeted organism (http://blast.ncbi.nlm.gov/Blast.cgi?PAGE=Proteins), this short consensual amino-acid sequence for IgLK fave a correspondence to 97 different proteins which were mostly IgL proteins according to NCBI database. Distance tree of this analysis (Fig. 41) confirmed the relevance of this consensual amino-acid sequence to rodents and especially in *mus musculus* part of the IgLK region sequences (Fast Minimum Evolution, 0.90 of max sequence difference, distance of Grishin for proteins).

IgHG clonotypes	RR status	organ	collected clusters	JUNCTION decryption	calculated AA sequence
1	sick RR	CLN-derived total B cells	IgHG IGB cluster 24	(1)-8{5}-5(8)-4{3}+1(23)	X Q E G X G I S M L W T T
2	sick RR	CLN-derived total B cells	IgHG IGB cluster 210	(8)-1{1}+1(10)-7{10}-10(12)	X A R R X W S X W X X X V W
3	sick RR	CLN-derived total B cells	IgHG IGB cluster 20	(8)-1{3}-1(17)-5{5}-2(15)	C X X X Y X Y G S T A W F A X W
4	sick RR	CLN-derived total B cells	IgHG IGB cluster 59	(8)-1{8}-5(7)-5{4}-9(6)	X A R W G G G F X Y X
5	sick RR	CLN-derived total B cells	IgHG IGB cluster 60	(9)0{11}-13(5)-5{20}-21(2)	C A R R G X X S X S X X X X S
6	sick RR	CLN-derived total B cells	IgHG IGB cluster 215	(9)0{16}-12(11)0{3}-6(9)	C A R R G Y X X X S X Y X X Y X
7	sick RR	CLN-derived total B cells	IgHG IGB cluster 53	(9)0{2}-7(8)-2{5}-2(15)	C A R V G N L A W F X Y W
8	healthy RR	CLN-derived total B cells	IgHG IGB cluster 422	(9)0{3}-4(7)+1{17}-15(2)	C A R R L G R E X X X X X
9	sick RR	CLN-derived total B cells	IgHG IGB cluster 50	(9)0{3}-8(9)	C A R G X Y W
10	sick RR	CLN-derived total B cells	IgHG IGB cluster 56	(9)0{6}-8(12)-3{6}-2(15)	C A R G G Y G S S P A W F A X X
11	sick RR	CLN-derived total B cells	IgHG IGB cluster 54	(9)0{9}-6(4)-1{2}-8(9)	C A R E R X G X X Y X
					No consensual AA sequence
IgLK clonotypes					
1	healthy RR	CLN-derived total B cells	IgLK IGB cluster 477	(23)-3{0}-1(10)	C Q Q H Y X T P Y T X
1	sick RR	brain-derived total B cells	IgLK IGB cluster 42	(23)-3{0}-1(10)	C Q Q Y Y S Y P Y T F
2	sick RR	brain-derived total B cells	IgLK IGB cluster 32	(23)-3{0}0(10)	X Q N D H S Y P F T X
2	sick RR	brain-derived total B cells	IgLK IGB cluster 30	(23)-3{0}0(10)	C X Q N X E X P W T F
3	sick RR	brain-derived total B cells	IgLK IGB cluster 37	(24)-2{1}-2(8)	C V Q G T H F P X T F
3	healthy RR	CLN-derived total B cells	IgLK IGB cluster 473	(24)-2{1}-2(8)	C Q N D X S X P X T X
3	sick RR	CLN-derived MOG B cells	IgLK IGB cluster 81	(24)-2{1}-2(8)	C Q Q H X S X P X T X
4	sick RR	CLN-derived total B cells	IgLK IGB cluster 48	(25)-2{0}-2(8)	C Q Q H N E X X W X X
4	sick RR	CLN-derived total B cells	IgLK IGB cluster 117	(25)-2{0}-2(8)	C Q Q G S S S P L T X
4	sick RR	brain-derived total B cells	IgLK IGB cluster 33	(25)-3{0}-2(8)	C Q Q Y X S Y P R T X
5	sick RR	CLN-derived total B cells	IgLK IGB cluster 47	(28)0{0}-5(5)	C Q Q R S S Y P X T X
5	sick RR	CLN-derived total B cells	IgLK IGB cluster 64	(28)0{0}-5(5)	C Q Q W S S Y P L T X
5	sick RR	CLN-derived MOG B cells	IgLK IGB cluster 63	(28)0{0}-5(5)	C Q Q X S G X P X T X
6	sick RR	CLN-derived total B cells	IgLK IGB cluster 46	(28)0{0}-6(5)	C Q Q X S S Y P P T X
7	healthy RR	CLN-derived total B cells	IgLK IGB cluster 483	(8)-20{16}-2(8)	X Q X G V V T X S R
8	healthy RR	CLN-derived total B cells	IgLK IGB cluster 461	(8)-20{17}-4(7)	C Q X X V V T H P X
9	sick RR	CLN-derived total B cells	IgLK IGB cluster 66	(9)-17{43}-8(2)	X C K V G R F R G R X X R X X X X X
10	healthy RR	CLN-derived total B cells	IgLK IGB cluster 474	(16)-10{9}-3(7)	C Q Q S N X G Q P R
11	sick RR	CLN-derived total B cells	IgLK IGB cluster 79	(20)-6{2}-2(8)	C L Q Y D N L X T X
12	sick RR	CLN-derived total B cells	IgLK IGB cluster 44	(22)-4{4}-2(7)	X X Q G X S X X X T X
13	sick RR	brain-derived total B cells	IgLK IGB cluster 31	(26)-2{1}-4(6)	X Q Q W D S Y P P T F
			consensual AA sequence from selected clonotypes		C Q Q W S S Y P L T

Table 7 : Comparison of the IMGT sequence submission results.
AA: amino_acid; iGB: induced germinal center B cells; in deep blue and pink are the genomic clonotypes read more than once; in red box correspond to an undefined amino-acid.

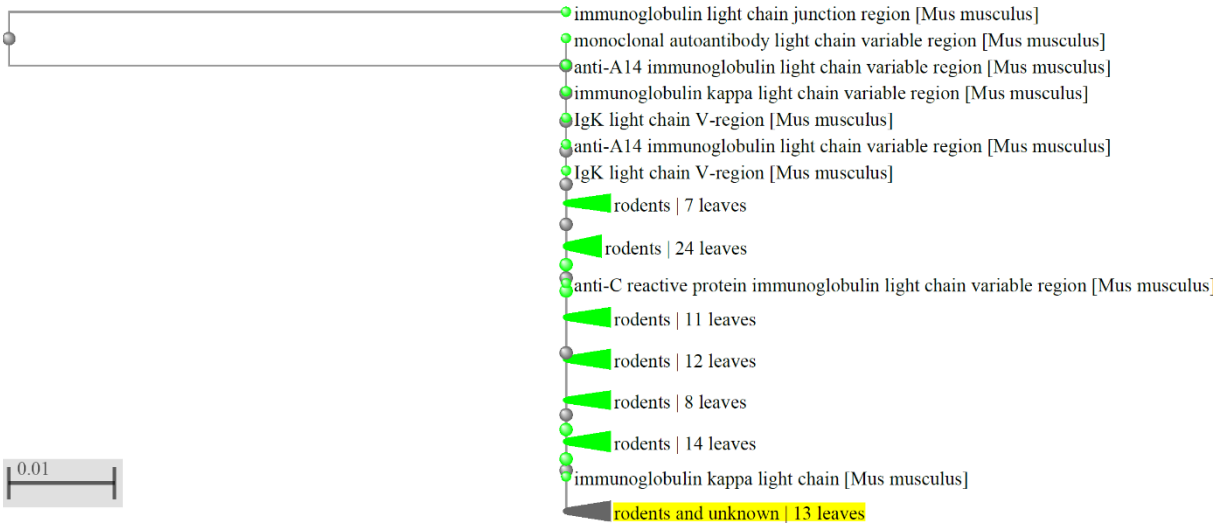

Figure 41 : Distance tree of NCBI protein blast.
Distance tree of NCBI protein blast with mus musculus (taxid:10090) as targeted organism and the short consensual sequence CQQWSSYPLT observed in our sequence analysis (Fast Minim Evolution, 0.90 of max sequence difference, distance of Grishin for proteins).

V. Discussion.

TCR^{1640} mice bred in our animal facility in Lille show a moderately different phenotype of TCR^{1640} mice compared to TCR^{1640} mice mice bred in the Munich such that spontaneous disease developed later, without any difference between male and female and with a relapsing-remitting phenotype in half of the colony. Trying to characterize the anti-MOG response in our colony, we found that, (i) serum anti-MOG titers in disease-free and diseased TCR^{1640} mice have no correlation with age of mice, time after EAE onset, or EAE clinical score, (ii) percentages of MOG$_{tet}^{+}$ B cells in CLN and brain of diseased TCR^{1640} mice were not correlated with the time after EAE onset, (iii) however serum from diseased TCR^{1640} mice appeared to significantly increase EAE incidence and EAE severity compared to serum from disease-free TCR^{1640} mice when transferred into 2D2 mice, suggesting potential different pathogenic humoral features between disease-free and diseased TCR^{1640} mice. Lastly (iv) the iGB single cell culture approach did not lead to a successful and sufficient B cells amplification and only few clonotypes were obtained for unpaired IgHG and IgLK chains. However, we found some few common clonotypes between CLN-derived-B cells from disease-free and diseased TCR^{1640} mice and brain-derived-B cells from diseased TCR^{1640} mice.

The strength of the work was based on the efficiency of the MOGtet as we showed that it could detect MOG-specific B cells in a cell suspension containing 1 MOG-specific B cell into 3000 cells. This tool allowed to detect more than 70% of MOG-specific B cells in homozygous IgH^{MOG} mice (having more than 95% of MOG-specific B cells). Despite its efficiency, less than 2 % of MOG$_{tet}^{+}$ B cells were detected in CLN and brain of diseased TCR^{1640} mice, which is not unexpected given that MOG$_{tet}^{+}$ B cells are recruited/expanded from an endogenous B cell repertoire in this model. Of course, it is also possible that the MOG$_{tet}^{+}$ B cells in TCR^{1640} mice

have a lower affinity for MOG compared to B cells from IgH^{MOG} mice, which contain the heavy chain of an anti-MOG antibody with very high affinity (8.18c5), which is reflected in a slightly lower MFI of the MOGtet staining in TCR^{1640} vs IgH^{MOG} mice (Figure 6).

The main limit of the study was the transcriptomic approach based on a B cell expansion method-iGB single-cell culture) which appeared not appropriate for activated B cells. Indeed iGB single-B cell was quite efficient with non-activated B cells as B cells isolated from spleen B cells of BALB/c or NTL SJL/J mice, and clonal efficiency was better with BALB/c B cells, maybe because 40LB feeder cells are BALB/c 3T3 fibroblasts [88]. We obtained as expected 70% clonal efficiency and more than 10000 expansion fold with spleen-derived B cells from BALB/c mouse, and this result was closed to Kuraoka's results [88]. However, clonal efficiency and expansion fold dramatically dropped with B cells isolated from CLN and brain of disease-free and diseased TCR^{1640} mice, especially for B cells from brains and brain-derived- MOG_{tet}^{+} B cells. Indeed, B cell isolation from brain may stress the cells and even if only live B cells were sorted to be seeded in iGB single cell culture, those brain-derived B cells are probably more activated and stressed and thus more prone to dying in the iGB culture. Kuraoka already described a lower clonal efficiency of iGB single-cell culture used for expansion of activated B cells (clonal efficiency of 23% versus 60% usually) [88]. Given the paucity of sorted MOG_{tet}^{+} B cells, we could not explore the phenotype of the sorted cells further before seeding them on 40LB for the iGB single cell culture. We confirm that iGB single-cell culture is not appropriate for a representative expansion of MOG_{tet}^{+} B cells from TCR^{1640} mice. The absence of anti-MOG activity detected in supernatant from cultures of TCR^{1640} mice brain-derived B cells may come to the low expansion fold. Moreover, despite the fact that IgG1 and anti-MOG antibodies were measured in supernatants from cultures derived from CLN-B cells, very few IgHG and IgLK sequences were obtained from the B cells clusters collected at term. Genomic clonotypes

obtained notably for IgLK allowed to obtain a consensual amino-acid sequence which could align with 97 proteins and most are variable parts of IgL chains. A single cell sequencing approach could at this step allow us to isolate more precisely in terms of quality and quantity the whole Ig components of each of our mice.

The TCR^{1640} mouse model we have worked on was imported from the native model from Munich. Berer *et al*. already demonstrated that the development of spontaneous EAE in TCR^{1640} mice model is dependent on the microbiota and no EAE developed in germ-free conditions. In SPF conditions, the Munich team described that 80% of TCR^{1640} mice developed EAE between 20 and 30 weeks of age [62]. In our SPF conditions 80% of the mice presented EAE after 42 weeks of age, and this could be due to mildly different environment and microbiota in both sites. Pöllinger *et al*., described a predominantly recurrent phenotype (71%) in female and more often chronical in male TCR^{1640} mice (53%). In Lille, independent of the gender, half of mice presented chronical spontaneous disease [61].

Pöllinger showed that in TCR^{1640} mice, serum auto-antibodies were specific for MOG and not for other myelin proteins [61]. In line with the published hypothesis that MOG_{tet}^{+} B cells in TCR^{1640} mice could be recruited either in CNS tissue or in CNS draining cervical lymph nodes with MOG imported from the CNS via lymphatic vessels [62], we did not find any MOG_{tet}^{+} B cells in other lymphoid organs than in CLN, especially none in mesenteric lymph nodes and Peyer's Patches (data not shown). The anti-MOG activity measured in the supernatants of iGB single cells cultures from CLN of disease-free and diseased TCR^{1640} mice confirmed the presence of MOG_{tet}^{+} B cells recruited to the CLN. The absence of data in brain B cells of disease-free and diseased TCR^{1640} mice in our work, potentially due to an inappropriate expansion method, did not allow conclusions on the recruitment or not of MOG_{tet}^{+} B cells to

the CNS of TCR^{1640} mice. Otherwise, transfer experiments suggest a different pathogenic humoral feature between disease-free and diseased TCR^{1640} mice: while other soluble factors such as cytokines may also contribute to this difference, it is possible that the repertoire of MOG_{tet}^{+} B cells undergoes pathogenic changes before and after EAE onset. Therefore, the analysis of the dynamic change of this repertoire could help to understand how recruitment of MOG_{tet}^{+} B cells may induce and perpetuate the disease.

VI. Conclusions and prospects.

In TCR^{1640} mice, where anti-MOG activity is detected early long before and after EAE without any correlation between anti-MOG titers and age, time after EAE and EAE score, differences observed between the influence of the disease-free serum or diseased serum in transfer experiments suggest different anti-MOG antibodies properties between disease-free and diseased status and dynamic changes of MOG-specific B cell repertoire.

Studying how purified anti-MOG antibodies from TCR^{1640} sera may influence EAE incidence and EAE severity in transfer experiments would help to confirm the different pathogenic humoral feature between disease-free and diseased status of those mice. We also suggest in perspective to directly evaluate the FACS-sorted MOG-specific B cells repertoire directly from CLN and CNS of disease-free and early diseased TCR^{1640} mice, to better understand how B cell act in developing a chronical inflammatory and demyelinating process.

Bibliography.

1. Browne, P. *et al.* Atlas of Multiple Sclerosis 2013: A growing global problem with widespread inequity. *Neurology* **83**, 1022–1024 (2014).
2. Dendrou, C. A. *et al.* Immunopathology of multiple sclerosis. *Nature Reviews Immunology* **15**, 545–558 (2015).
3. Compston, A. *et al.* Multiple sclerosis. *Lancet* **372**, 1502–1517 (2008).
4. Willer, C. J. *et al.* Twin concordance and sibling recurrence rates in multiple sclerosis. *Proc Natl Acad Sci U S A* **100**, 12877–12882 (2003).
5. Patsopoulos, N. A. *et al.* Fine-mapping the genetic association of the major histocompatibility complex in multiple sclerosis: HLA and non-HLA effects. *PLoS Genet* **9**, e1003926 (2013).
6. Sawcer, S. *et al.* Genetic risk and a primary role for cell-mediated immune mechanisms in multiple sclerosis. *Nature* **476**, 214–219 (2011).
7. Hedström, A. K. *et al.* Smoking and multiple sclerosis susceptibility. *European journal of epidemiology* **28**, 867-874 (2013).
8. Levin, L. I. *et al.* Temporal relationship between elevation of epstein-barr virus antibody titers and initial onset of neurological symptoms in multiple sclerosis. *JAMA* **293**, 2496–2500 (2005).
9. Munger, K. L. *et al.* Body size and risk of MS in two cohorts of US women. *Neurology* **73**, 1543–1550 (2009).
10. Ascherio, A. *et al.* Vitamin D as an early predictor of multiple sclerosis activity and progression. *JAMA Neurol* **71**, 306–314 (2014).
11. Thompson, A. J. *et al.* Diagnosis of multiple sclerosis: 2017 revisions of the McDonald criteria. *Lancet Neurol* **17**, 162–173 (2018).

12. Izquierdo, G. *et al.* Intrathecal IgG synthesis: marker of progression in multiple sclerosis patients. *Acta Neurologica Scandinavica* **105**, 158–163 (2002).
13. Tintoré, M. *et al.* Optic neuritis, brain stem syndromes and myelitis: rapid conversion to multiple sclerosis. *Med Clin (Barc)* **112**, 693–694 (1999).
14. Filippi, M. *et al.* Assessment of lesions on magnetic resonance imaging in multiple sclerosis: practical guidelines. *Brain* **142**, 1858–1875 (2019).
15. Friese, M. A. *et al.* Mechanisms of neurodegeneration and axonal dysfunction in multiple sclerosis. *Nat Rev Neurol* **10**, 225–238 (2014).
16. Bramow, S. *et al.* Demyelination versus remyelination in progressive multiple sclerosis. *Brain* **133**, 2983–2998 (2010).
17. Goverman, J. *et al.* Autoimmune T cell responses in the central nervous system. *Nat Rev Immunol* **9**, 393–407 (2009).
18. Lucchinetti, C. *et al.* Heterogeneity of multiple sclerosis lesions: implications for the pathogenesis of demyelination. *Ann Neurol* **47**, 707–717 (2000).
19. Kuhlmann, T. *et al.* An updated histological classification system for multiple sclerosis lesions. *Acta Neuropathol* **133**, 13–24 (2017).
20. Serafini, B. *et al.* Detection of ectopic B-cell follicles with germinal centers in the meninges of patients with secondary progressive multiple sclerosis. *Brain Pathol* **14**, 164–174 (2004).
21. Mitsdoerffer, M. *et al.* Tertiary Lymphoid Organs in Central Nervous System Autoimmunity. *Front Immunol* **7**, 451 (2016).
22. Frischer, J. M. *et al.* The relation between inflammation and neurodegeneration in multiple sclerosis brains. *Brain* **132**, 1175–1189 (2009).
23. Goebels, N. *et al.* Repertoire dynamics of autoreactive T cells in multiple sclerosis patients and healthy subjects: epitope spreading versus clonal persistence. *Brain* **123 Pt 3**, 508–518 (2000).

24. Li, R. *et al.* Reassessing B cell contributions in multiple sclerosis. *Nat Immunol* **19**, 696–707 (2018).
25. Vanderlugt, C. L. *et al.* Epitope spreading in immune-mediated diseases: implications for immunotherapy. *Nat Rev Immunol* **2**, 85–95 (2002).
26. Li, R. *et al.* Proinflammatory GM-CSF–producing B cells in multiple sclerosis and B cell depletion therapy. *Science Translational Medicine* **7**, 310ra166-310ra166 (2015).
27. Ireland, S. J. *et al.* Seeking Balance: Potentiation and Inhibition of Multiple Sclerosis Autoimmune Responses by IL-6 and IL-10. *Cytokine* **73**, 236–244 (2015).
28. Louveau, A. *et al.* Structural and functional features of central nervous system lymphatic vessels. *Nature* **523**, 337–341 (2015).
29. Wekerle, H. Tackling multiple sclerosis. *Nature* **420**, 39–40 (2002).
30. Steenbrugghe, F. H. Prise en charge globale de la sclérose en plaques. HAL **161**. (2016).
31. Trapp, B. D. *et al.* Axonal Transection in the Lesions of Multiple Sclerosis. *New England Journal of Medicine* **338**, 278–285 (1998).
32. Lampron, A. *et al.* Inefficient clearance of myelin debris by microglia impairs remyelinating processes. *J Exp Med* **212**, 481–495 (2015).
33. Vaughn, C. B. *et al.* Epidemiology and treatment of multiple sclerosis in elderly populations. *Nature reviews. Neurology* **15**, 329-342 (2019).
34. Vojdani, A. Molecular mimicry as a mechanism for food immune reactivities and autoimmunity. *Altern Ther Health Med* **21** Suppl 1, 34–45 (2015).
35. Liu, Y. *et al.* Myelin-specific multiple sclerosis antibodies cause complement-dependent oligodendrocyte loss and demyelination. *Acta Neuropathol Commun* **5**, (2017).
36. Bradl, M. *et al.* Neurologic autoimmunity: mechanisms revealed by animal models. *Handb Clin Neurol* **133**, 121–143 (2016).

37. Obermeier, B. *et al.* Matching of oligoclonal immunoglobulin transcriptomes and proteomes of cerebrospinal fluid in multiple sclerosis. *Nat Med* **14**, 688–693 (2008).
38. Wagner, C. A. *et al.* Pathogenic T cell cytokines in multiple sclerosis. *Journal of Experimental Medicine* **217**, (2019).
39. Fernández, O. *et al.* Survey of diagnostic and treatment practices for multiple sclerosis (MS) in Europe. Part 2: Progressive MS, paediatric MS, pregnancy and general management. *Eur. J. Neurol.* **25**, 739–746 (2018).
40. Bermel, R. A. *et al.* Interferon-beta treatment for multiple sclerosis. *Neurotherapeutics* **4**, 633–646 (2007).
41. Schubert, R. D. *et al.* Interferon-β treatment requires B cells for efficacy in neuro-autoimmunity. *J Immunol* **194**, 2110–2116 (2015).
42. Fridkis-Hareli, M. *et al.* Direct binding of myelin basic protein and synthetic copolymer 1 to class II major histocompatibility complex molecules on living antigen-presenting cells--specificity and promiscuity. *Proc Natl Acad Sci U S A* **91**, 4872–4876 (1994).
43. Edan, G. *et al.* Sclérose en plaques agressive: Définition et indication thérapeutique particulière. *La Presse Médicale* **33**, 187–191 (2004).
44. Martinelli Boneschi, F. *et al.* Mitoxantrone for multiple sclerosis. *Cochrane Database Syst Rev* CD002127 (2005).
45. Polman, C. H. *et al.* A randomized, placebo-controlled trial of natalizumab for relapsing multiple sclerosis. *N Engl J Med* **354**, 899–910 (2006).
46. Zivadinov, R. *et al.* Effect of teriflunomide on gray and white matter brain pathology in multiple sclerosis using volumetric and diffusion-tensor imaging MRI measures. *J Neurol Sci* **388**, 175–181 (2018).
47. Montes Diaz, G. *et al.* Dimethyl fumarate treatment in multiple sclerosis: Recent advances in clinical and immunological studies. *Autoimmun Rev* **17**, 1240–1250 (2018).

48. Koch-Henriksen, N. *et al.* A comparison of multiple sclerosis clinical disease activity between patients treated with natalizumab and fingolimod. *Mult Scler* **23**, 234–241 (2017).
49. Ruck, T. *et al.* Alemtuzumab in Multiple Sclerosis: Mechanism of Action and Beyond. *Int J Mol Sci* **16**, 16414–16439 (2015).
50. Hauser, S. L. *et al.* B-cell depletion with rituximab in relapsing-remitting multiple sclerosis. *N Engl J Med* **358**, 676–688 (2008).
51. Matsushita, T. *et al.* Regulatory B cells inhibit EAE initiation in mice while other B cells promote disease progression. *J Clin Invest* **118**, 3420–3430 (2008).
52. Rivers, T. M. *et al.* Observations on attempts to produce acute disseminated encephalomyelitis in monkeys. *J Exp Med* **58**, 39–53 (1933).
53. Freund, J. *et al.* Isoallergic encephalomyelitis and radiculitis in guinea pigs after one injection of brain and Mycobacteria in water-in-oil emulsion. *J Immunol* **57**, 179–194 (1947).
54. Bittner, S. *et al.* Myelin Oligodendrocyte Glycoprotein (MOG35-55) Induced Experimental Autoimmune Encephalomyelitis (EAE) in C57BL/6 Mice. *J Vis Exp* **5**, e51275 (2014).
55. McPherson, R. C. *et al.* Induction of passive EAE using myelin-reactive CD4+ T cells. *Methods Mol Biol* **1193**, 187–198 (2014).
56. Scheikl, T. *et al.* Transgenic mouse models of multiple sclerosis. *Cell. Mol. Life Sci.* **67**, 4011–4034 (2010).
57. Ben-Nun, A. *et al.* From classic to spontaneous and humanized models of multiple sclerosis: Impact on understanding pathogenesis and drug development. *Journal of Autoimmunity* **54**, 33–50 (2014).
58. Bettelli, E. *et al.* Myelin Oligodendrocyte Glycoprotein–specific T Cell Receptor Transgenic Mice Develop Spontaneous Autoimmune Optic Neuritis. *Journal of Experimental Medicine* **197**, 1073–1081 (2003).

59. Krishnamoorthy, G. *et al.* Spontaneous opticospinal encephalomyelitis in a double-transgenic mouse model of autoimmune T cell/B cell cooperation. *J Clin Invest* **116**, 2385–2392 (2006).
60. Litzenburger, T. *et al.* B Lymphocytes Producing Demyelinating Autoantibodies: Development and Function in Gene-targeted Transgenic Mice. *J Exp Med* **188**, 169–180 (1998).
61. Pöllinger, B. *et al.* Spontaneous relapsing-remitting EAE in the SJL/J mouse: MOG-reactive transgenic T cells recruit endogenous MOG-specific B cells. *Journal of Experimental Medicine* **206**, 20 (2009).
62. Berer, K. *et al.* Commensal microbiota and myelin autoantigen cooperate to trigger autoimmune demyelination. *Nature* **479**, 538–541 (2011).
63. Sabatino, J. *et al.* B cells in autoimmune and neurodegenerative central nervous system diseases. *Nat Rev Neurosci* **20**, 728–745 (2019).
64. Muramatsu, M. *et al.* Pillars Article: Class Switch Recombination and Hypermutation Require Activation-Induced Cytidine Deaminase (AID), a Potential RNA Editing Enzyme. Cell. 2000. 102: 553-563. *J Immunol* **201**, 2530–2540 (2018).
65. Bowers, P. M. *et al.* Coupling mammalian cell surface display with somatic hypermutation for the discovery and maturation of human antibodies. *PNAS* **108**, 20455–20460 (2011).
66. Vazquez, M. I. *et al.* B cells responses and cytokine production are regulated by their immune microenvironment. *Cytokine* **74**, 318–326 (2015).
67. Li, R. *et al.* Cytokine-Defined B Cell Responses as Therapeutic Targets in Multiple Sclerosis. *Front Immunol* **6**, 626 (2015).
68. Walsh, M. J. *et al.* Immunoglobulin G, A, and M--clonal restriction in multiple sclerosis cerebrospinal fluid and serum--analysis by two-dimensional electrophoresis. *Clin Immunol Immunopathol* **35**, 313–327 (1985).

69. Carroll, W. M. *et al.* 2017 McDonald MS diagnostic criteria: Evidence-based revisions. *Mult Scler* **24**, 92–95 (2018).
70. Krumbholz, M. *et al.* BAFF is produced by astrocytes and up-regulated in multiple sclerosis lesions and primary central nervous system lymphoma. *J Exp Med* **201**, 195–200 (2005).
71. von Büdingen, H.-C. *et al.* B cell exchange across the blood-brain barrier in multiple sclerosis. *J Clin Invest* **122**, 4533–4543 (2012).
72. Keegan, M. *et al.* Relation between humoral pathological changes in multiple sclerosis and response to therapeutic plasma exchange. *Lancet* **366**, 579–582 (2005).
73. Magliozzi, R. *et al.* Meningeal B-cell follicles in secondary progressive multiple sclerosis associate with early onset of disease and severe cortical pathology. *Brain* **130**, 1089–1104 (2007).
74. Brändle, S. M. *et al.* Distinct oligoclonal band antibodies in multiple sclerosis recognize ubiquitous self-proteins. *Proc Natl Acad Sci U S A* **113**, 7864–7869 (2016).
75. Srivastava, R. *et al.* Potassium Channel KIR4.1 as an Immune Target in Multiple Sclerosis. *New England Journal of Medicine* **367**, 115–123 (2012).
76. Pröbstel, A.-K. *et al.* Multiple Sclerosis and Antibodies against KIR4.1. *The New England journal of medicine* **374**, 1496–1498 (2016).
77. Gontika, M. P. *et al.* Anti-Myelin Oligodendrocyte Glycoprotein and Human Leukocyte Antigens as Markers in Pediatric and Adolescent Multiple Sclerosis: on Diagnosis, Clinical Phenotypes, and Therapeutic Responses. *Multiple Sclerosis International* vol. 2018 e8487471
78. Pröbstel, A.-K. *et al.* Anti-MOG antibodies are present in a subgroup of patients with a neuromyelitis optica phenotype. *Journal of Neuroinflammation* **12**, 46 (2015).

79. Cobo-Calvo, A. *et al.* Clinical Features and Risk of Relapse in Children and Adults with Myelin Oligodendrocyte Glycoprotein Antibody–Associated Disease. *Annals of Neurology* **89**, 30–41 (2021).
80. Mayer, M. C. *et al.* Distinction and Temporal Stability of Conformational Epitopes on Myelin Oligodendrocyte Glycoprotein Recognized by Patients with Different Inflammatory Central Nervous System Diseases. *The Journal of Immunology* **191**, 3594–3604 (2013).
81. Klein, L. *et al.* Antigen presentation in the thymus for positive selection and central tolerance induction. *Nat Rev Immunol* **9**, 833–844 (2009).
82. Ramagopalan, S. V. *et al.* Multiple sclerosis: major histocompatibility complexity and antigen presentation. *Genome Med* **1**, 105 (2009).
83. Seifert, M. *et al.* Functional capacities of human IgM memory B cells in early inflammatory responses and secondary germinal center reactions. *PNAS* **112**, E546–E555 (2015).
84. Kappos, L. *et al.* Ocrelizumab in relapsing-remitting multiple sclerosis: a phase 2, randomised, placebo-controlled, multicentre trial. *Lancet* **378**, 1779–1787 (2011).
85. Araki, M. *et al.* Clinical improvement in a patient with neuromyelitis optica following therapy with the anti-IL-6 receptor monoclonal antibody tocilizumab. *Mod Rheumatol* **23**, 827–831 (2013).
86. Disanto, G. *et al.* The evidence for a role of B cells in multiple sclerosis. *Neurology* **78**, 823–832 (2012).
87. Häusser-Kinzel, S. *et al.* The Role of B Cells and Antibodies in Multiple Sclerosis, Neuromyelitis Optica, and Related Disorders. *Front. Immunol.* **10**, (2019).
88. Kuraoka, M. *et al.* Complex Antigens Drive Permissive Clonal Selection in Germinal Centers. *Immunity* **44**, 542–552 (2016).

89. Nojima, T. *et al.* In-vitro derived germinal centre B cells differentially generate memory B or plasma cells in vivo. *Nat Commun* **2**, 465 (2011).

Abstracts

The project aims to clarify the involvement of B cells in the initiation and progression of multiple sclerosis (MS) using a transcriptomic analysis of B cells in cervical lymph nodes (CLNs) and brain of a transgenic mouse model of spontaneous experimental autoimmune encephalomyelitis (EAE). In this model called TCR^{1640}, transgenic TCR (T cell receptor) for $MOG_{92\text{-}106}$ are supposed to recruit MOG-specific B cells from the endogenous repertoire. The objective of the thesis was to evaluate the dynamics of MOG-specific B cells at the initiation of EAE in the secondary lymphoid organs and the brain. In this TCR^{1640} model in Lille, the EAE incidence was from 85% at 700 days of life. We checked the performance of a MOG tetramer to detect and isolate MOG-specific B cells. This MOG tetramer allowed us to identify rare MOG_{tet}^{+} B cells primarily in CLNs and brains of diseased TCR^{1640} mice. Anti-MOG antibodies in serum were quantified by ELISA and detected in disease-free and diseased TCR^{1640} mice, without correlation with their age, delay of EAE and clinical score. However, serum transfer experiments showed that there was a difference in humoral activity between sera of disease-free and diseased TCR^{1640} mice, which aggravated incidence and severity of EAE in the 2D2 mouse (another EAE model). These results suggested the dynamics of the repertoire of MOG_{tet}^{+} or MOG_{tet}- B cells to a pathogenic repertoire for the EAE development. Induced germinal center B cells culture (iGB) and expansion (on fibroblasts called 40LB cells) of MOG_{tet}^{+} or total B cells sorted from CLNs and brain of disease-free and diseased TCR^{1640} mice allowed to define only few clonotyps for IgLKappa chains and IgHG chains. Our findings highlight the difficulty of the iGB single cell culture to expand effector cells and suggest to go directly to single cell sequencing of sorted derived-CLNs and derived-CNS (central nervous system) MOG_{tet}^{+} B cells from TCR^{1640} mice.

Résumé

Le projet vise à préciser l'implication des lymphocytes B dans l'initiation et la progression de la sclérose en plaque (SEP) au travers d'une analyse transcriptomique des lymphocyes B dans les ganglions cervicaux lymphatiques (CLN) et cerveau d'un modèle murin transgénique d'encéphalomyélite auto-immune expérimentale (EAE) spontanée. Dans ce modèle appelé TCR^{1640}, les TCR (récepteurs membranaire des lymphocytes T) transgéniques pour $MOG_{92\text{-}106}$ sont supposés recruter des lymphocytes B spécifiques de MOG du répertoire endogène. L'objectif de la thèse était d'évaluer la dynamique des lymphocytes B spécifiques de MOG à l'initiation de EAE, à la fois dans les organes lymphoïdes secondaires et le cerveau. Dans ce modèle TCR^{1640} à Lille, l'incidence de l'EAE était de 85% à 700 jours de vie. Nous avons vérifié la performance d'un tétramère de MOG pour détecter et isoler des lymphocytes B spécifiques de MOG. Ce tétramère de MOG nous a permis d'identifier de rares lymphocytes B MOG_{tet}^{+} essentiellement dans les CLN et le cerveau des souris TCR^{1640} malades. Les anticorps anti-MOG sériques ont été dosés par ELISA et retrouvés chez les souris TCR^{1640} encore saines et les souris malades, sans corrélation avec leurs âges, leurs durées d'EAE et leurs scores cliniques. Cependant, les expériences de transferts sériques montraient qu'il existait une différence d'activité humorale entre les sérums de souris TCR^{1640} encore saines et les sérums de souris TCR^{1640} malades, qui pour ces derniers aggravaient l'incidence et la sévérité de l'EAE chez la souris 2D2 (autre model d'EAE). Ces résultats suggéraient la dynamique du répertoire des lymphocytes B MOG_{tet}^{+} ou MOG_{tet}- vers un répertoire pathogène pour le développement de l'EAE. La culture et l'expansion cellulaire en cellule unique (sur fibroblastes appelés 40LB) de lymphocytes B MOG_{tet}^{+} ou B totaux triés des CLN et du cerveaux de souris TCR^{1640} saines et malades ont permis de définir quelques clonotypes pour les chaines lourdes des IgG et légères des IgKappa. Nos résultats soulignent la difficulté de la culture cellulaire iGB en cellule unique. Ce qui suggèrent de séquencer directement les cellules uniques purifiées par cytométrie à partir de lymphocytes B MOG_{tet}^{+} issus des CLN et système nerveux central de souris TCR^{1640}.